RESCEU / DENET Summer School 2010 @ Kochi

Density Probability Distribution Function of SDSS Galaxies in Redshift Space

○Kensuke Fukunaga(The University of Tokyo),
Takahiro Nishimichi, Toshiya Kashiwagi,
Atsushi Taruya, Yasushi Suto,
and Yun-Young Choi

We measure the probability distribution function (PDF) of galaxies in the Seventh Data Release of the Sloan Digital Sky Survey.

In particular, we consider the dependence of PDFs on galaxy properties such as color, luminosity and morphology by constructing the volume-limited samples.

$$P(\delta^r) \xrightarrow{\text{check by N-body simulation}} P(\delta^s)$$

approximately Log-normal.(Kayo et al.)

We measure PDF of DM in redshift space.

Galaxy biasing

probe galaxy properties

$$P(\delta^r_{\mathrm{gal}}) \xrightarrow[\text{Redshift distortion}]{} P(\delta^s_{\mathrm{gal}})$$

We measure this of SDSS galaxies.

PDF of dark matter

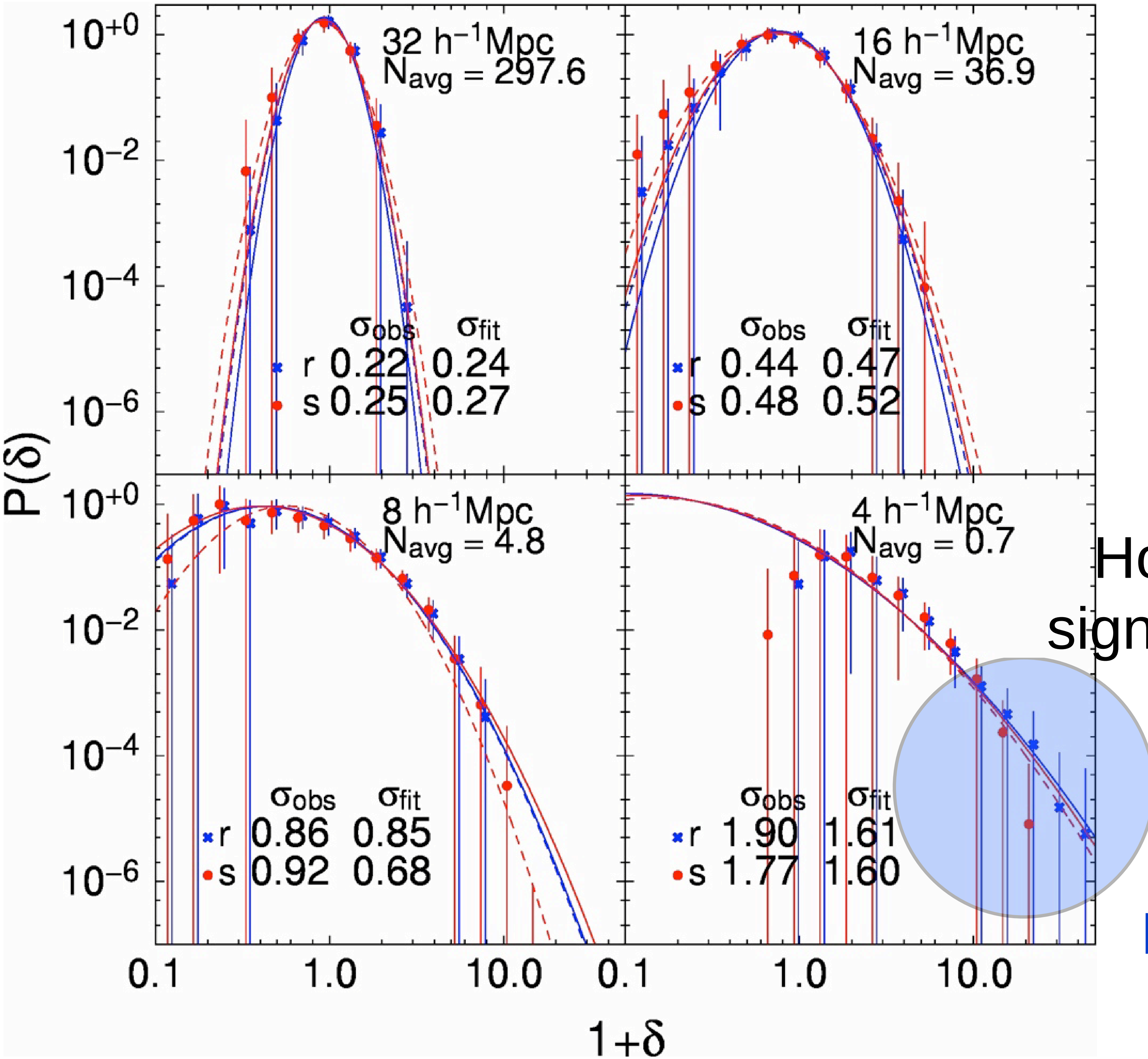

solid line:LN(obs)

dashed line:LN(fit)

Basically,
PDF is well
described by LN.

However, we detect
significant departure @
small R.

Redshift distortion!

PDF of SDSS galaxies

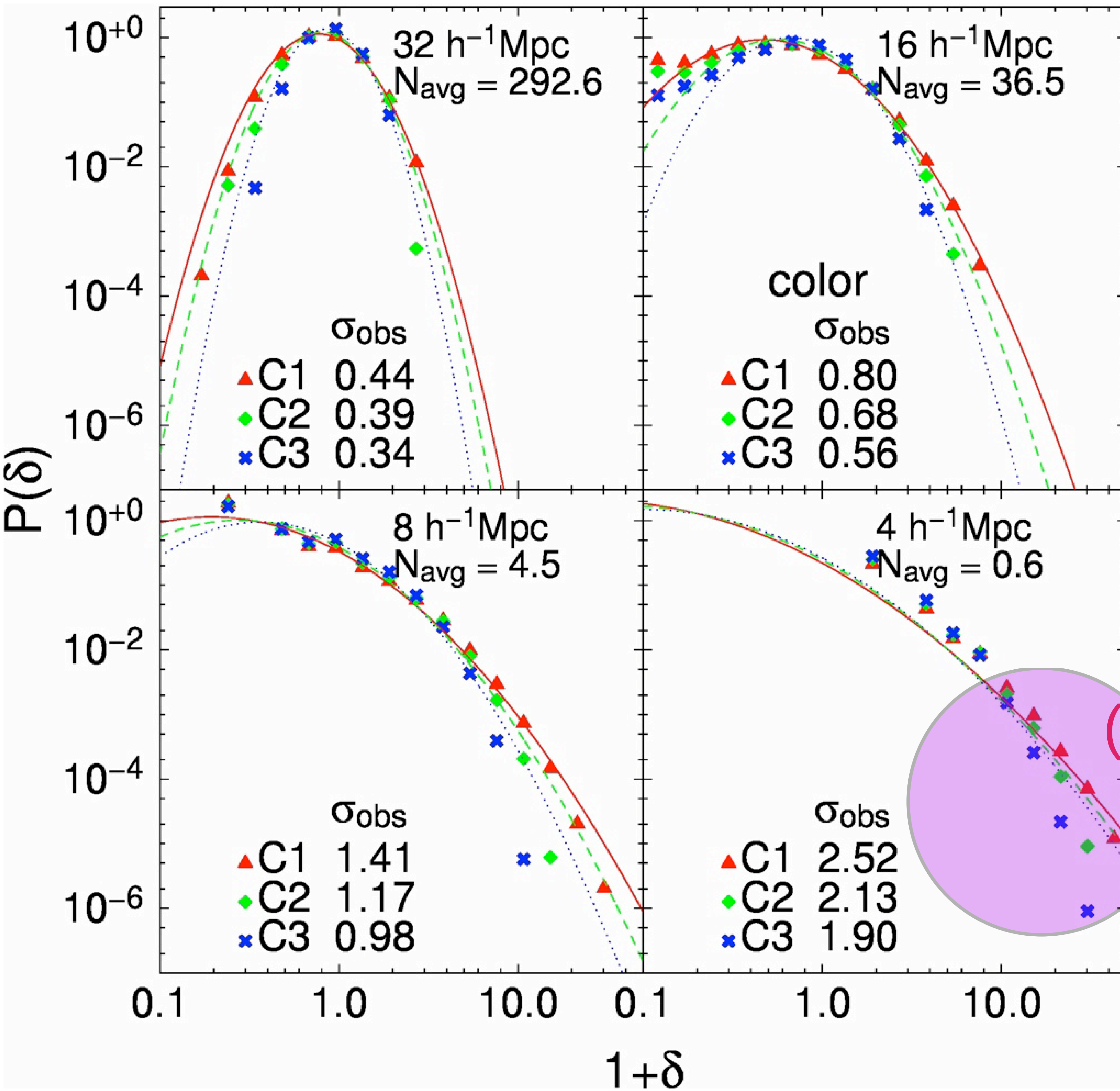

line:LN(obs)

C1:Red galaxies

C2:Intermediate

C3:Blue galaxies

Basically,
PDF is also well
described by LN.

Nonlinear biasing
(density-morphology)

+

Redshift distortion
(Finger-of-God)

X-ray Universe and it's instruments

Junko S. Hiraga (Research Center for the Early Universe, U. Tokyo)

1. Probe for the nuclear synthesis

My research interests is the origin of heavy elements and Cosmic-ray origin using observational data of supernova remnants(SNRs) by X-ray space observatory. Junko is a SWG member of Suzaku satellite.

Suzaku detected Mn and Cr K emission lines.

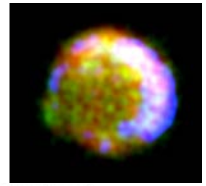

Suzaku Image of Tycho SNR

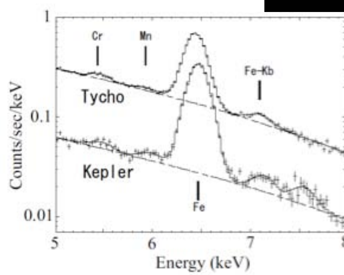

2. Instrumentation is now being developed

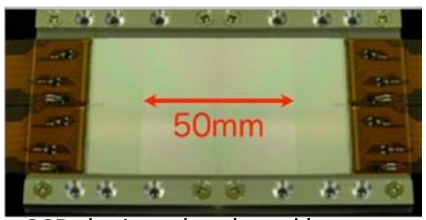

CCD devices developed by Hamamatsu Photonics. K.K.

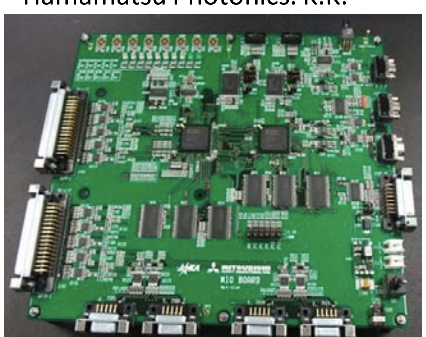

Digital Electronics Board developed for SXI(BBM)

Junko is also a member of Astro-H project. Astro-H employs the world's first instrument, SXS (Soft X-ray Spectrometer). SXS will carry out high resolution(FWHM=7eV@6keV) spectroscopy even in diffuse objects with 3'x 3' FOV. Junko is especially working on SXI (Soft X-ray Imager) development as a CCD expert. SXI will strongly support SXS observation taking with full advantages of its large FOV of 30'x 30' and medium energy resolution (〜150eV).

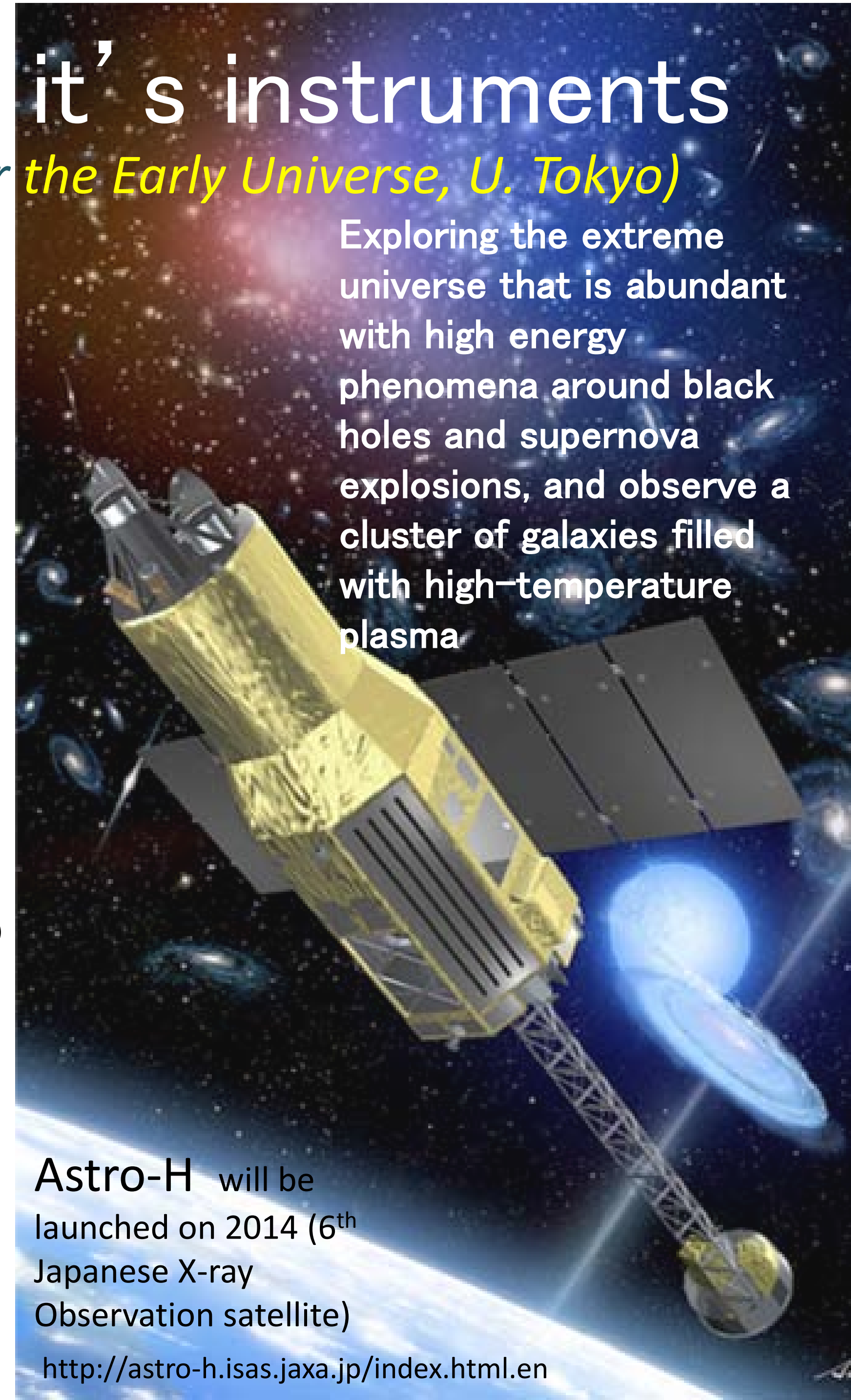

Exploring the extreme universe that is abundant with high energy phenomena around black holes and supernova explosions, and observe a cluster of galaxies filled with high-temperature plasma

Astro-H will be launched on 2014 (6th Japanese X-ray Observation satellite)

http://astro-h.isas.jaxa.jp/index.html.en

Affleck-Dine field, parametrising flat direction in MSSM, is represented by a complex scalar field + global U(1) symmetry. Its potential in gravity mediation is

$$\ddot{\Phi} + DH\dot{\Phi} - \frac{1}{a^2}\nabla^2\Phi = -V'(\Phi)$$

$$V(\Phi) = m^2 |\Phi|^2 \left[1 + K\log\left(\frac{|\Phi|^2}{M_*^2}\right)\right] - cH^2|\Phi|^2 + NR$$

1-loop corrections from gauginos $\quad K = -0.01 \sim -0.1$

Enqvist, McDonald, PLB 1998

$V(\Phi)/|\Phi|^2$ has a minimum at $\Phi \neq 0$

This system has a non-topological soliton named Q-ball

Results : Formation process (3D) $N = 128^3$

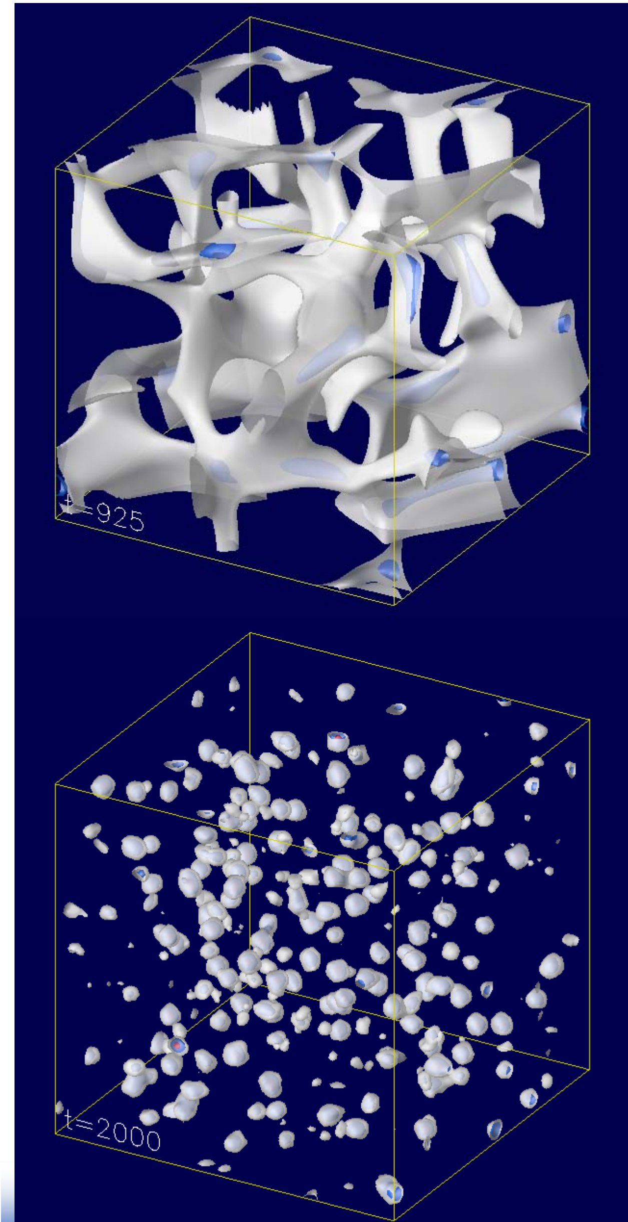

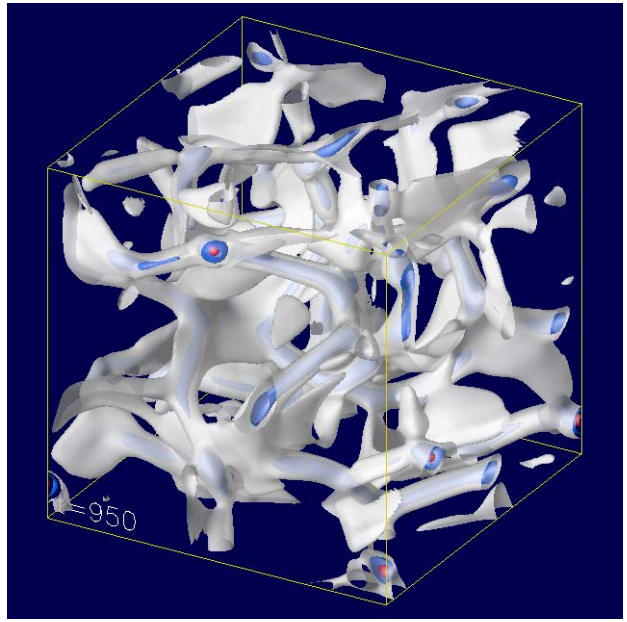

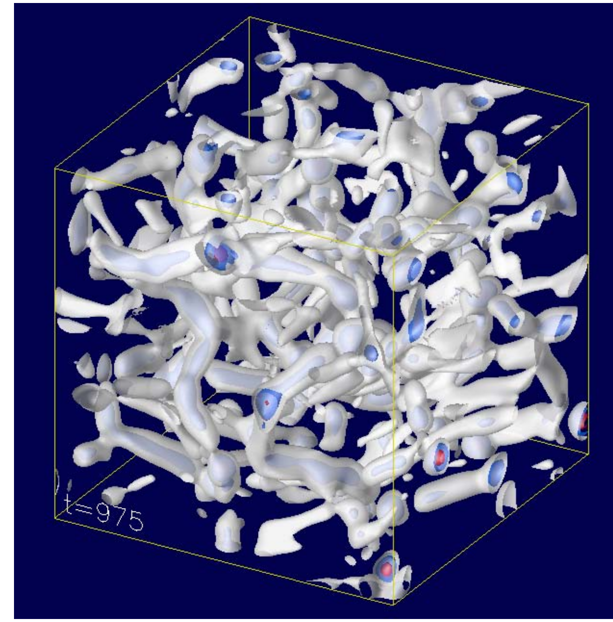

t

background oscillation | formation | relaxation

From these lattice simulaitions, we identify Q-balls, and obtain the charge distributions, charge/energy relation, and chage/size relation.

TH, Kawasaki, Takahashi, JCAP 06(2010)008 [arXiv:1003.1779]

Furthermore, we computed the GW spectra from Q-balls.

TH, Takahashi, Yamaguchi, in preparation

Results : Charge distribution/GWs

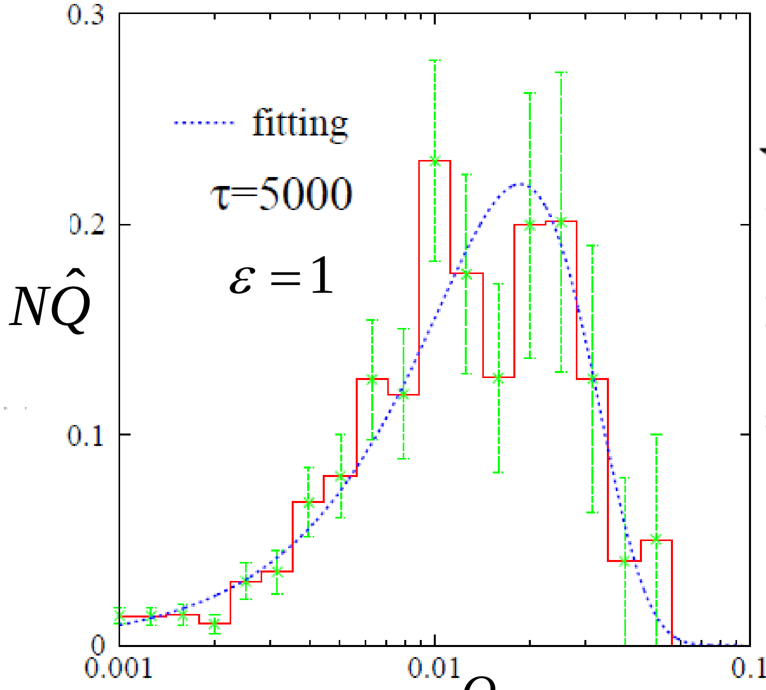

$$\hat{Q} \equiv \frac{Q}{|\Phi_{in}|^2 m^{-2}}$$

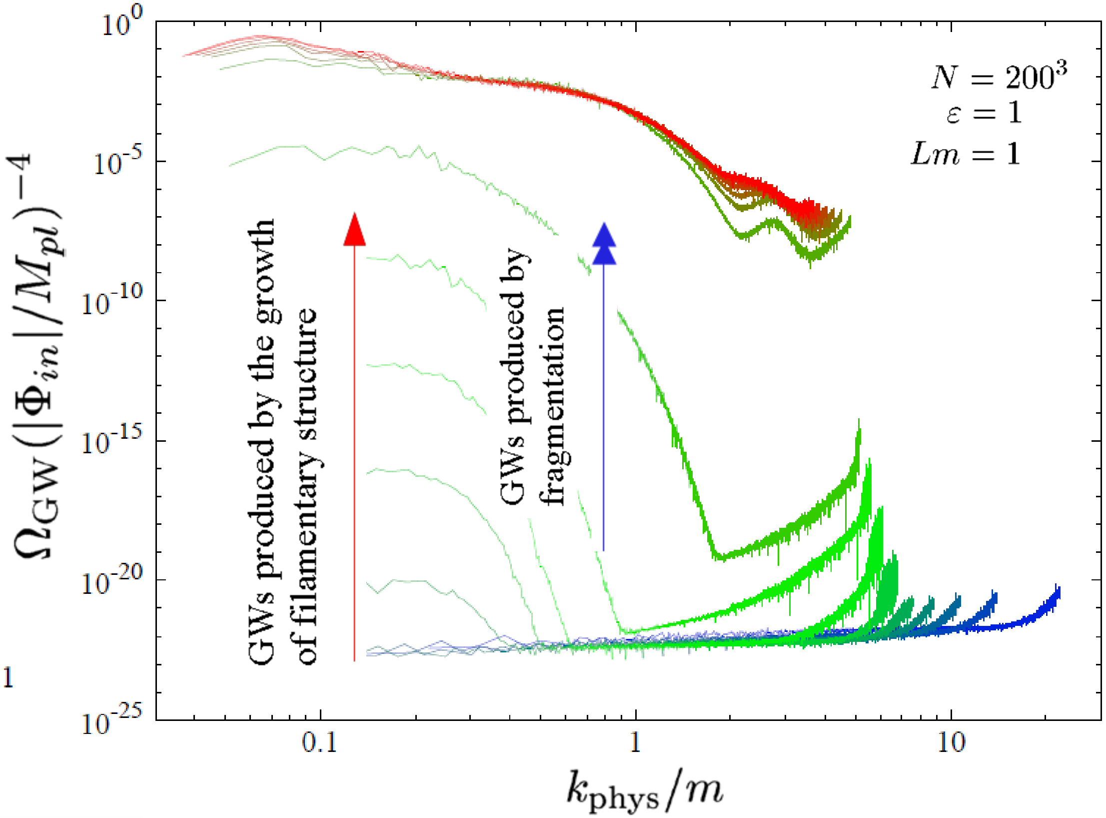

$$Q_{peak} = 1.9\times 10^{-2}\,|\Phi_{in}|^2\,m^{-2}$$

∼60% larger than $Q_{\max}^{(KK)} = 1.2\times 10^{-2}\,|\Phi_{in}|^2\,m^{-2}$

Kasuya, Kawasaki, PRD 2000

$$\rho_{\rm GW} = \frac{1}{32\pi G}\langle \dot{h}_{ij}\dot{h}_{ij}\rangle$$

$$\Omega_{\rm GW} = \frac{1}{\rho_c}\frac{d\rho_{\rm GW}}{d\log k}$$

Results : Formation process with $\varepsilon = 0.01$

Recall $\Phi(t_{in}) = M_*$ $\dot{\Phi}(t_{in}) = imM_*\varepsilon$

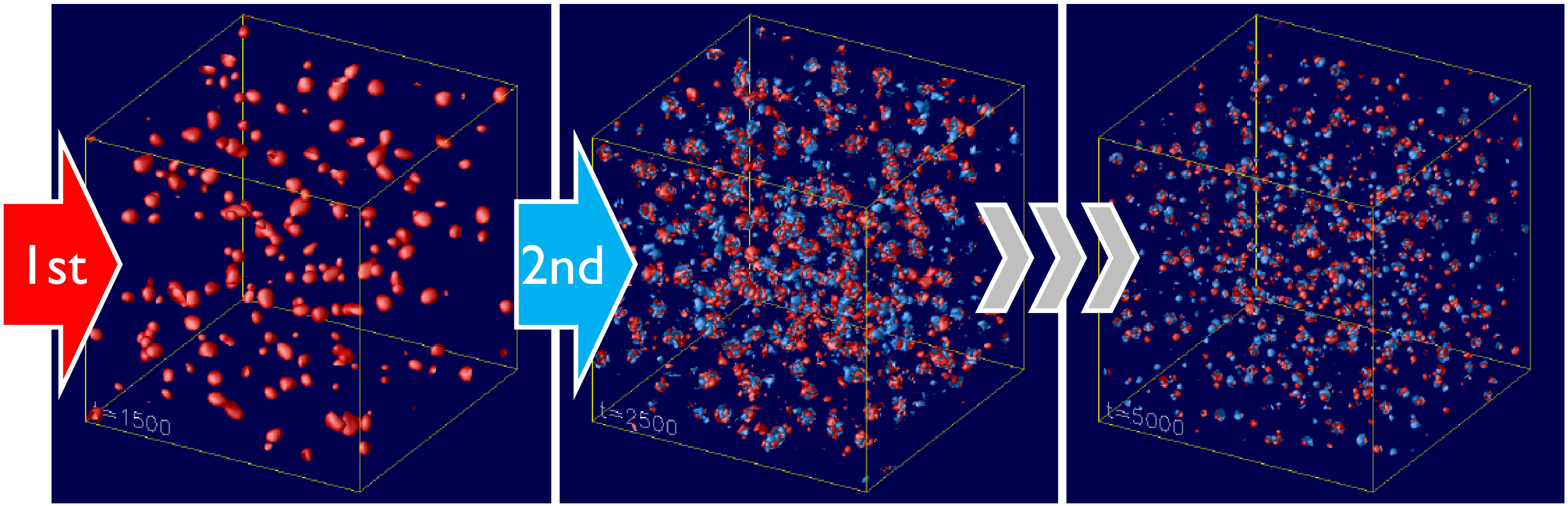

(a) $\tau = 1500$ (b) $\tau = 2500$ (c) $\tau = 5000$

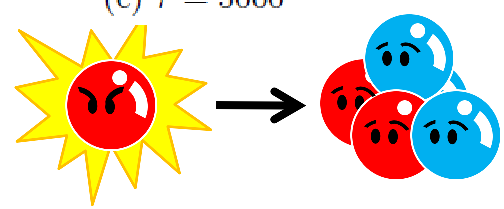

- 1^{st} -generation Q-ball : positive, excited
- 2^{nd} -generation Q-ball : positive+negative, mildly excited

Excited Q-balls release their excessive energy, producing negative Q-balls

Gravitational wave background from inflation

Sachiko Kuroyanagi (ICRR)

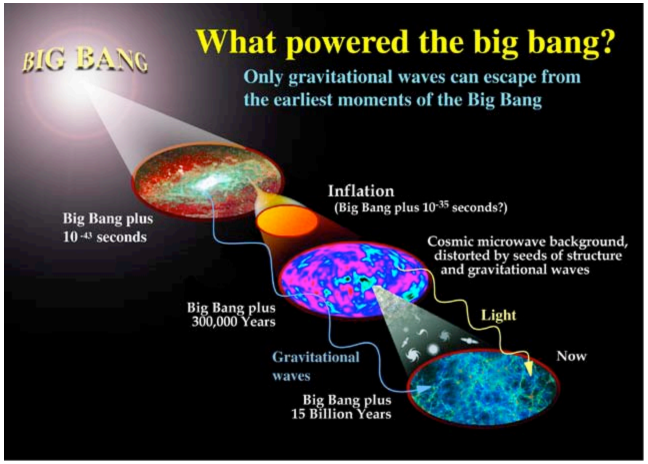

is…

- originating from quantum fluctuations in the space time metric
- only way to directly observe inflation
- one of the main targets of DECIGO and BBO (next-generation satellite experiment for direct detection of gravitational waves)

<u>Work 1</u> The precise spectrum is calculated by taking into account…

- dynamics of slow-rolling scalar field during inflation
- changes in the effective number of degrees of freedom g_*
- reheating (decay of the scalar field + radiation production)
- neutrino anisotropic stress

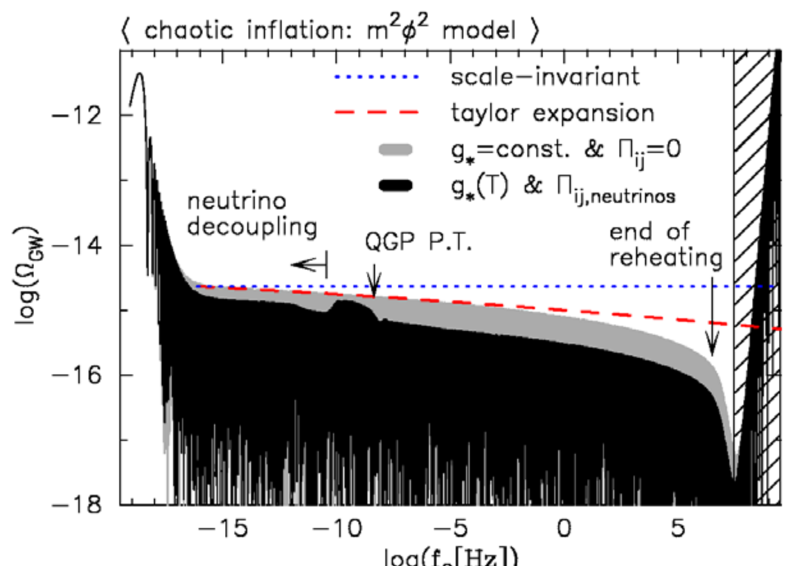

S. Kuroyanagi, T. Chiba and N. Sugiyama, Phys. Rev. D 79, 103501 (2009)

Work 2

How well can the inflationary parameters be constrained by future direct detection experiments for the GWs? and how does it complement the information from CMB?

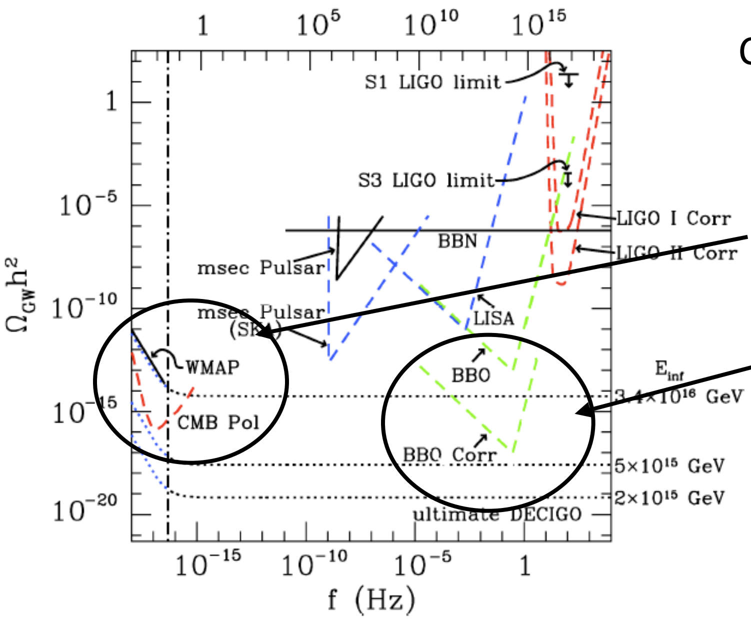

CMB B-mode polarization

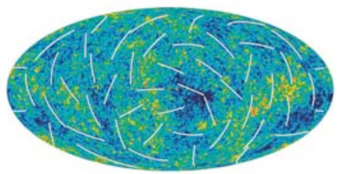

Direct detection

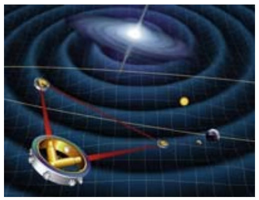

→ looking at two different frequency.

expected to provide independent information from each other.

Direct detection has power to improve the constraint from the CMB experiment!

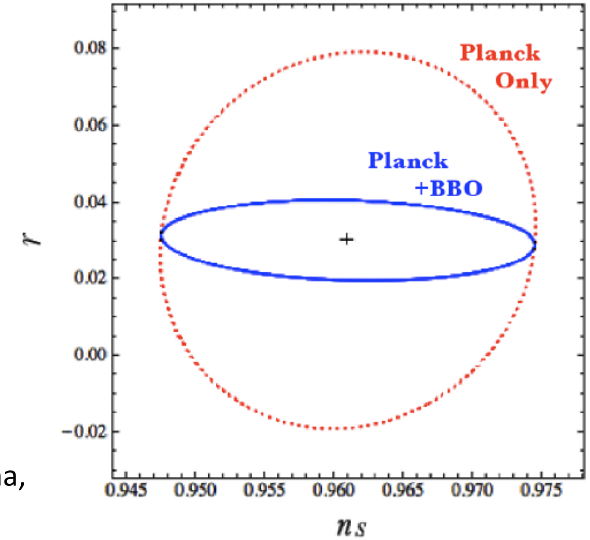

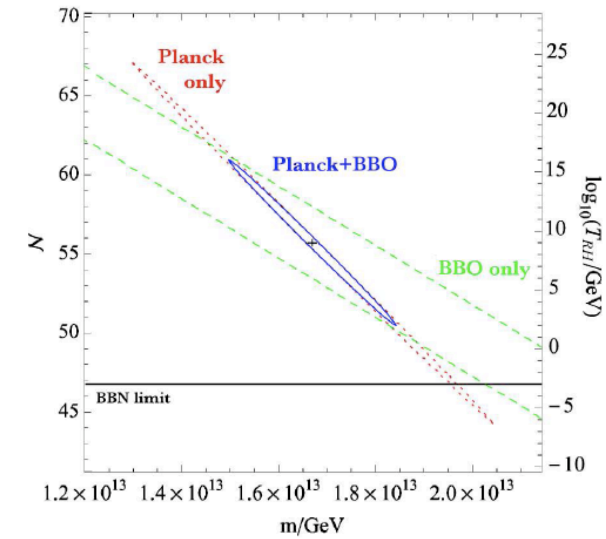

S. Kuroyanagi, C. Gordon, J. Silk and N. Sugiyama, Phys. Rev. D 81, 083524 (2010)

Tsz Yan Lam (IPMU)

Research interests:

1. Structure formation
   - ✴Excursion set approach in halo and void abundances
   - ✴First crossing probability of moving barriers and correlated steps
   - ✴Constraints on primordial non-Gaussianity
2. Peculiar Velocity Field and f_{nl} models
   - ✴Pairwise velocity PDF
   - ✴Redshift space distortions

Primordial non-G & Pairwise Velocity PDF

TYL, Nishimichi & Yoshida (2010)

1. peculiar velocity field & redshift space distortions also affected by primordial non-Gaussianity (See TYL, Desjacques & Sheth 2010 for calculation using ellipsoidal collapse model)

2. The idea was proposed almost 20 years ago (Scherrer 1992; Catelan & Scherrer 1995; Schmidt 2010) -- all of them used linear theory

3. This work: compare predictions to N-body measurements & Evolution is important (linear theory fails to match the effect of f_{nl})!

4. Non-vanishing three-point functions: $\langle v_{||}^3 \rangle$ and $\langle v_{||} v_{\perp}^2 \rangle$

term missed in earlier studies; it induces correlation between velocities in parallel and perp directions

Why evolution is important

Parallel to line of separation

Perpendicular to line of separation

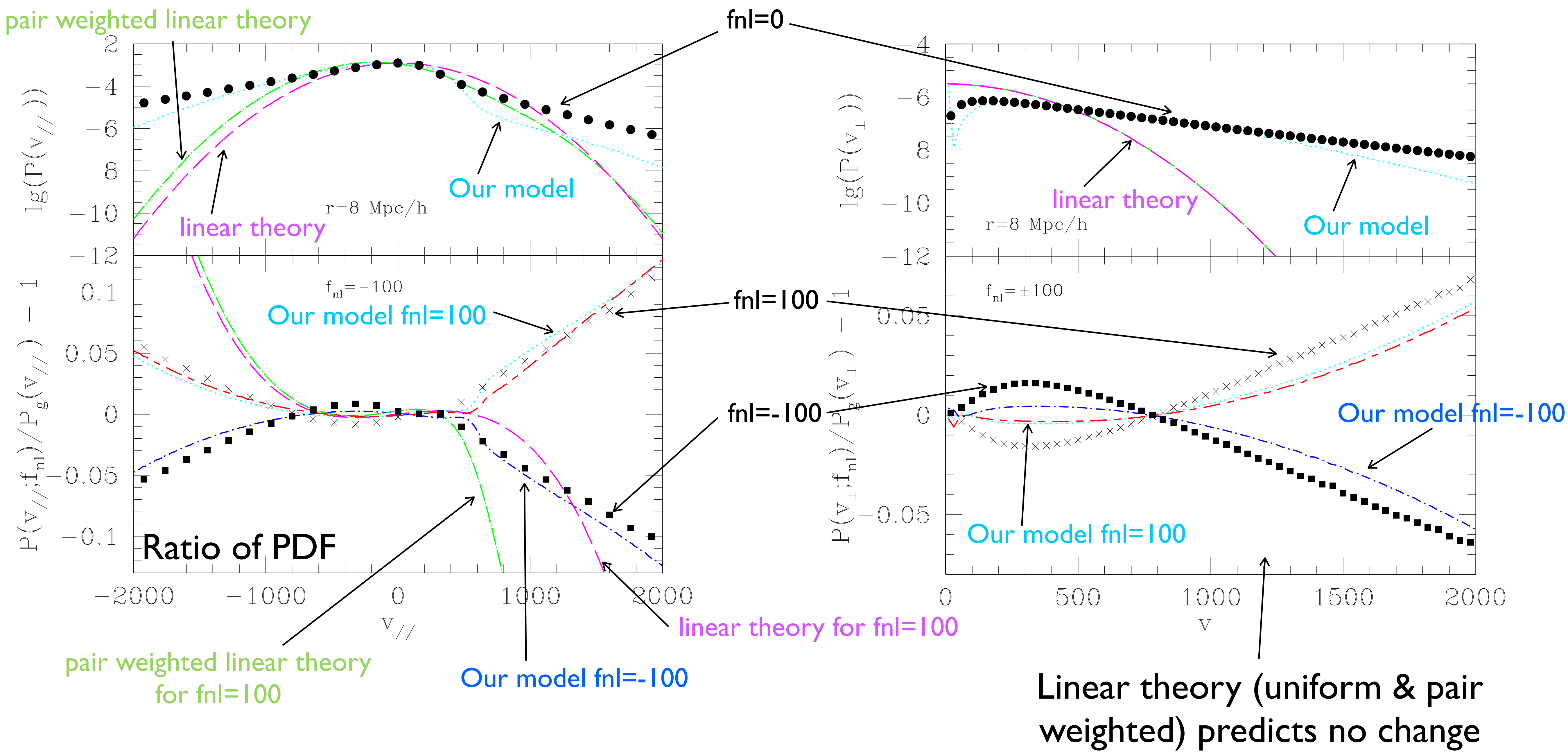

- Linear theory predictions fail in both parallel and perpendicular directions
- Our model agrees with measurements, both the profile when $f_{nl}=0$ and the ratio of PDF

Ongoing work

i. Redshift space distortion in f_{nl} model (including evolution model)
ii. Peculiar velocity of biased tracers
iii. Monte-Carlo simulations with correlated steps (TYL & Sheth, in preparation)
iv. Excursion set beyond 1D
v. Void abundances measurements

Development of Precise Weak Lensing Measurement Method

Hironao Miyatake (Ph. D Student, University of Tokyo) and Masahiro Takada (IPMU)

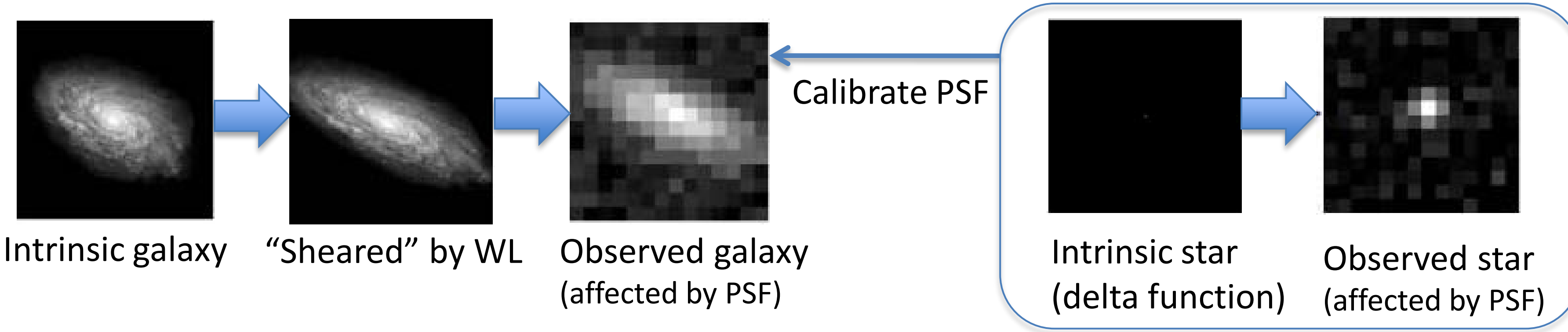

Bridle et al. 2009

-Weak lensing signal (shear) is the powerful tool for exploring cosmology.

-However, there are difficulties to obtain weak lensing signals.

- Statistics: Weak lensing (WL) distortion of the galaxies acts as an elliptical coordinate transformation. Since galaxies have intrinsic ellipticity we cannot obtain the lensing shear from a single galaxy. However, under the assumption that the intrinsic ellipticity has a random orientation between different galaxies, shear can be estimated by averaging the observed ellipticities over a sufficient number of galaxies.

- PSF correction: The image of an galaxy is smeared and distorted when the photons from the object pass through the atmosphere and telescope. This effect is called Point Spread Function (PSF). We have to correct for the PSF effect using images of stars that are not affected by WL.

-A few percent accuracy is needed for future weak lensing survey such as HSC, DES, and LSST.

BJ02 Method

Bernstein & Jarvis 2002

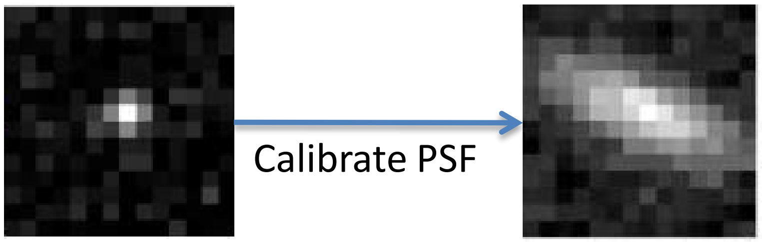

Observed star   Observed galaxy

1. Represent star images by Gauss Laguerre (GL) Functions to obtain PSF.
2. Convolve elliptical GL Functions with the PSF to create a new basis to be used for galaxy image expansion.
3. Find the ellipticity of the GL which makes coefficients of the ψ_{20} and ψ_{02} (quadrupole momemt) of the above basis zero.
4. Statistically estimate the shear by using the obtained ellipticities of a population of galaxies

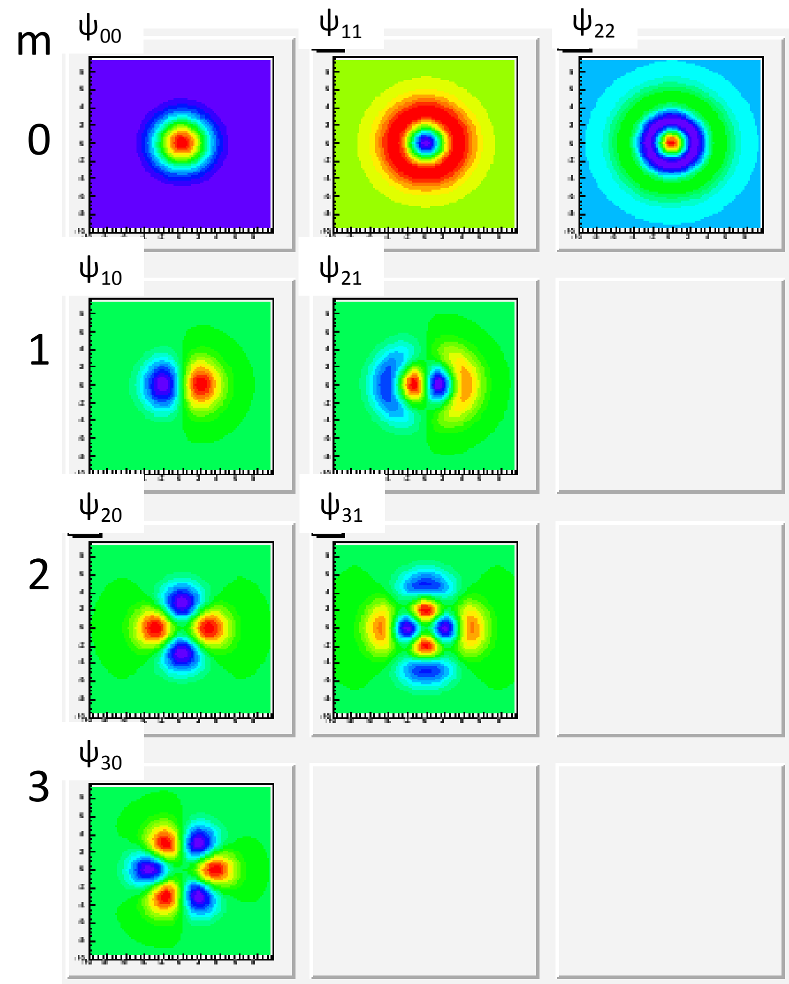

<u>We are implementing this method.</u>

Ring Test

-Generate galaxies that have ellipticity magnitude *e* evenly on a ring in the ellipticity plane (solid line).
-In the absence of shear δ, the average of the measured ellipticities should be zero.
-In the presence of shear δ, the ring is off from center (dashed line). The input shear should be reconstructed after averaging the measured ellipticities.

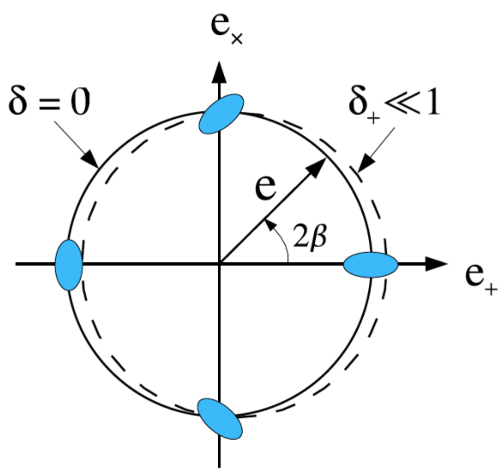

Nakajima & Bernstein 2006

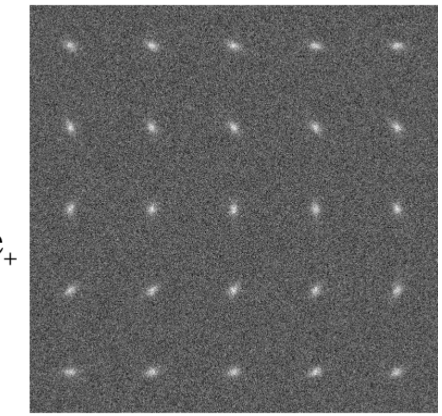
Simulation Image

Test Parameters
-Input shear (0.02,0)
-Galaxy: elliptical exponential profile
-Ellipticity magnitude = {0.1, 0.2, 0.3, 0.4}
-SN = {100,40,20}
-PSF: Gaussian FWHM=0.7”

A few % accuracy is achieved.

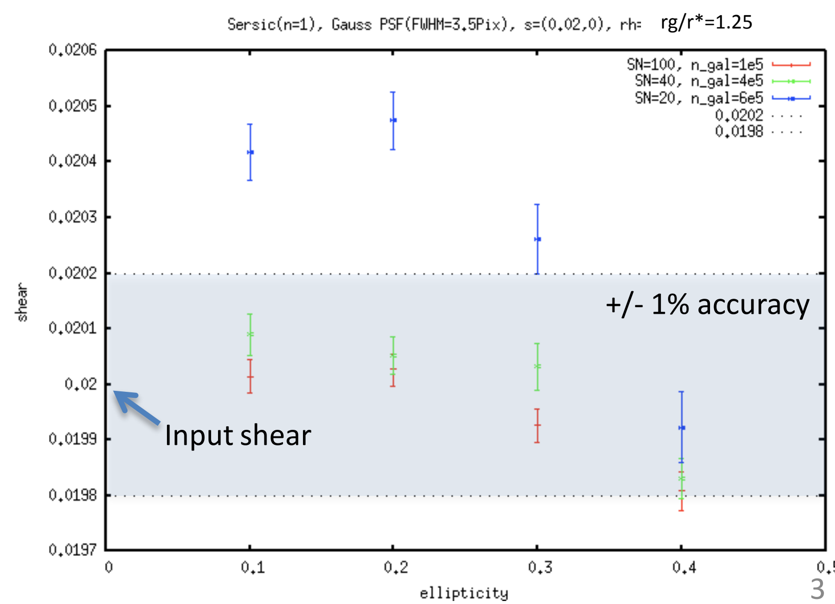

Toward Realistic Image

More realistic test

-Intrinsic ellipticity distribution: Gaussian

-Galaxy: elliptical exponential profile

-SN=20

-PSF: Gaussian FWHM = {0.5, 0.7, 0.9}

A few % accuracy is achieved.

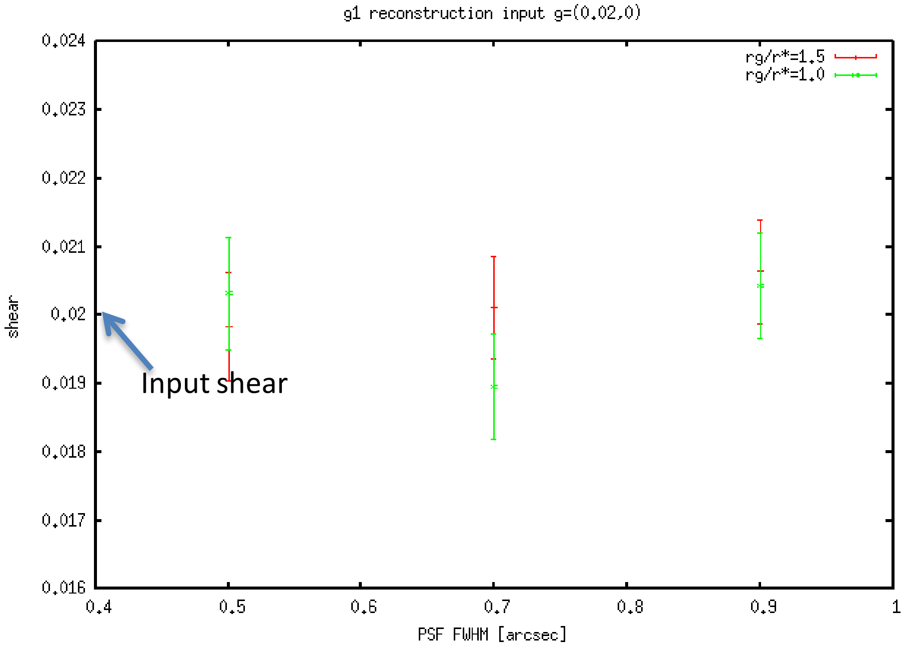

Future Works

-Test the method using more realistic simulation images such as glafic (Oguri 2010), STEP (Heymans et al. 2006, Massey et al. 2007) and GREAT08 (Bridle et al. 2009)

-Apply this method to a cluster of galaxies and extract cosmological information.

Growth rate of cosmological density perturbations in an $f(R)$ model and cosmological constraints from large surveys of galaxies

Nakamura Gen

HIROSHIMA UNIVERSITY

Collaborators : K.Yamamoto, T.Narikawa, G.Huetsi, T.Sato
(Tartu Obs.)

Refs : PRD 81, 103517 (2010)

f(R) model

Modified Action $S = \frac{1}{16\pi G}\int d^4x\sqrt{-g}(R + f(R))$

The viable models ($z \lesssim 1$) $\boxed{f(R) = -\lambda R_c \left[1 - \left(\frac{R_c}{R}\right)^{2n}\right]}$

Growth history in f(R) model

Modification of the gravity

$$\ddot{\delta} + 2\frac{\dot{a}}{a}\dot{\delta} - 4\pi G_{\rm eff}(a,k)\rho\delta = 0,$$

$$\frac{G_{\rm eff}(a,k)}{G} = 1 + \frac{1}{3}\frac{k^2/a^2}{k^2/a^2 + 1/(3f_{RR})}$$

$$\frac{1}{3f_{RR}} = k_c^2\left(\frac{\Omega_0/a^3 + 4(1-\Omega_0)}{\Omega_0 + 4(1-\Omega_0)}\right)^{2n+2}$$

Difference of growth history

Growth factor

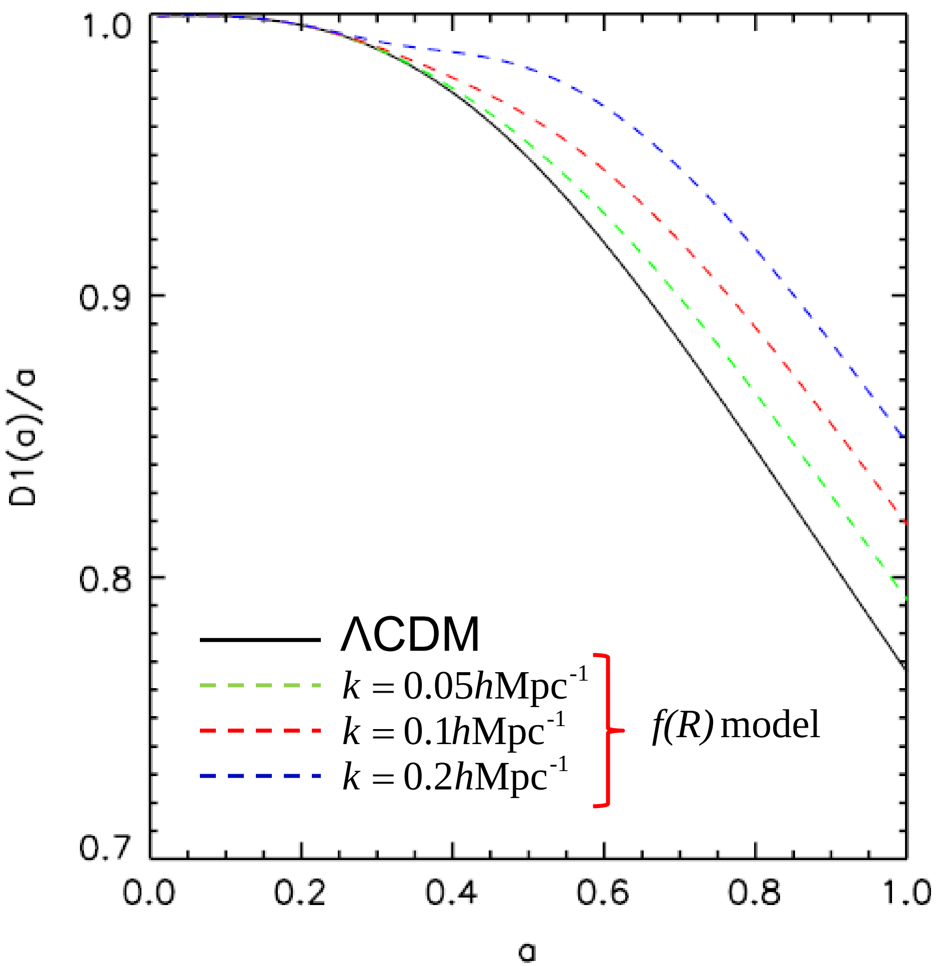

Growth rate

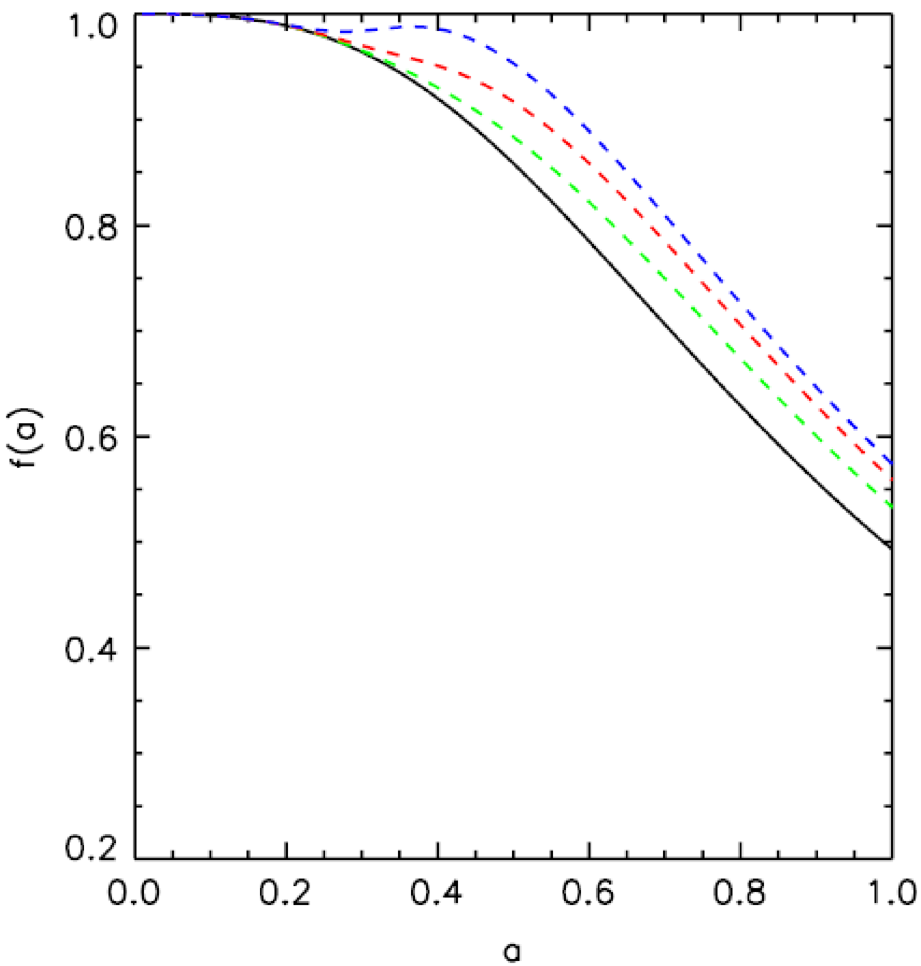

$$n = 1, k_c = 0.05h\mathrm{Mpc}^{-1}$$

Constraint from SDSS LRG galaxy sample

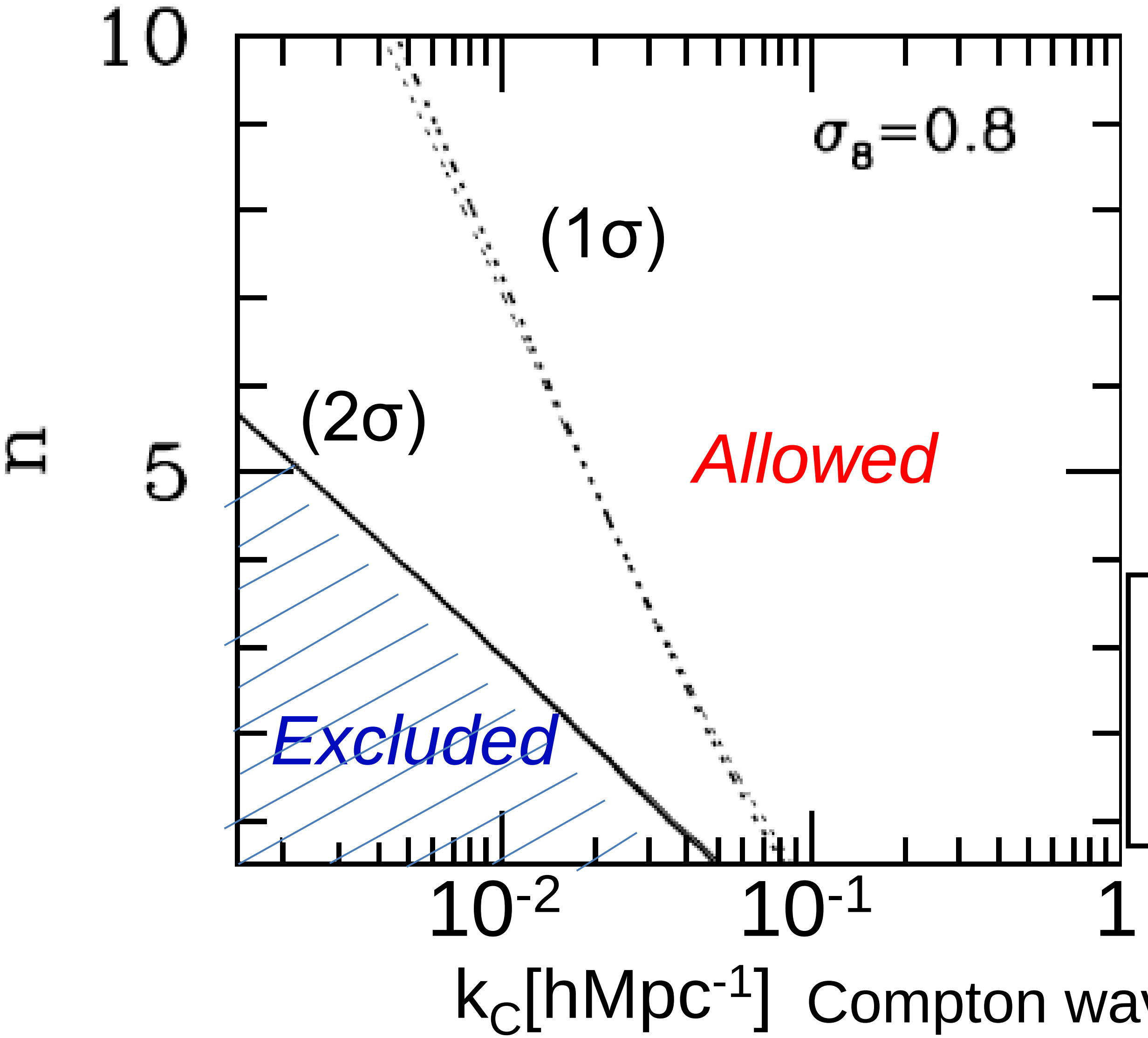

Compton wavelength parameter

Using mulitipole power spectrum, P_0,P_2

Large k_C model fits better, while small k_C model is excluded.

Probing primordial non-gaussianity from *magnification*-lensing & *magnification*-ISW cross-correlations

Toshiya Namikawa (The University of Tokyo)

collaboration with

Tomohiro Okamura (Tohoku University)

Atsushi Taruya (The University of Tokyo)

10th-RESCEU/DENET Summer School @ Kochi, Aug.29th – 31st, Sep. 1st , 2010

Motivation & Purpose

☆ **Information on primordial non-gaussianity can be obtained from galaxy observations through galaxy bias** (see Okamura's presentation).

☆ **Recent studies explore primordial non-gaussianity from cross-correlation between galaxy number density and CMB observables** (Jeong +09, Takeuchi +10).

☆ **However, *observed* galaxy number density is modified by gravitational lensing (Magnification effect)** (Moessner +98, Matsubara 00).

$$\delta_h \to \delta_h + \boxed{(5s-2)\kappa}$$

slope **convergence**

$$s = \frac{d\log_{10} N(<m)}{dm}$$

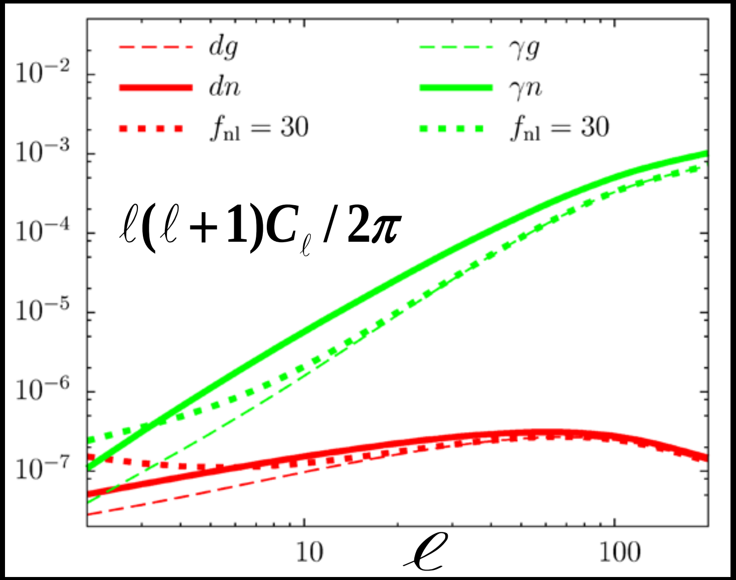

Power spectrum is enhanced by magnification effect at large scale where the effect of non-gaussianity become important.

We estimate systematic bias due to ignoring magnification.

Details of Calculation

[Survey]

CMB experiment : Planck

Galaxy survey : $f_{\rm sky} = 0.5$ $N_g = 1\,[\mathrm{arc\,min}^{-2}]$

[Model of galaxy samples]

Redshift distribution of galaxy $n(z) = N_g \delta_D(z - z_s)$ $[\mathrm{arc\,min}^{-2}]$

bias $b = 2.0$

Source redshift

[Systematic bias]

$$\Delta p_i = \sum_j ((F^{Xg})^{-1})_{ij} \sum_\ell^{1000} \frac{dC_\ell^{Xg}}{dp_i} \left(\frac{(2\ell+1) f_{\rm sky}}{(C_\ell^{gg} + 1/N_g) C_\ell^{XX} + (C_\ell^{Xg})^2} \right) (C_\ell^{Xn} - C_\ell^{Xg})$$

Fisher matrix

$p_i^{\rm inferred} - p_i^{\rm true}$

$$F_{ij}^{Xg} = \frac{dC_\ell^{Xg}}{dp_i} \boxed{\left(\frac{(2\ell+1) f_{\rm sky}}{(C_\ell^{gg} + 1/N_g) C_\ell^{XX} + C_\ell^{Xg}} \right)} \frac{dC_\ell^{Xg}}{dp_j}$$

Inverse of the covariance

We consider…

$X = \Theta$ (Temperature) d (CMB deflection angle) γ (galaxy shear)

Results

[Systematic bias and 1 sigma constraint on fnl]

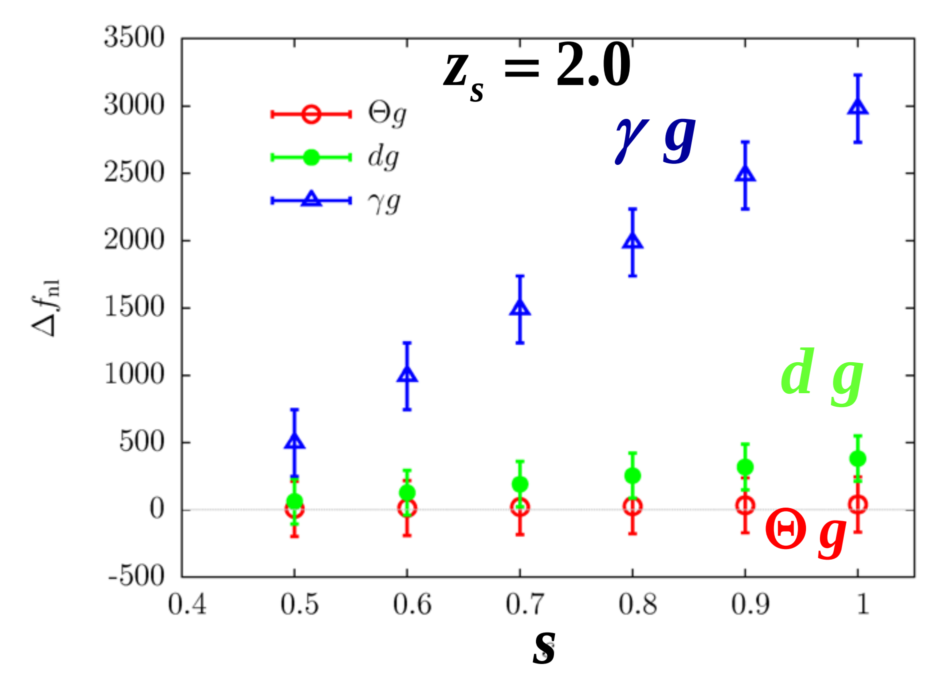

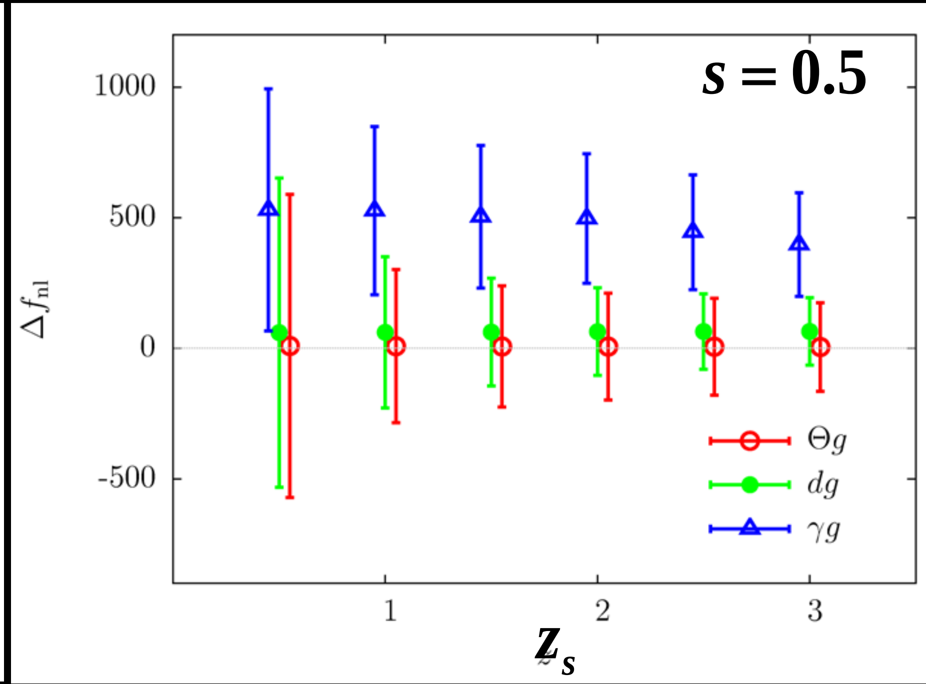

☆ From left panel…

Θg & dg : The systematic bias and constraint are insensitive to slope.
γg : Estimated fnl is highly biased due to ignoring magnification

☆ From right panel…

The systematic bias on fnl is not so sensitive to redshift, but constraint on fnl is improved at higher redshift.

ISW of Local structures and CMB correlation

A.J. Nishizawa(Tohoku U.) and K.T. Inoue(Kinki U.)

Abstract
CMB temperature fluctuation is generated not only at z~1100 but during the photons pass through the LSS of the Universe, that is, (k,t)-SZ, ISW, WL effects. Here, we present a effect of ISW effect of large clusters and voids, which typically ~200 Mpc/h in diameter.
The amount of ΔT(~10μK) caused by those structures well accounts for the CMB large scale temperature fluctuations.

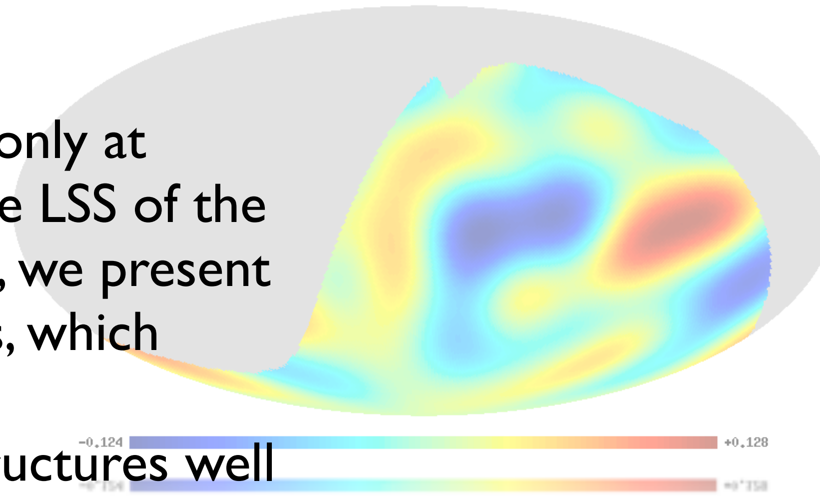

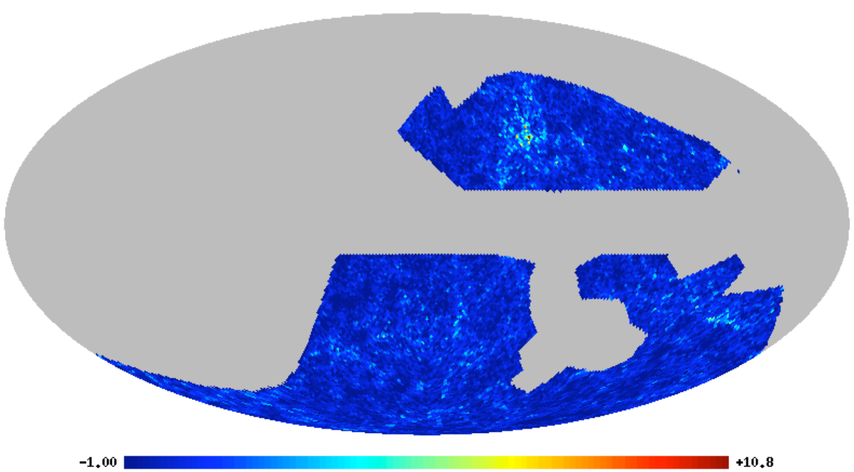

Data
- LSS data
+ 6 degree Field(6dF) spectroscopic sample(z<0.3)
+ Ks(2MASS) < 12.8 flux limited sample
+ redshift slice(dz=0.05)
+ Harmonic Inpainting the masked region

- CMB data
+ WMAP Q band (not ILC)

ISW of Local structures and CMB correlation

ISW map

The ΔT(iSW) map can be computed from the density fluctuations given the galaxy biases.

$$\Delta T^{isw}_{\ell m} = 8\pi\kappa(-i)^{\ell} \int dr \frac{\partial}{\partial\tau} \int \frac{d^3k}{(2\pi)^3} Y_{\ell m}(\hat{k}) j_{\ell}(kr) \frac{\delta(k,t)}{k^2 a}$$

$$\simeq 2\kappa(-i)^{\ell} \int dr \left(\frac{r}{\ell}\right)^2 \frac{\partial}{\partial\tau} \left[\frac{\delta_{\ell m}(\tau)}{b(\tau)} \frac{1}{a}\right]$$

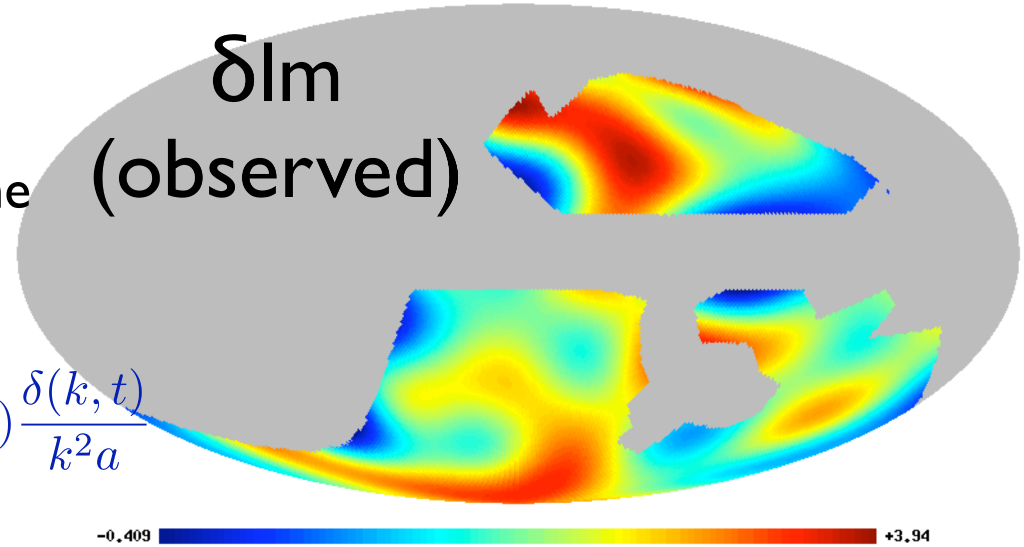

Harmonic inpainting

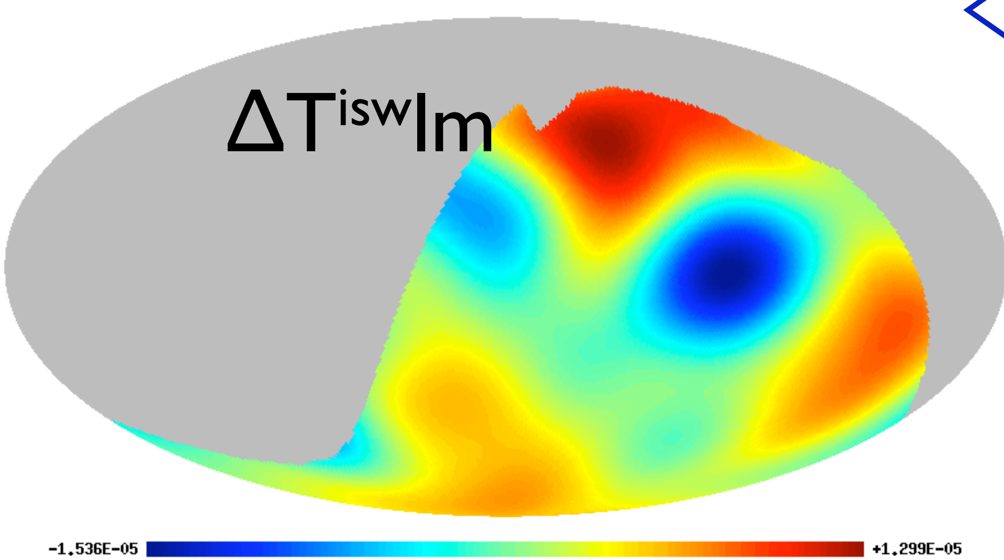

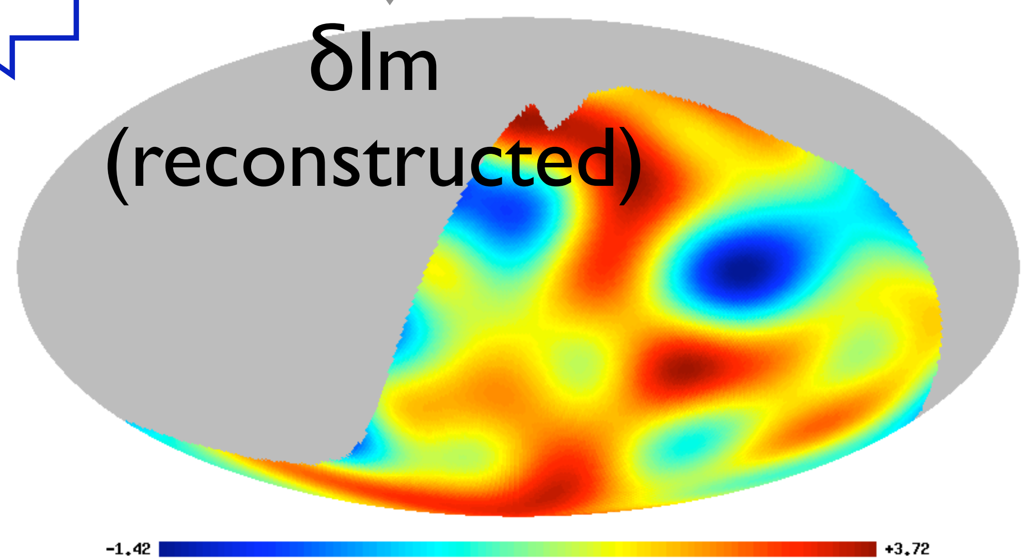

ISW of Local structures and CMB correlation

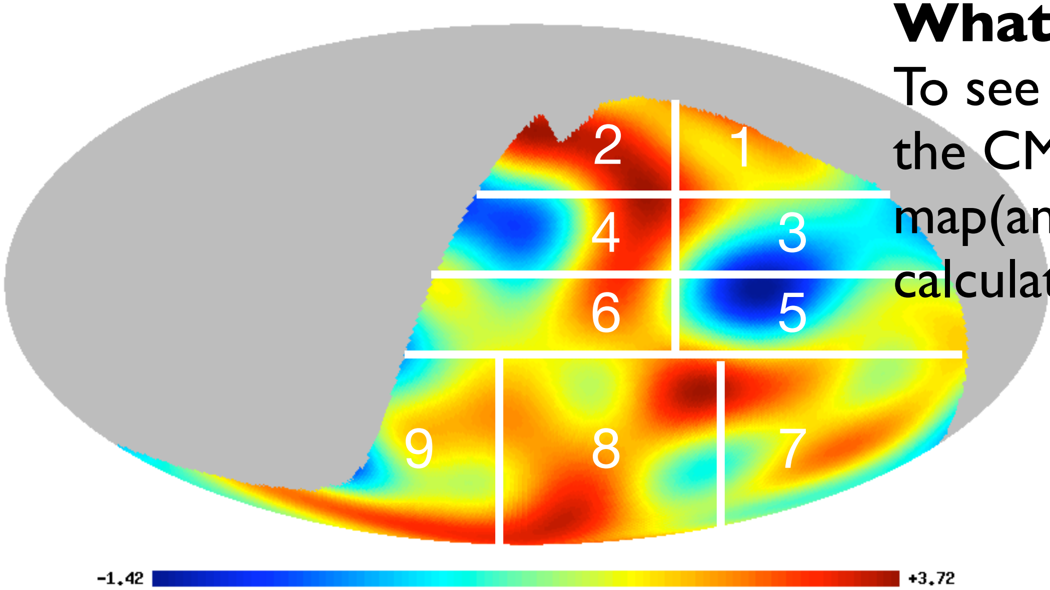

What is the prominent structure?

To see which large scale structures contributes to the CMB correlation, we divide the reconstructed map(and also CMB) and remove one region to calculate cross-correlation power spectrum.

$$C^{g-CMB}/\sqrt{C^{gg}C^{CMB}}$$

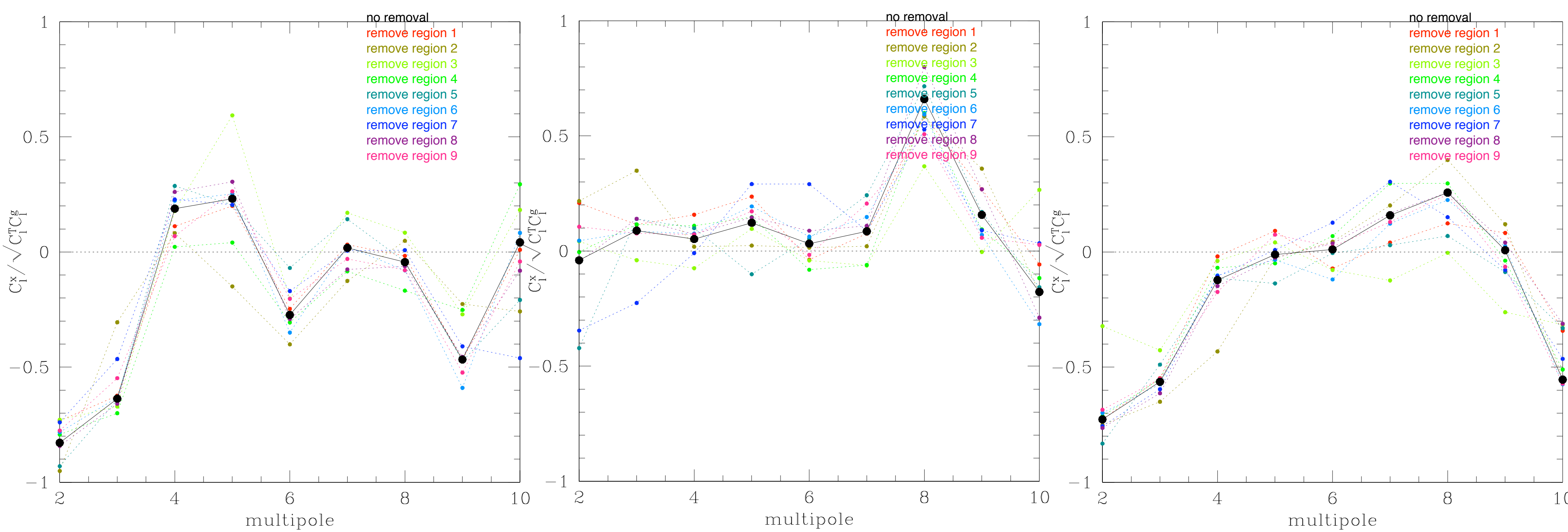

Assisted dark energy

Physical Review D 80, 103513 (2009)

Junko Ohashi and Shinji Tsujikawa , Tokyo University of Science

INTRODUCTION

Cosmological scaling solutions, which give rise to a scalar-field density proportional to a background fluid density during radiation and matter eras, are attractive to alleviate the energy scale problem of dark energy because the solutions enter the scaling regime even if the field energy density is initially comparable to the background fluid density. However the condition required for the existence of scaling solutions is incompatible with the condition for the existence of a late-time accelerated solution. Hence, in the single field case, the scaling solution cannot be followed by the scalar-field dominated solution responsible for dark energy. One of the ways to allow a transition from the scaling regime to the epoch of a late-time cosmic acceleration is to consider multiple scalar fields. We study cosmological dynamics of a multi-field system in details for a general Lagrangian density having scaling solutions.

DYNAMICAL SYSTEM

First action

scalar curvature

background fluid

$$S = \int d^4x \sqrt{-g}\left[\frac{R}{2} + p(X,\phi)\right] + S_f(\phi)$$

Lagrangian density

condition of scaling solution

$$\rho_\phi / \rho_f = \text{const.}$$

$$X = -g^{\mu\nu}\partial_\mu\phi\partial_\nu\phi/2$$

$$p(X,\phi) = X g(X e^{\lambda\phi})$$

arbitrary function

multiple fields

$$p = \sum_{i=1}^{n} X_i g(X_i e^{\lambda_i \phi_i})$$

The multiple fields evolve to give dynamics matching a single-field model with

$$\frac{1}{\lambda_{\rm eff}^2} = \sum_{i=1}^{n} \frac{1}{\lambda_i^2}$$

We shall study the case in which one of the fields has a large slope λ_1 to satisfy the BBN bound and other field join the scalar-field dominated attractor at late times.

(1) Radiation-dominated scaling solution

- Field density parameter

$$\Omega_{\phi_1} = \frac{4p_{,X}}{\lambda_1^2} \lesssim 0.045$$

constraint of BBN

(2) Matter-dominated scaling solution

$$\Omega_\phi = \frac{3p_{,X}}{\lambda_{\rm eff}^2} \Rightarrow \boxed{\lambda_{\rm eff}^2 > 3p_{,X}}$$

is required.

(3) Assisted field-dominated point

- Equation of state

$$w_\phi = -1 + \frac{\lambda_{\rm eff}^2}{3p_{,X}}$$

$$\Rightarrow \lambda_{\rm eff}^2 < 2p_{,X}$$

condition for acceleration

- Stability

$$\boxed{\lambda_{\rm eff}^2 < 3p_{,X}}$$

EXPONENTIAL POTENTIALS

Lagrangian

$$p_i = X_i - c_i e^{-\lambda_i \phi_i}$$

$$g(X_i e^{\lambda_i \phi_i}) = 1 - c_i/(X_i e^{\lambda_i \phi_i})$$

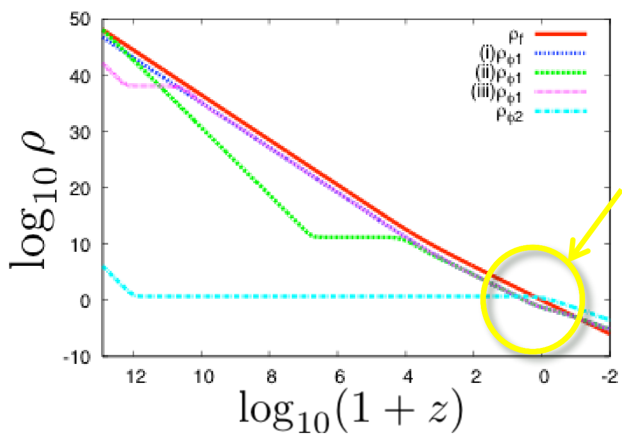

Finally the system enters the assisted field dominated epoch.

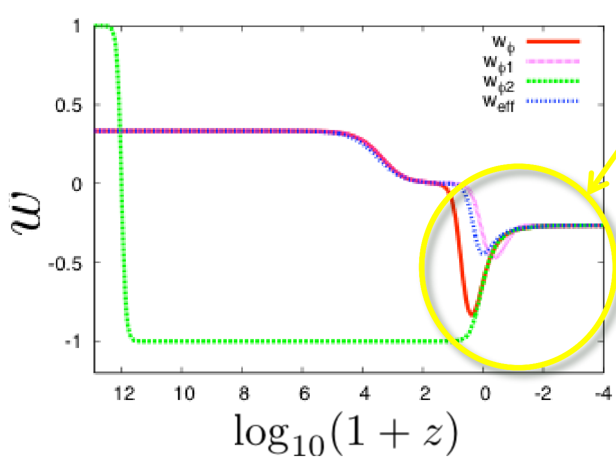

w_ϕ first reaches a minimum and then starts to grow toward the assisted attractor.

DILATONIC GHOST CONDENSATE

Lagrangian

$$p_i = -X_i + c_i e^{\lambda_i \phi_i} X_i^2$$

$$g(X_i e^{\lambda_i \phi_i}) = -1 + c_i (X_i e^{\lambda_i \phi_i})$$

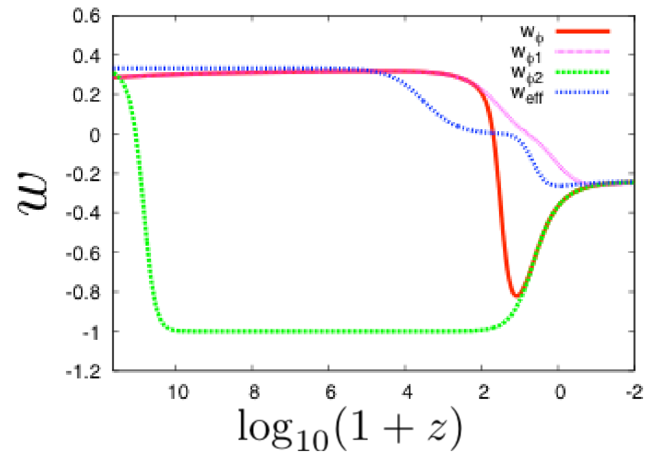

As we add more fields, we obtain smaller values of w_ϕ .

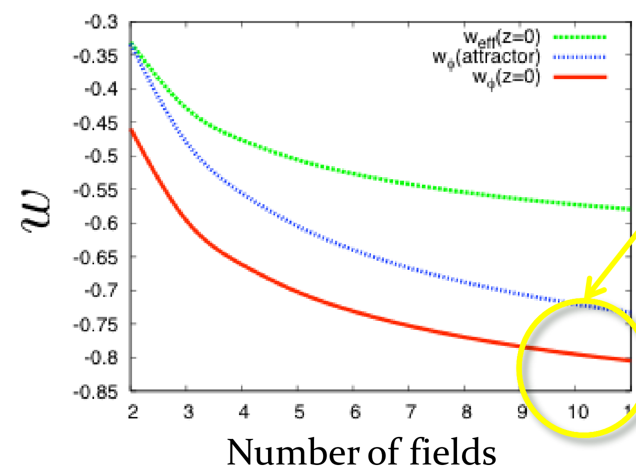

We require at least ten scalar fields to realize the acceleration $w_\phi < -0.8$ $(z=0)$.

CONCLUSION

We have studied cosmological dynamics of assisted dark energy for the Lagrangian density $p = \sum_{i=1}^{n} X_i g(X_i e^{\lambda_i \phi_i})$. In the presence of multiple scalar fields the scaling matter era can be followed by the phase of a late-time cosmic acceleration as long as more than one field join the assisted attractor. Since the effective slope $\lambda_{\rm eff}$ is smaller than the slope λ_i of each field, the presence of multiple scalar fields can give rise to cosmic acceleration even if none is able to do so individually. This is a nice feature from the viewpoint of particle physics because there are in general many scalar fields (dilaton, modulus, etc) with the slopes λ_i larger than the order of unity. For quintessence with exponential potentials and the multi-field dilatonic ghost condensate model, we have shown that a thawing property of assisting multiple scalar fields allows the field equation of state w_ϕ smaller than -0.8 today.

References

[1] F. Piazza and S. Tsujikawa, JCAP 0407, 004 (2004).
[2] S. Tsujikawa and M. Sami, Phys. Lett. B 603, 113 (2004).
[3] A. R. Liddle, A. Mazumdar and F. E. Schunck, Phys. Rev. D 58, 061301 (1998).
[4] S. A. Kim, A. R. Liddle and S. Tsujikawa, Phys. Rev. D 72, 043506 (2005).
[5] S. Tsujikawa, Phys. Rev. D 73, 103504 (2006).
[6] J. Ohashi and S. Tsujikawa, Phys. Rev. D 80, 103513 (2009).

Magnification effect on the galaxy-galaxy Power Spectrum and a primordial non-Gaussianity

Tomohiro OKAMURA (Tohoku Univ.)
in collaboration with T. Namikawa (Tokyo Univ.)
T. Futamase (Tohoku Univ.)

Usually, I work on weak lensing analysis using Subaru S-cam data. If you are interested in it, please talk to me !!

10th RESCEU/DENET Summer School: Dark Energy in the Universe @ Kochi Palace Hotel , 29-31/Aug, 1/Sep, 2010

Motivation

- In the presence of primordial non-Gaussianity (NG), the halo bias has an additional scale dependent term (Dalal+08, Matarrese+08) :

$$\Delta b(k) = \frac{3(b_0 - 1) f_{\rm NL} \Omega_m H_0^2 \delta_c}{D(z) k^2 T(k)}$$

- To constrain NG, we need the large scale power spectrum ($\because \Delta b \propto 1/k^2$) .
  → Prefer large-sky coverage and high-z samples (individual z information is not important).
  ex. NVSS (Xia+ 2010)

- Such magnitude limited survey, magnification effects change the galaxy number count (Matsubara 00, LoVerde+08, Hui+08A, Hui+08B) :

$$\delta_n = \delta_g + \delta_\mu = \delta_g + (5s - 2)\kappa$$

where "*s*" characterizes the slope of the number count function ($s \sim O(1)$).

✓ Q1. Comparing scale dependent bias, how much magnification effects change the galaxy-galaxy Power Spectrum ?

✓ Q2. How much magnification effects affect the estimation of primordial NG ?

※ Future large galaxy survey can constraint $\sigma(f_{NL}) \sim 1$ (Carbone+08).

A1. Power Spectra

We assume s=1.2, b_0=2.3.

Gal dis. $$W(z) = \frac{1}{\sqrt{2\pi}\sigma} \exp\left[-\frac{(z-z_0)^2}{\sigma^2}\right]$$

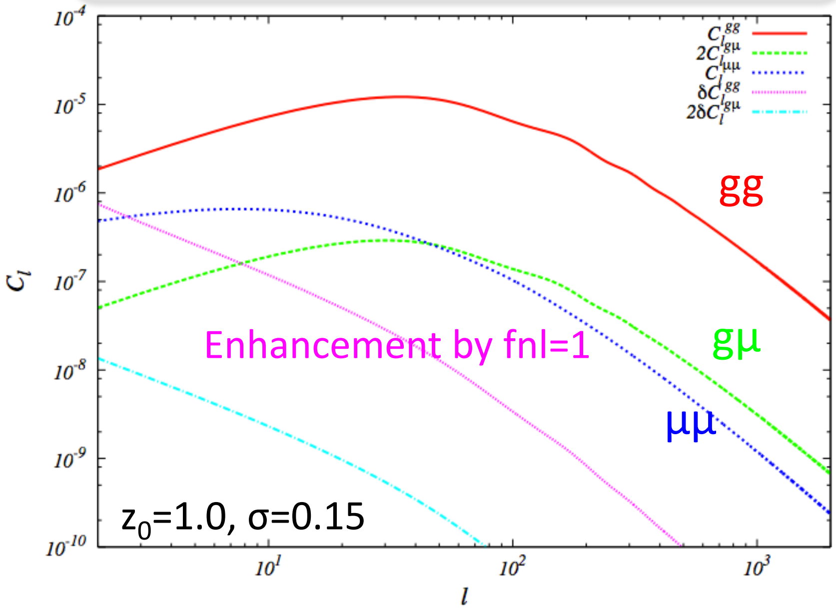

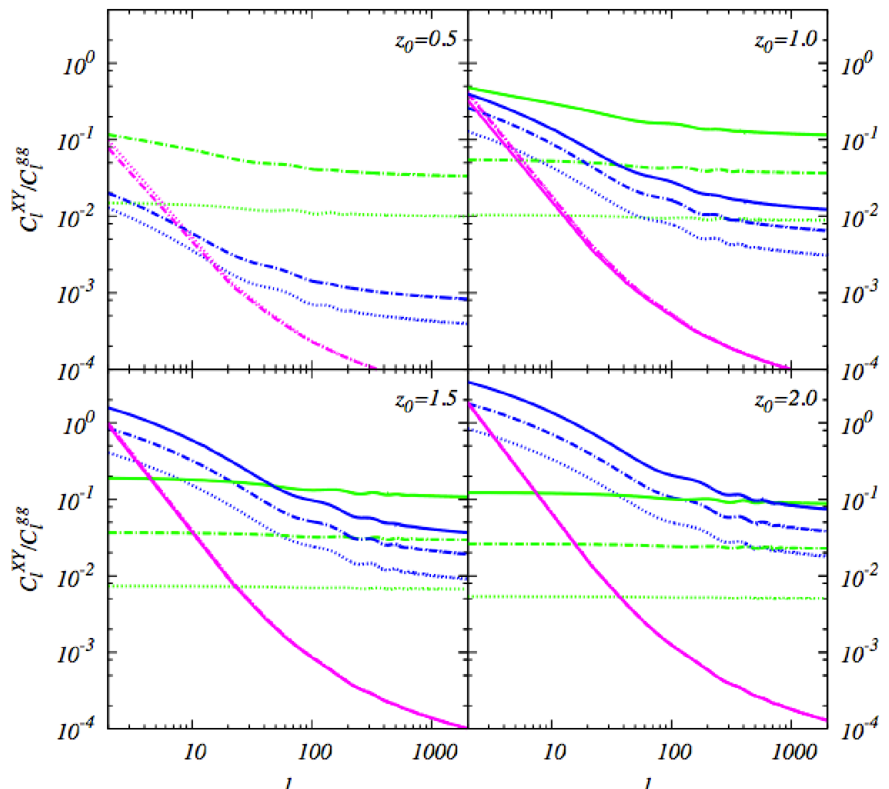

- μμ has a large scale power comparably to scale dependent bias.
- gμ looks like gg except an amplitude.

- Broad sample is highly affected by both gμ and μμ.
- High-z sample is highly affected by μμ.

We cannot neglect magnification effects in the estimation of NG especially deep & broad survey.

A2. bias & constraint

<Bias> Magnification effects change the model power spectrum and we get the wrong NG, Δf_{NL}.

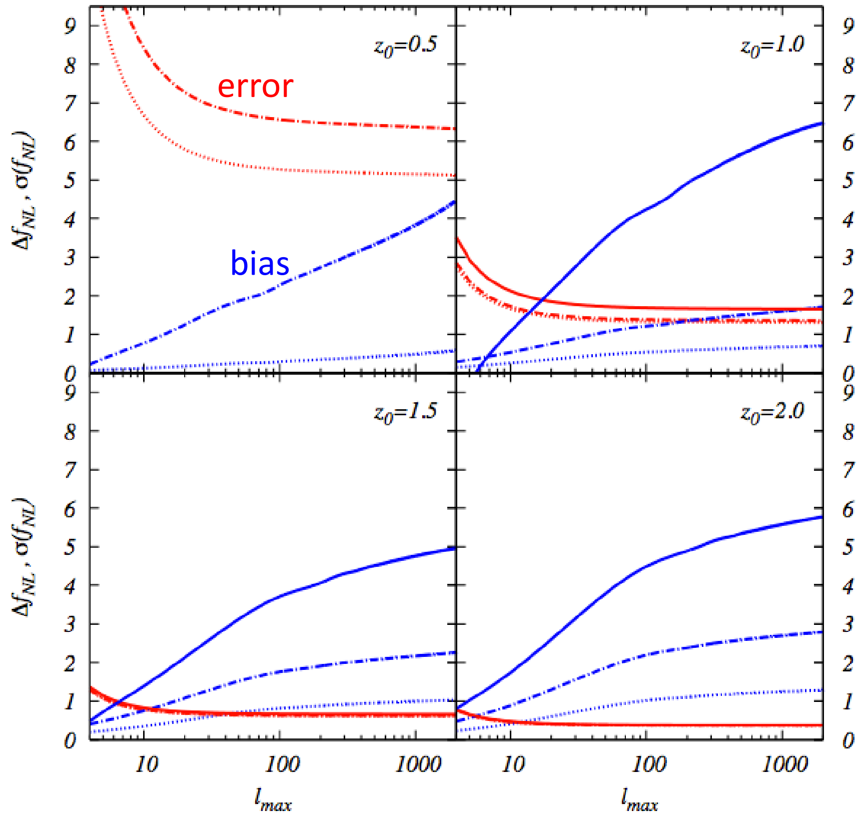

<Error> Magnification effects add to nuisance power and shade off f_{NL}'s characteristic.

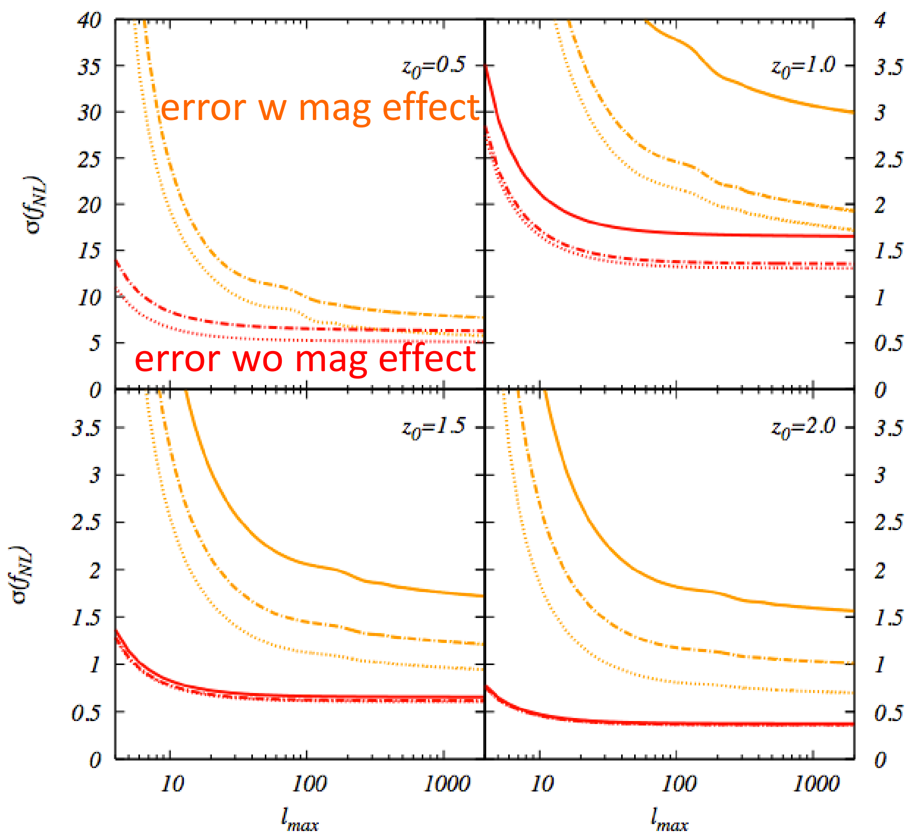

※ CV limited, f_{sky}=1

Magnification effects distort the estimation of f_{NL} more than 1 sigma error, and make the constraint on NG, $\sigma(f_{NL})$, weaker up to 3 times.

Copula Cosmology based on Sato, Ichiki, Takeuchi, submitted

Masanori Sato with Kiyotomo Ichiki, Tsutomu T. Takeuchi (Nagoya U., Japan)

RESCEU/DENET summer school, 29, August, 2010

Motivation

- Sato et al.(2009) find that the probability distribution function of weak lensing power spectrum is well approximated by the chi-square distribution.
- The chi-square distribution deviates from Gaussian distribution on large scales because number of modes corresponding to degrees of freedom are very small.
- We have to include these informations accurately when we constrain the cosmological parameters.

For cosmological parameter estimation, almost all authors use chi-square method in weak lensing analysis (e.g. Hamana et al.2003, Fu et al.2008, Semboloni et al.2010).

see, below fig!

The copula helps to solve this problem!

Is all distribution really Gaussian ?

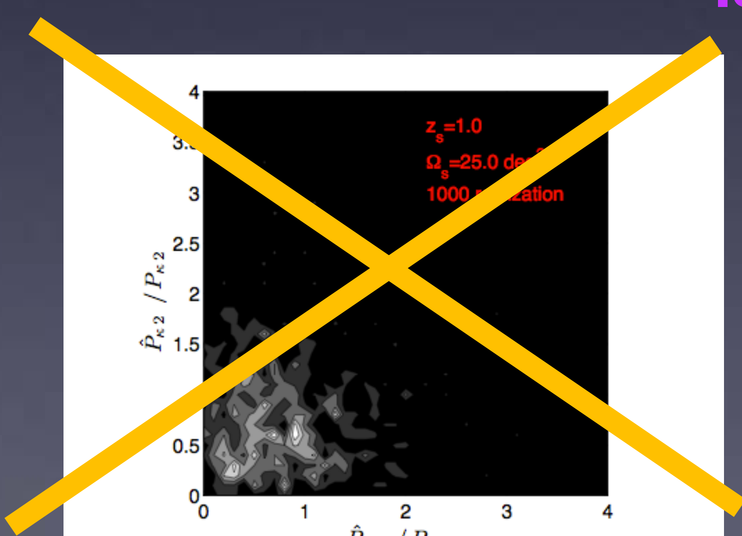

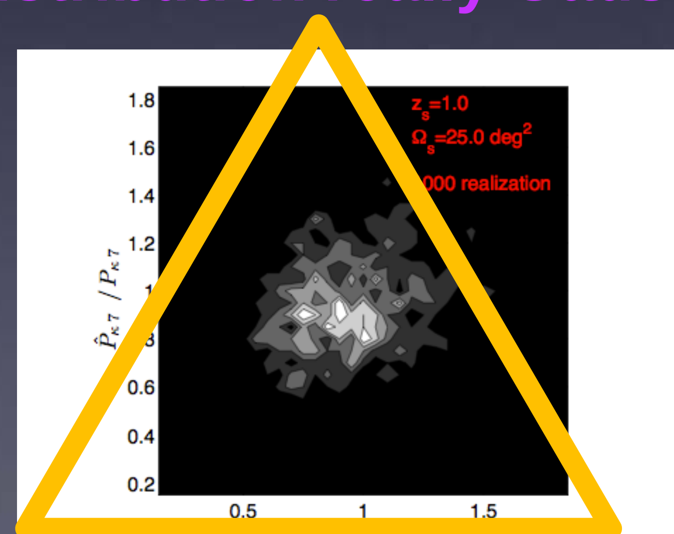

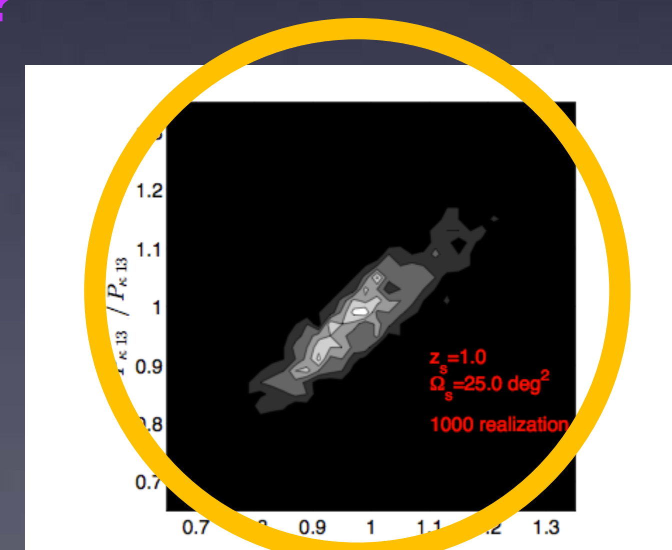

The two-dimensional probability distribution of convergence power spectrum is calculated from Sato et al.2009 simulations.

linear regime

quasi-linear regime

non-linear regime

What is a copula?

$$\mathrm{P}_{\mathrm{prob}}(x_1 \le \hat{x}_1, x_2 \le \hat{x}_2, \ldots, x_n \le \hat{x}_n) \equiv F(\hat{x}_1, \hat{x}_2, \ldots, \hat{x}_n) = \underbrace{C}_{\text{Copula}}(F_1(\hat{x}_1), F_2(\hat{x}_2), \ldots, F_n(\hat{x}_n))$$

$$F(\hat{x}_1, \hat{x}_2, \ldots, \hat{x}_n) = \int_{-\infty}^{\hat{x}_1} \int_{-\infty}^{\hat{x}_2} \cdots \int_{-\infty}^{\hat{x}_n} f(x_1, x_2, \ldots, x_n) \mathrm{d}x_1 \mathrm{d}x_2 \ldots \mathrm{d}x_n$$

$F(\hat{x}_1, \hat{x}_2, \ldots, \hat{x}_n)$ is n-point cumulative distribution function. $F_i(\hat{x}_i)$ is one-point cumulative distribution function.

Copulas are functions that join or couple multivariate distribution functions to their one-dimensional marginal distribution functions.

The copula has been used in the field of mathematical finance, although there is only one application to cosmology (Scherrer et al.2010)

Constructing a likelihood function using Gaussian copula

$$C(u_1, u_2, \ldots, u_n) \equiv \Phi\left(\Phi_1^{-1}(u_1), \Phi_1^{-1}(u_2), \ldots, \Phi_1^{-1}(u_n)\right)$$

Gaussian copula

$$\Phi(\hat{x}_1, \hat{x}_2, \ldots, \hat{x}_n) = \int_{-\infty}^{\hat{x}_1} \int_{-\infty}^{\hat{x}_2} \cdots \int_{-\infty}^{\hat{x}_n} \frac{1}{\sqrt{(2\pi)^n \det(\mathrm{Cov})}} \exp\left(-\frac{1}{2}(\boldsymbol{x} - \boldsymbol{\mu})^{\mathrm{T}} \mathrm{Cov}^{-1} (\boldsymbol{x} - \boldsymbol{\mu})\right) \mathrm{d}x_1 \mathrm{d}x_2 \ldots \mathrm{d}x_n,$$

$\Phi(\hat{x}_1, \hat{x}_2, \ldots, \hat{x}_n)$ is n-point cumulative Gaussian distribution function

$\Phi_1(\hat{x}_1)$ is one-point cumulative Gaussian distribution function

$u_i(\hat{x}_i)$ is one-point cumulative general distribution function

The likelihood function based on Gaussian copula model is (see Sato et al. submitted for details of derivation)

$$-2\ln \mathcal{L}(\hat{x}_1, \hat{x}_2, \ldots, \hat{x}_n) = \sum_{i=1}^{n} \sum_{j=1}^{n} (q_i - \mu_i) \mathrm{Cov}^{-1} (q_j - \mu_j) - \sum_{i=1}^{n} \frac{(q_i - \mu_i)^2}{\sigma_i^2} - 2 \sum_{i=1}^{n} \ln f_i(\hat{x}_i)$$

$$q_i = \sigma_i \Psi_1^{-1}(u_i) + \mu_i$$

we abbreviate constant term.

where Ψ_1^{-1} is the cumulative standard normal distribution

Results: Two-dimensional marginalized constraints on estimated convergence power spectrum.

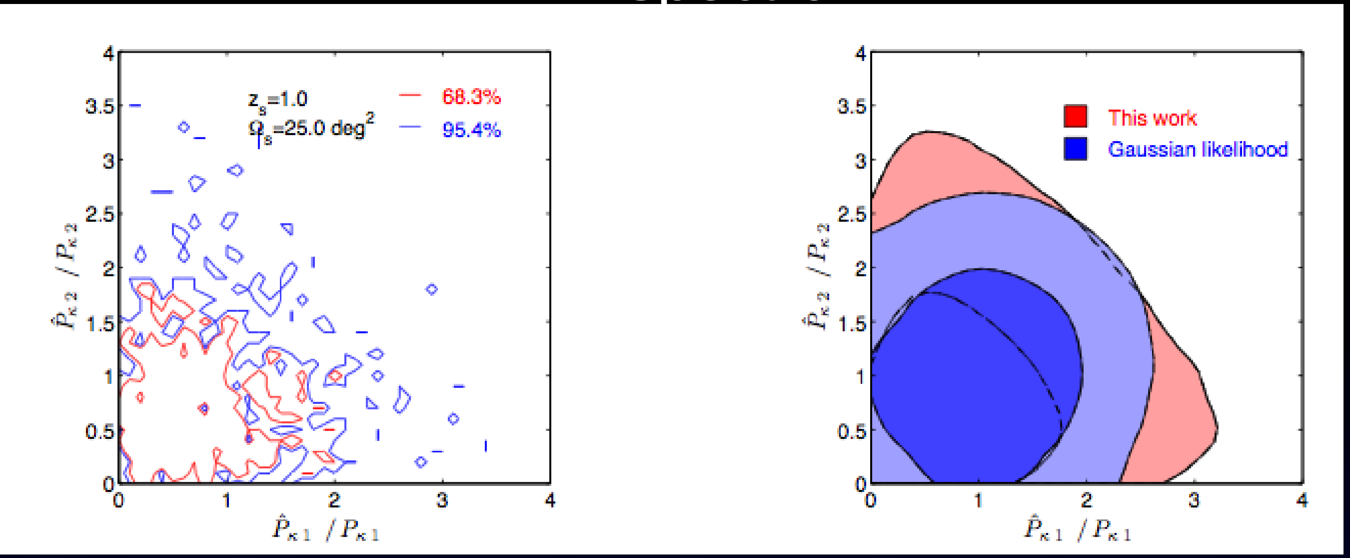

bin1 and bin2

Left panel: Two-dimensional joint PDF from ray-tracing simulations

Right panel: Two-dimensional marginalized constraints on convergence power spectrum

The one-point PDF is normalized so that mean convergence power spectrum estimated at each bin gives unity.
The bin1 and bin2 correspond to multipole l=72 and l=97.
We can see that our likelihood based on Gaussian copula is more plausible than Gaussian likelihood for cosmic shear power spectrum.

Especially, results of our likelihood function capture the feature of maximum probability deviates from each mean value.

bin6 and bin7

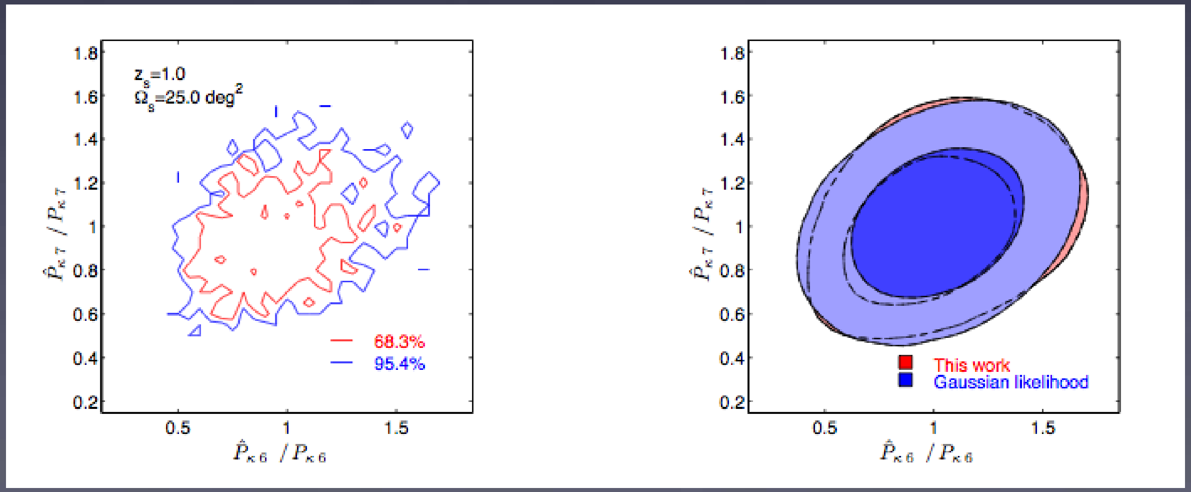

bin12 and bin13

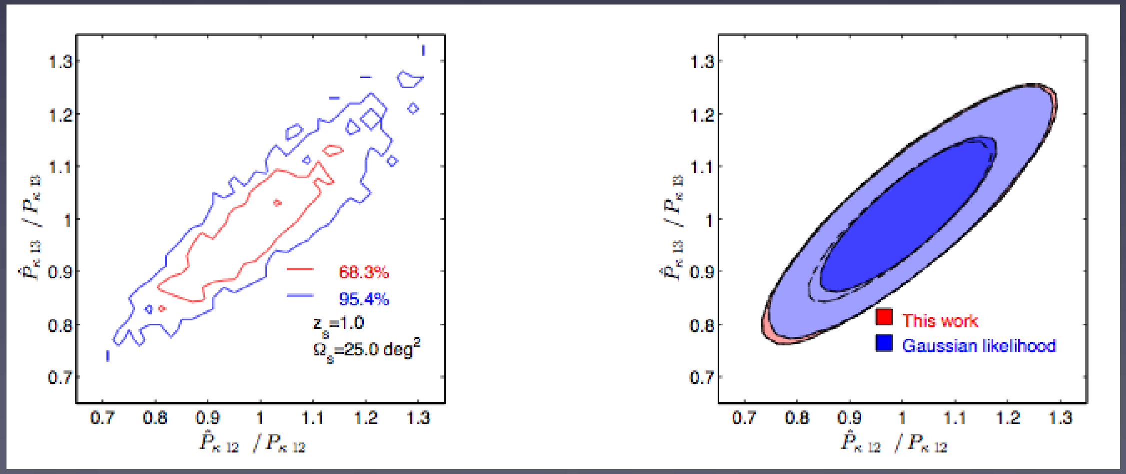

The bin6 and bin7 correspond to multipole l=323 and l=436.

The bin12 and bin13 correspond to multipole l=1952 and l=2635.

Results: Impact on Cosmological parameter estimation

For simplicity, we work with two cosmological parameter

$$\boldsymbol{p} = (\Omega_{\rm dm}, \ln 10^{10}\Delta_{\rm R}^2)$$

Two-dimensional marginalized constraints on Ωm and σ8

weak lensing only

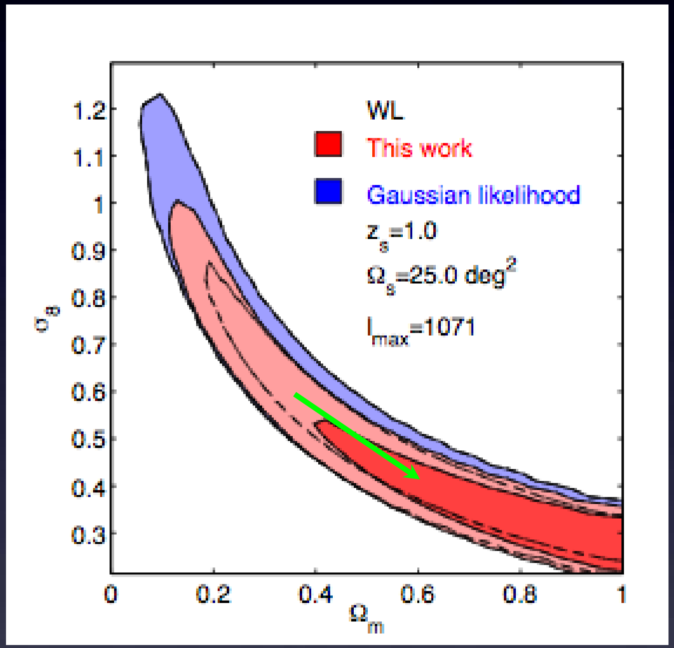

direction to decrease the power

When we estimate the equation of state parameter w, combined with another probe of WMAP 3yr, we work with three cosmological parameter

$$\boldsymbol{p} = (\Omega_{\rm dm}, w, \ln 10^{10}\Delta_{\rm R}^2)$$

Two-dimensional marginalized constraints on Ωm and w

weak lensing + WMAP3

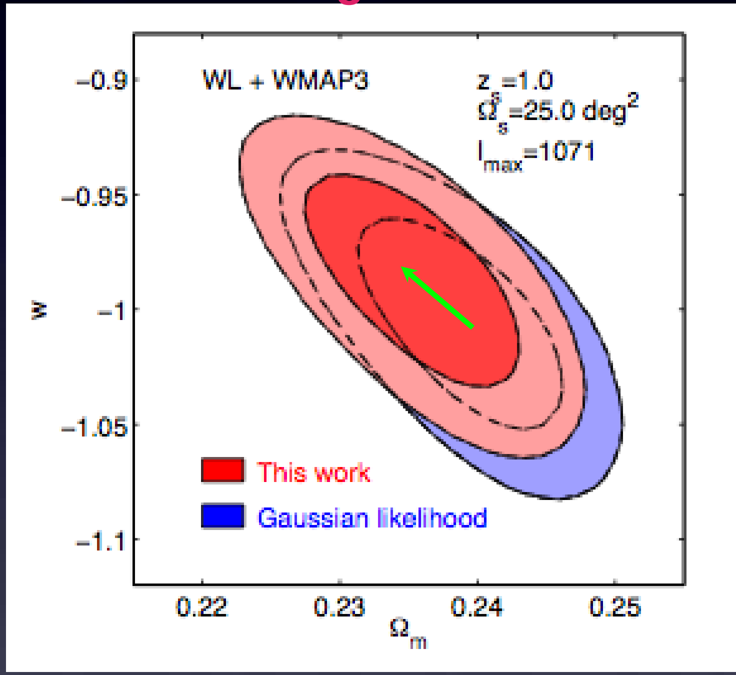

The contours obtained with our likelihood is shifted toward a parameter region that gives a lower convergence power compared to that from the Gaussian likelihood.
The result is attributed to the fact that median of chi-square distribution for the convergence power spectrum is smaller than that of the Gaussian distribution.

We found that for the 25 deg2 weak lensing survey, the results can be different even combined with CMB data, depending on which likelihood functions is used. The difference is as large as a few percent.
Thus, the copula likelihood should be used in the future cosmological observations.

Relativistic astrophysics with resonant multiple inspiral

-Evolution and final fate of a "trojan compact object" around a massive BH binary-

Naoki Seto and Takayuki Muto (Kyoto University) arxiv1005.3114

1 Introduction

MBHs: important target for LISA

MBH+MBH

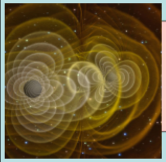

high SNR
Dark energy study
...

A combination must be interesting
our target here

EMRI

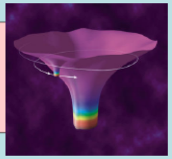

precision mapping of BH
complicated waveform

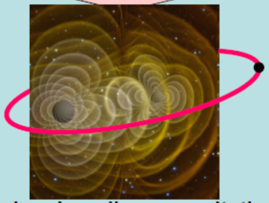

We might study a dynamical and nonlinear gravitational field with a test particle!!

Can this triple system really exist?

our scenario

- MBH binary: resonantly traps a third body
  - e.g. interaction with circumbinary disk?
- orbital decay by GW radiation
- evolve into relativistic regime
- observe with LISA

(last three: in this poster)

simplify the problem

circular restricted three body(m_3=0)
1:1 resonance (trojan type)
post-Newton for point particles

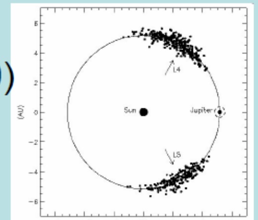

Trojans of Jupiter

see also Schnittman arXiv:1006.0182

2 Stability of the third body

linear analysis without GWR

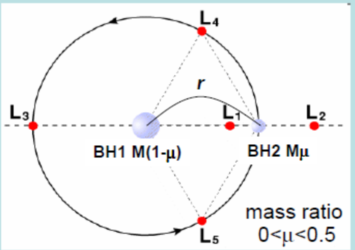

parameters for the parent binary

masses: BH1, M(1-μ), BH2: Mμ

orbital separation: *r*

eccentricity *e=0*

→ five equilibrium points; $L_{1\text{-}5}$

Newtonian analysis (known from 1800s)

solve characteristic eqs. for perturbative motions around the points

The third body around
- $L_{1,2,3}$ are unstable.
- **$L_{4,5}$ are stable for the mass ratio**

$$\mu < \frac{1}{2} - \frac{\sqrt{69}}{18} = 0.0385$$

The perturbative motion can be decomposed into two modes; *e*: epicyclic, *l*: libration

their frequencies

$$\omega_e(\mu) > \omega_l(\mu) \qquad (\omega_e(\mu) = \omega_l(\mu)\ \ for\ \mu = 0.0385)$$

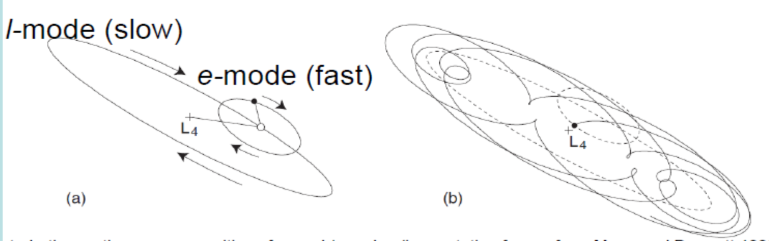

perturbative motion: a superposition of *e*- and *l*- modes (in corotating frame, from Murry and Dermott 1999)

1PN analysis (e.g. Maindl & Hagel 1996)

The two frequencies get dependence on *r*

$$\omega_e(\mu,r),\ \omega_l(\mu,r)$$

The stability condition is modified as

$$\mu < 0.0385 - 0.291M / r$$

Now depends on the separation *r* of the parent binary
→ interesting effects

3 Numerical Method

1PN evolution with GWR (now dissipative)

①use Einstein-Infeld-Hoffman form for 1PN EoM
②dr/dt (for parent binary) by quad. formula
③evolution of the parent given almost analytically
④solve the third body around parent binary

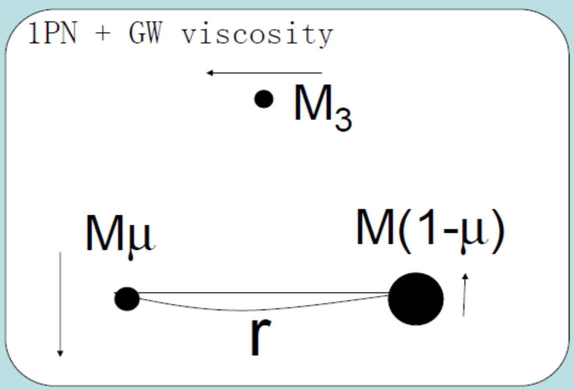

Even for M_3→0, the third body has a finite dissipative acceleration due to an interference effect of waves!!
e.g. Landau & Lifshitz

4 Quasi Stationary Phase

intermediate stages of our numerical study

Evolution around L_5 in the normalized (r=1) corotating frame

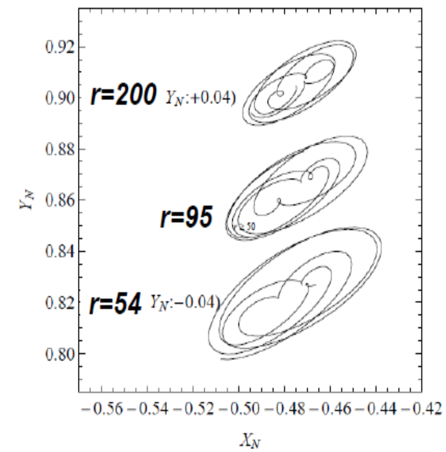

FIG. 1: Evolution of the orbit of a test particle around the L_5 point in the normalized corotating frame (X_N, Y_N). The mass ratio of the parent binary is $\mu = 0.027$. We show the orbits at three different separations $r_b = 200$, 95 and 54. Each figure is given for ~ 8 rotation cycles of the parent binary. The initial conditions are $q_x = 0.002$, $q_z = 0.001$ at $r_b = 200$. The upper and bottom figures are shifted toward the vertical direction by ± 0.004.

What we found

The amplitude of the perturbation grows mildly.
In the normalized frame and at *r*>50, roughly scales as $r^{-1/4}$
(similar to evolution of Trojans, see Fleming & Hamilton 2000)

5 Instability

Evolve further and become unstable

The binary separation *r* where the third body becomes unstable

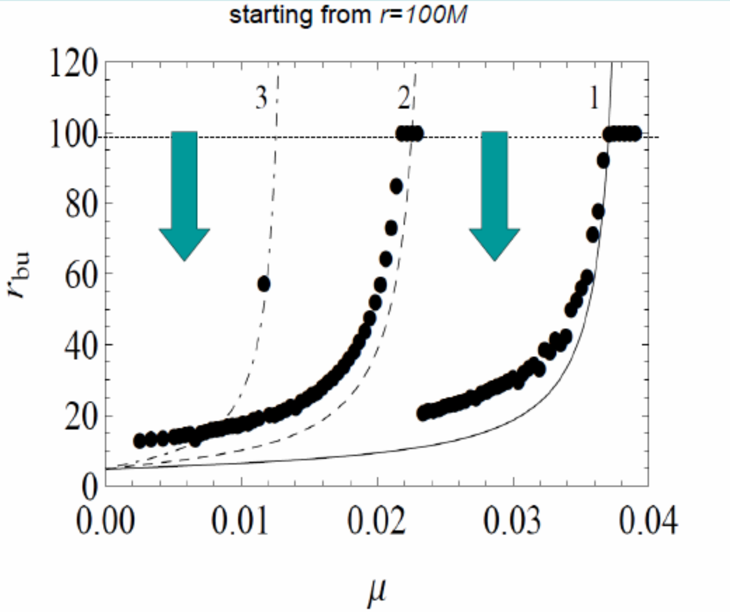

FIG. 2: The unstable separation r_{bu} of a parent binary as a function of its mass ratio μ. The points are given from the evolution of the test particle initially placed around the L_5 point at $r_b = 100$. The solid curve is derived from the stability condition $\omega_L = \omega_E$ at 1PN and has the asymptotic profile $r_{bu} \to \infty$ at $\mu = 0.038521$. The dashed and dot dashed curves are given for $\omega_E = 2\omega_L$ and $\omega_E = 3\omega_L$ with the critical mass ratios $\mu = 0.024293$ and $\mu = 0.013516$. respectively.

We define the ratio $R = \omega_e(\mu,r)/\omega_l(\mu,r)$
The simple stability condition in Sec.2 was $R>1$

We have two new branches at R=2 and 3!!

These are the resonant couplings of *e*- and *l*-modes (e.g. Deprit et al. 1967 for Newtonian analysis)

How does this happen?

With 1PN, the ratio *R* depends on *r*.
R can go through the resonantly unstable condition *R*=*n* (*n*=2,3…)!!

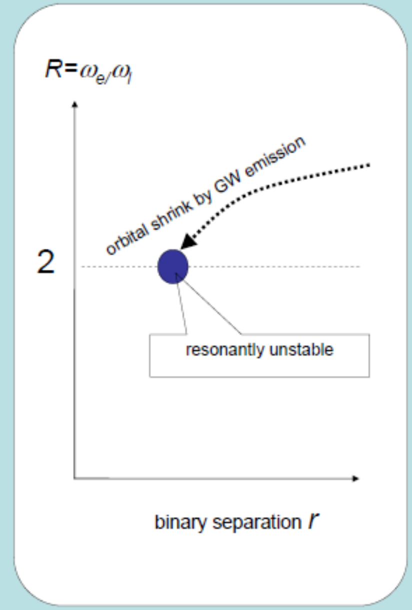

GR enhances resonance instability

6 Final fate of the third body

After the instability, three possible fates

1) plunge into BHs

If the third body is a WD, it might be tidally disrupted.
We might determine the host galaxy with EMW obs.!
→helps dark energy study

2) scattered as a hyper-velocity star

The escape velocity can be more than 0.2c

3) formation of an EMRI

If decoupled from the parent binary

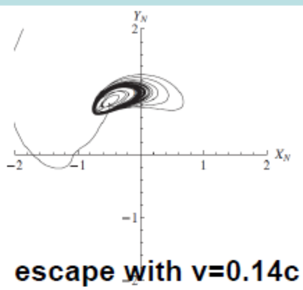

escape with v=0.14c

FIG. 3. Ejection of a test particle around the binary separation $r_b = 24.6$ after $N \sim 1.1 \times 10^5$ cycles from $r_b = 200$. The ejection velocity is $\sim 0.14c$. The initial conditions are the same as Fig. 1. The larger BH is at (0.027,0,0) and the smaller one is at $(-0.973, 0, 0)$. They rotate counterclockwise.

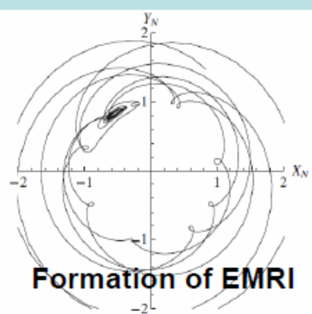

Formation of EMRI

FIG. 4. Dynamical formation of an EMRI system around $r_b = 13.0$ with $\mu = 0.0025$. The initial positions are $q_x = 0.004$ and $q_z = 0.08$ at $r_b = 77$ (9.9×10^4 cycles to $r_b = 13.0$).

7 Implications for LISA

- From the strong parent binary signal, we can determine their parameters M, μ,…
- the epoch of the instability predictable!
- This prior information helps us to search for a weak GW signal by the third body
- Interaction with the smaller (second) BH might be detectable with LIGO
- With EMRI, we can accurately estimate the parameters of the merged BH

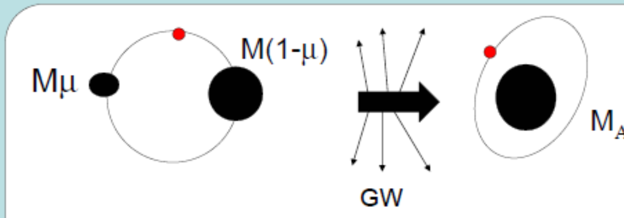

check energy budget with EMRI!
$M > M_A$

additional works in progress
e=0, m_3=0, 2PN, 1:2 etc …

The persistent filamentary structure of the universe

T. Sousbie

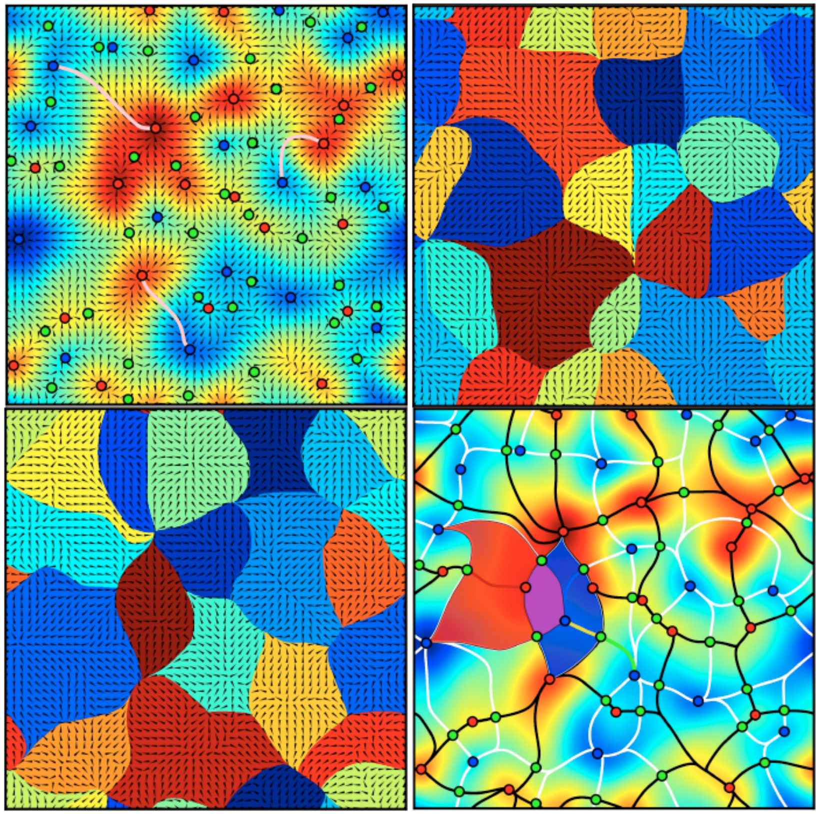

Figure 2. A 2D density field with its gradient (top left), its descending 2-manifolds (top right), its ascending 2-manifolds (bottom left), and its Morse-Smale complex (bottom right, see the black and white network). The maxima/saddle points/minima are represented as red/green/blue circled disks respectively and three integral lines are drawn in pink on the top left frame. On the central left part of the bottom right frame, an arc (*i.e.* a 1-cell) is represented in yellow (intersection of a green ascending 1-manifold and a blue descending 2-manifold) and a quad (*i.e.* a 2-cell) in purple (intersection of a red descending 2-manifold and a blue ascending 2-manifold).

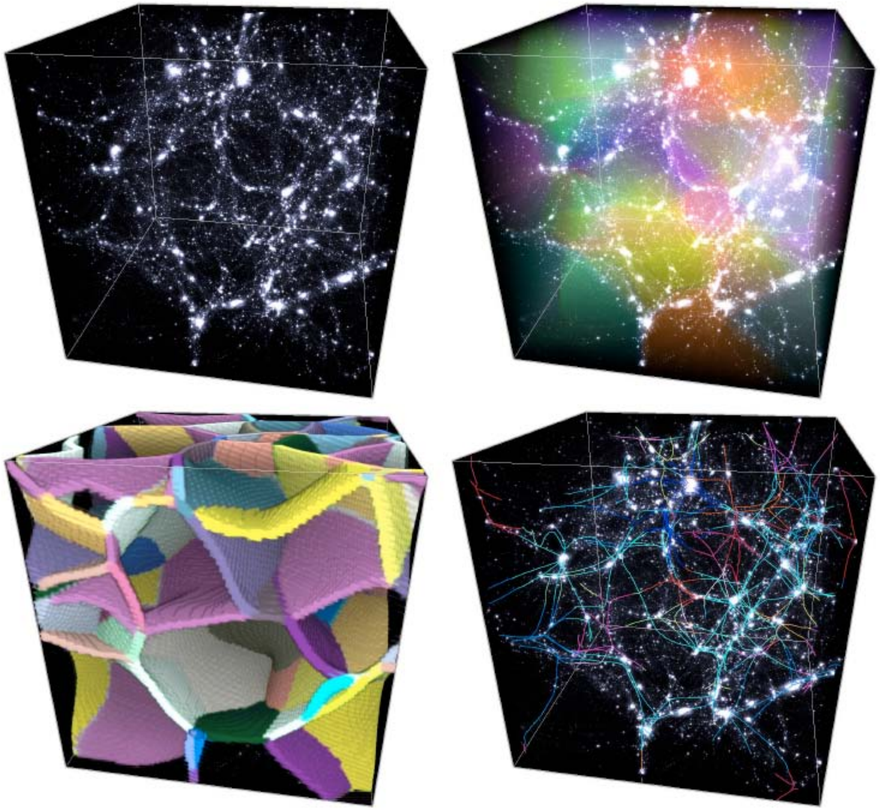

Figure 1. The dark matter density distribution in a $50\,h^{-1}$ Mpc large cosmological simulation (top left frame), with its ascending 3-manifolds (*i.e.* the voids, top right frame), ascending 2-manifolds (*i.e.* the walls, bottom left frame) and ascending 1-manifolds (*i.e.* the filaments, bottom right frame). The manifolds were computed using the method introduced in Sousbie et al. (2009).

Persistence

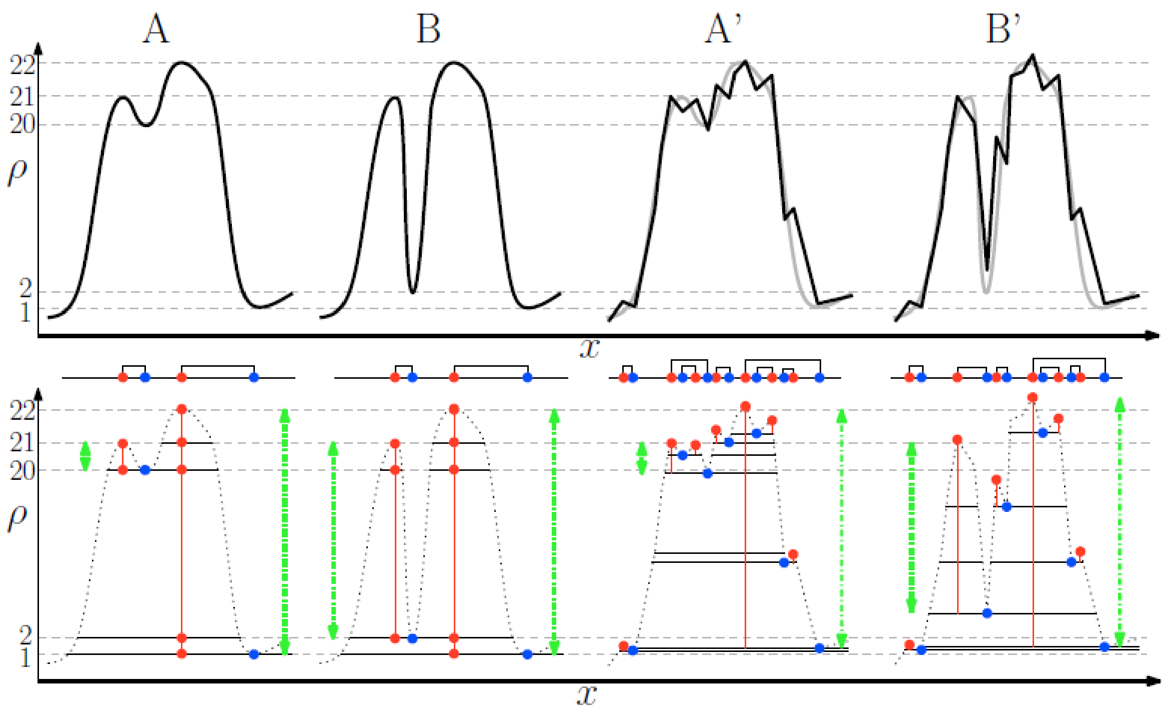

Figure 5. Illustration of the concept of persistence over a 1D functions. The upper panel shows two functions (left) and their discretely sampled counterparts, with noise added (right). The lower panel displays the evolution of sublevel-sets of these functions at the level of different critical points. The green dash-dotted vertical arrows emphasize the lifetime of components in the sublevel-sets, the persistence pairs are displayed in the central part over the function's Morse-Smale complex.

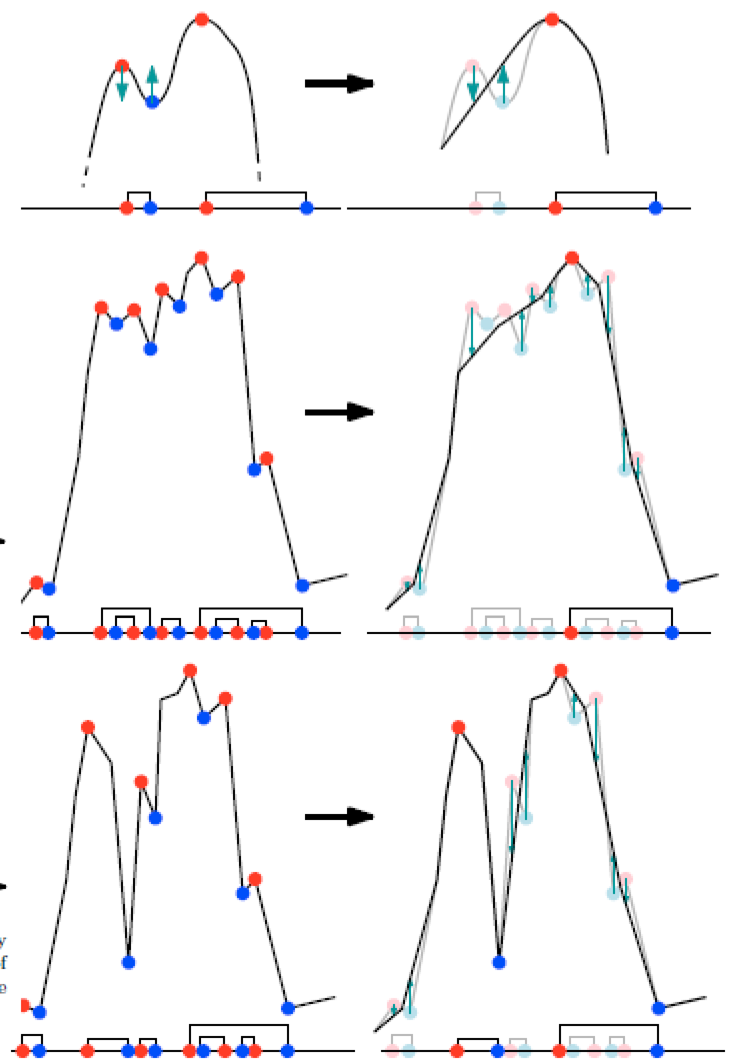

Figure 6. Illustration of the topological simplification process applied to functions A, A' and B' defined on figure 5 (see top, central and bottom panel). The diagram under each function represents its Morse-Smale complex and persistence pairs.

Topological simplification

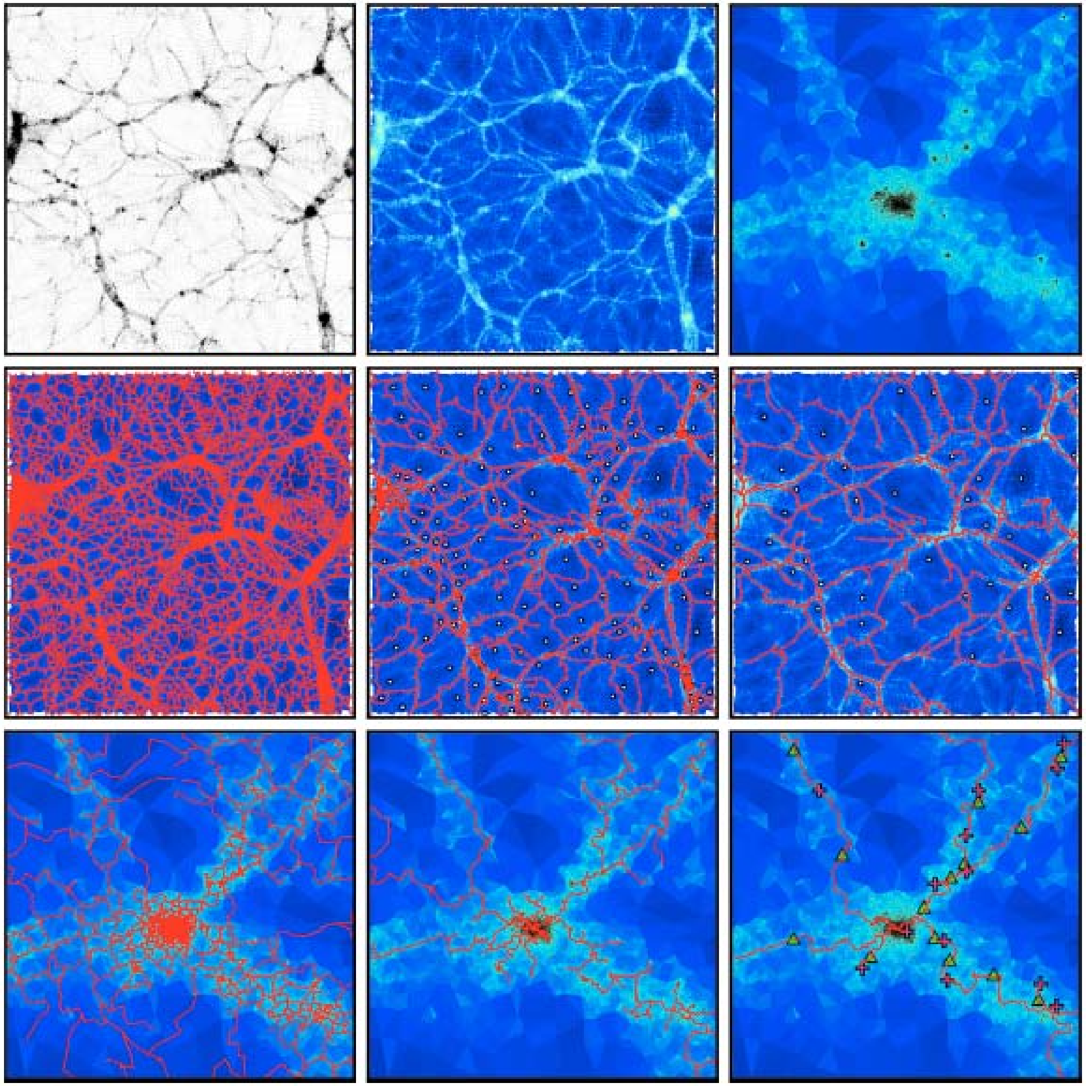

Figure 13. The filaments measured in a 2D distribution obtained by projecting the particles from a slice of an N-Body cosmological simulation. The initial discrete distribution, its Delaunay tesselation and a zoom on a Halo (from the upper central part of the distribution) are displayed on the top raw, with colour corresponding to the DTFE density. The filamentary structure is traced in red on the middle raw, as the geometry of the arcs remaining after cancellation of persistence pairs with significance less than $0-\sigma$ (middle left), $2-\sigma$ (center) and $4-\sigma$ (middle right). A zoom around a projected Halo is shown on the bottom raw. The white disks, green triangles and purple crosses stand for the minima, saddle-points and maxima respectively (notes that they only represented on some panels for clarity reasons).

The SDSS DR7

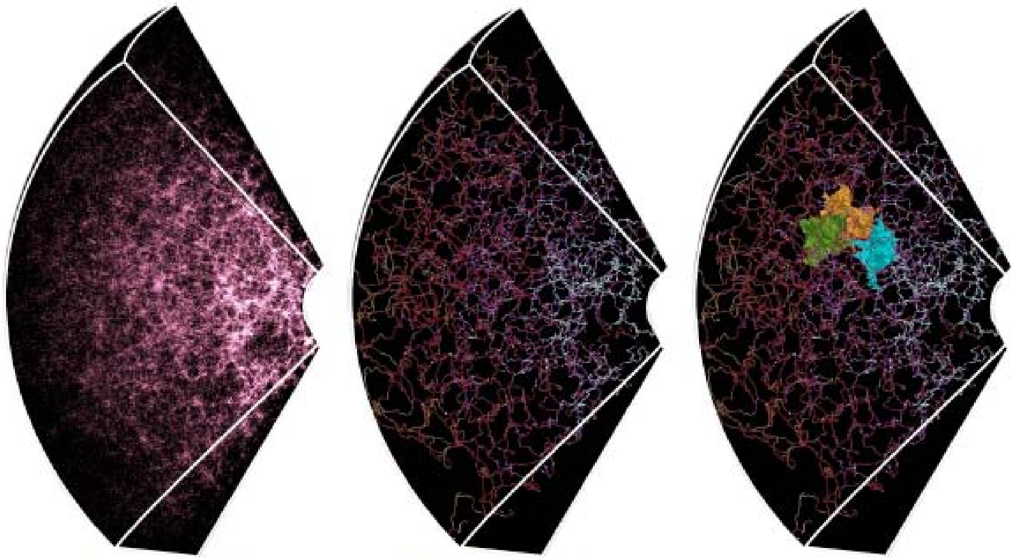

(a) A portion of SDSS DR7 (b) The filamentary structure (c) Three voids

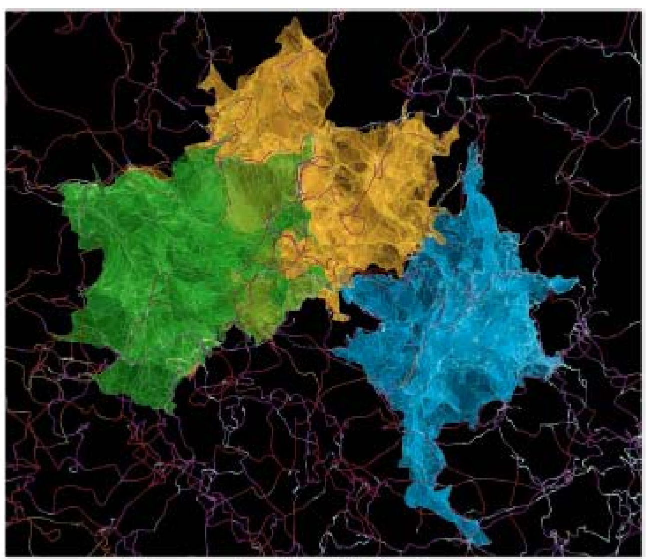

(d) A zoom on the voids and the filamentary structure

Figure 26. The detected filamentary structure at a significance level of $5-\sigma$ and three voids within a portion of SDSS DR7. Note that only the upper half of the distribution shown on figure 23 is displayed here for clarity reasons. The color of the filaments corresponds the the logarithm of the density field.

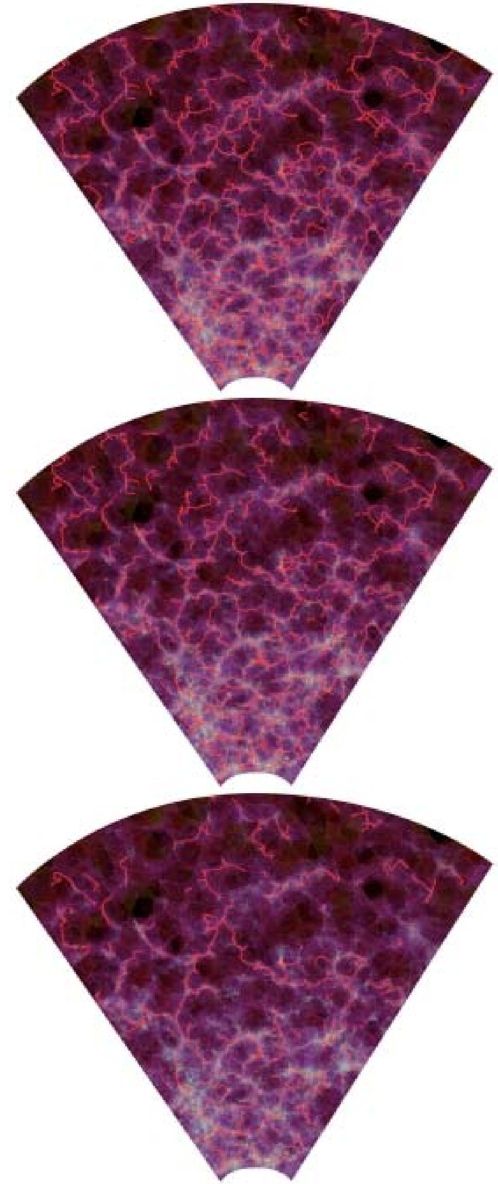

Figure 25. From top to bottom, the filamentary structure in a $\sim 40\,h^{-1}$ Mpc thick slice of the SDSS Dr7 galaxy catalog at a significance level of 3, 4 and $5-\sigma$ respectively. The distribution is represented by the non bounding subset (see main text) of the Delaunay tesselation used to compute the DMC, shaded according to the logarithm of the density. The depth of a filament can be judged by how dimmed its shade is. Note that filaments that seem to stop for no apparent reason actually enter or leave the slice.

Non-linear curvature perturbation for general multi fields beyond δN *formalism*

東北大学D1杉山尚徳

First we make clear what is the curvature perturbation. We define it as the conserved quantity at super-horizon scale if the fluid dominants universe and satisfies the adiabatic condition : $p = p[\rho]$. It is defined very generally as follow,

$$\zeta \equiv \psi + \frac{1}{3}\int_{\bar{\rho}(t)}^{\rho(x,t)} \frac{d\rho}{\rho + p[\rho]}$$

Or the metric perturbation under uniform density gauge, $\rho(x.t) = \bar{\rho}(t)$.

$$\psi\Big|_{\delta\rho=0} = \zeta - \dot{\zeta}\frac{\delta\rho}{\dot{\bar{\rho}}}$$

$$ds^2 = -N^2 dt^2 + a^2 e^{2\psi}\gamma_{ij}dx^i dx^j$$

We show our model. We will mainly consider the models of multi-scalar fields having the following general lagrangian.

$$\mathcal{L} = P(X, \varphi^I)$$

where $X \equiv -G_{IJ} g^{\mu\nu} \partial_\mu \varphi^I \partial_\nu \varphi^J$, $I = 1, 2, \cdots, n_f$. n_f is the number of scalar fields and G_{IJ} is general metric of scalar fields space, and we assume that it is the function of scalar fields : $G_{IJ} = G_{IJ}\left[\varphi^K\right]$.

We have defined the base vectors in the space of the field by the following relation.

$$\bar{G}_{IJ} e_n^I e_m^J = \delta_{nm}$$

We define

$$Z_{nm} \equiv \bar{G}_{IJ} e_n^I D_t e_m^J$$

$$D_t e_n^I \equiv \dot{e}_n^I + \Gamma^I_{JK} \dot{\bar{\varphi}}^J e_n^K$$

where Γ^I_{JK} are Christoffel symbols generated by the field space metric $\bar{G}_{IJ}$.

$$\delta\varphi^I = Q^{(n)} e_n^I, \quad (n = 1, 2, 3, \cdots)$$

$$e_r^I \equiv \frac{\dot{\bar{\varphi}}^I}{\sqrt{\bar{X}}}$$

where $Q^{(1)}$ is called adiabatic mode and $Q^{(n)}$ for $n \geq 2$ is called isocurvature mode respectively, and we define that $e_1^I \equiv e_r^I$.

Note that the upper right indices means the components with respect to this basis here.

we construct the quantity that correspond to $\psi|_{\delta\rho=0}$ at super-horizon scale, that is, correspond to the comoving curvature perturbation $\mathcal{R}$ of first order perturbation.(In first order, $\mathcal{R} \equiv \psi + H\delta u \to \psi|_{\delta\rho=0}$ at super horizon scale.)

$$\boxed{\begin{aligned}\psi|_{\delta\rho=0} = &\psi - \frac{H}{\dot r}Q^{(1)} + \frac{1}{2}\left(\frac{H\ddot r}{\dot r^3} - \frac{H}{\dot r^2} - \frac{H}{\dot r}w_{(1)(1)(1)}\right)(Q^{(1)})^2 \\ &- \sum_{n\ge 2}\frac{H}{\dot r^2}Z_{(n)(1)}Q^{(1)}Q^{(n)} \\ &- \frac{1}{2}\frac{H}{\dot r^2}\sum_{m,n\ge 2}Z_{(m)(n)}\partial^{-2}\partial^i W_i^{(n)(m)} \\ &- \frac{1}{2}\frac{H}{\dot r^2}\sum_{m\ge 2}\dot Q^{(m)}Q^{(m)} - \frac{1}{2}\frac{H}{\dot r^2}\sum_{m\ge 2}\partial^{-2}\partial^i V_i^{(m)} \\ &- \frac{H}{\dot r}\frac{1}{2}\sum_{n,m\ge 2}w_{(n)(m)(1)}Q^{(n)}Q^{(m)} \\ &- \sum_{n\ge 2}\frac{H}{2\dot r^3\bar P_X}\left[2c_s^2\dot r^2\bar P_{Xn} - (1+c_s^2)\bar P_n\right]Q^{(1)}Q^{(n)}\end{aligned}}$$

$$\left(\begin{aligned} V_i^{(m)} &\equiv \dot Q^{(m)}\partial_i Q^{(m)} - Q^{(m)}\partial_i \dot Q^{(m)} \\ W_i^{(n)(m)} &\equiv Q^{(n)}\partial_i Q^{(m)} - Q^{(m)}\partial_i Q^{(n)} \\ \Gamma^K_{IJ}e^I_n e^J_m e^L_1 \bar G_{LK} &\equiv w_{(n)(m)(1)}\end{aligned}\right)$$

$$\Updownarrow$$

$$\psi|_{\delta\rho=0} = N_I\delta\varphi^I_* + \frac{1}{2}N_{IJ}\delta\varphi^I_*\delta\varphi^J_* + \dots$$

As a special case we consider general single field inflationary model, and the relation between our approach and δN formalism. We consider general lagrangian for scalar field. $\mathcal{L} = P(X, \varphi)$ where $X \equiv -\partial^\mu \varphi \partial_\mu \varphi$.

Then we can prove that the scalar field perfect fluid satisfies adiabatic condition $p = p[\rho]$ and $\psi|_{\delta\varphi=0} = \zeta$ is conserved only at super-horizon scale.

$$\psi|_{\delta\rho=0} = \zeta = \psi(x, t_i) - \left.\frac{H}{\dot{\bar{\varphi}}}\right|_{t=t_i} \delta\varphi(x, t_i) - \frac{1}{2}\left.\left(\frac{\dot{H}}{\dot{\bar{\varphi}}^2} - H\frac{\ddot{\bar{\varphi}}}{\dot{\bar{\varphi}}^3}\right)\right|_{t=t_i} \delta\varphi^2(x, t_i)$$

$$\Updownarrow$$

$$\psi|_{\delta\rho=0} = N'_* \delta\varphi_* + \frac{1}{2} N''_* \delta\varphi_* \delta\varphi_* + \dots$$

This form is equal to the one generated by using δN formalism.

Conclusion

- We gave a proof that δN formalism is valid for single field with general lagrangian.

- For general multi fields there are necessarily the non-local form

  The use of δN formalism for general multi-field model of inflation may miss such an important feature.

N-Body simulation on Moffat gravity

Yamaguchi University D2 Takayuki Suzuki

○ Basic theory and review of Moffat gravity

developed by John Moffat 2005

ACTION

$$S_G = -\frac{1}{16\pi}\int \frac{1}{G}(R+2\Lambda)\sqrt{-g}\,d^4x,$$

$$S_\phi = -\int \omega\left[\frac{1}{4}B^{\mu\nu}B_{\mu\nu} - \frac{1}{2}\mu^2\phi_\mu\phi^\mu + V_\phi(\phi)\right]\sqrt{-g}\,d^4x,$$

$$S_S = -\int \frac{1}{G}\left[\frac{1}{2}g^{\mu\nu}\left(\frac{\nabla_\mu G\nabla_\nu G}{G^2} + \frac{\nabla_\mu \mu\nabla_\nu \mu}{\mu^2} - \nabla_\mu\omega\nabla_\nu\omega\right) + \frac{V_G(G)}{G^2} + \frac{V_\mu(\mu)}{\mu^2} + V_\omega(\omega)\right]\sqrt{-g}\,d^4x.$$

It have a massive vector field $\varphi_\mu(x)$which couples with matter directly, and 3 scalar fields $G(x)$, $\omega(x)$ and $\mu(x)$. $B_{\mu\nu} = \partial_\mu\varphi_\nu - \partial_\nu\varphi_\mu$ and $V_\varphi(\varphi)$, $V_G(G)$, $V_\omega(\omega)$ and $V_\mu(\mu)$ denote self-interaction potentials. G(x) is gravitational constant.

- The equation of motion of a test particle is given by

$$m\left(\frac{du^\mu}{ds} + \Gamma^\mu_{\alpha\beta}u^\alpha u^\beta\right) = -\alpha\,\kappa\,\omega\, m\, B^\mu{}_\nu u^\nu .$$

- For weak fields the MOG acceleration law is

$$\frac{d^2r}{dt^2} = -\frac{G_N M}{r^2}\left[1+\alpha-\alpha(1+\mu r)e^{-\mu r}\right],$$

$$\alpha = \frac{M}{\left(\sqrt{M}+E\right)^2}\left(\frac{G_\infty}{G_N}-1\right), \qquad \mu = \frac{D}{\sqrt{M}}, \qquad D \cong 6250 M_\Theta^{1/2}\mathrm{kpc}^{-1},\ E \cong 25000 M_\Theta^{1/2},\ G_\infty \cong 20 G_N,$$

$$\frac{d^2r}{dt^2} = -\frac{G_{\mathrm{eff}} M}{r^2}, \qquad G_{\mathrm{eff}} = G_N\left[1+\alpha-\alpha(1+\mu r)e^{-\mu r}\right].$$

key point : Vector field is
couple with matter → Geodesic equation has external force term
massive → It has effective range → *Yukawa* like force

In fact,
Newton gravity we recognize = (1+α)×Gravitation of the inverse square law — Yukawa like Repulsive force

Moffat gravity can explain galaxy flat rotate curve without dark matter

galaxy mass $=10^{11}\ M_\odot$

G_{eff} $$G_{eff} = G_N\left[1+\alpha-\alpha(1+\mu r)e^{-\mu r}\right].$$

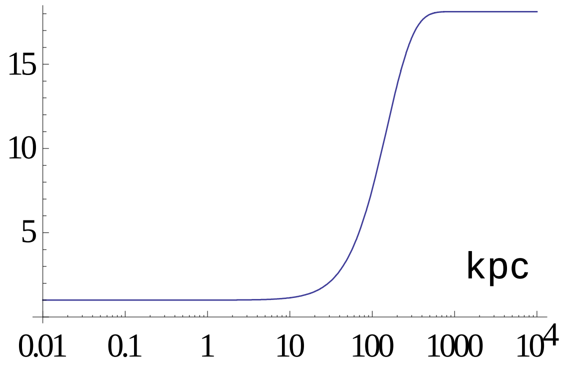

→linear plot

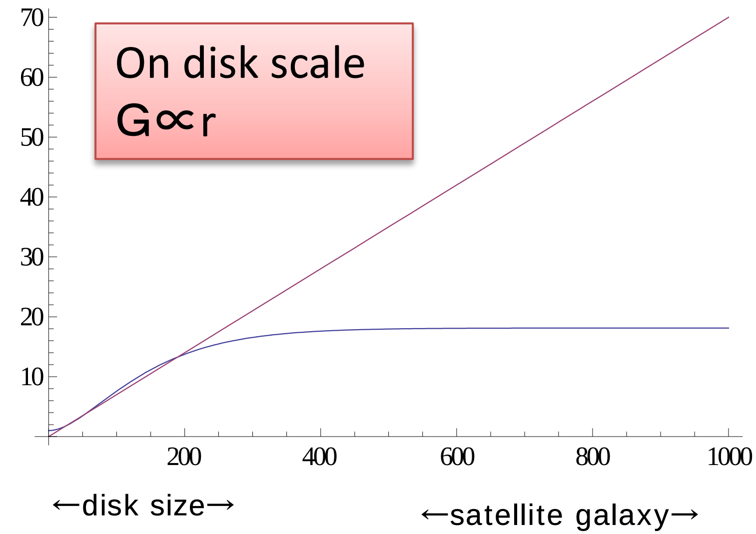

Equation of Kepler motion

$$\frac{GM}{r^2} = \frac{v^2}{r} \Rightarrow v = \sqrt{\frac{GM}{r}}$$

if $G \propto r$, v is constant.

How are MOG different from MOND(Mordehai Milgrom 1983)?

- It is not simple-minded phenomenalism.
  - ➢ It is relativistic gravity theory.
  - ➢ It can be derived from an action principle.
- It can explain without dark matter from small scale(galaxy) to large scale(cosmology).
- It can explain dark energy too. (**arXiv:0710.0364**)

Moffat says —

• A fitting routine has been applied to fit a large number of galaxy rotation curves (101 galaxies), using photometric data (58 galaxies) and a core model (43 galaxies) (J. R. Brownstein and JWM, 2005; J. R. Brownstein, 2009). The fits to the data are remarkably good for STVG. For the photometric data, only one parameter, the mass-to-light ratio M/L, is used.

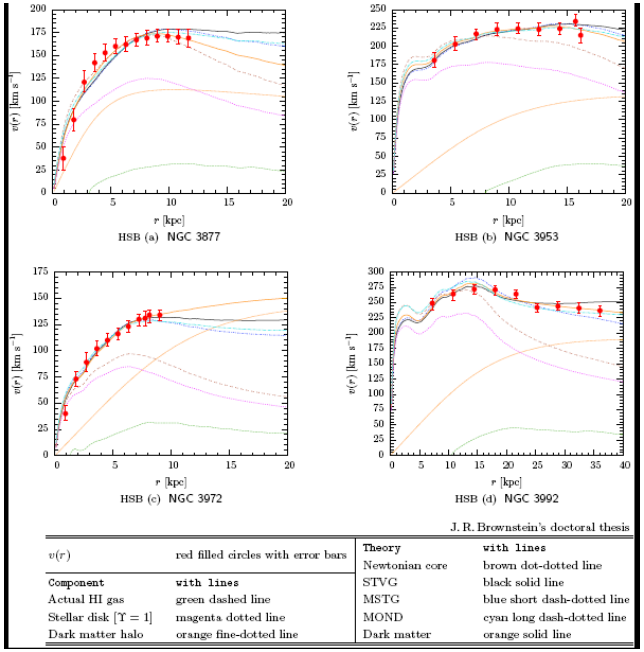

○ the theme of my study

But, This verification is the viewpoint from "statics".
It is necessary to examine it about the real galactic "kinetic" evolution more.
My study is verification of Moffat gravity from the viewpoint of N-body simulation.

$$a_i = -G_N \sum_j \frac{(r_j - r_i) m_i}{\left|r_j - r_i\right|^3} \left\{ 1 + \alpha\left(1 - \left(1 + \mu\left|r_j - r_i\right|\right) e^{-\mu\left(\left|r_j - r_i\right|\right)}\right) \right\}$$

Method is very simple.
performing normal N-body simulation after having changed equation of motion.

This is the modified equation of motion.(μ and α is decided by total system mass.
But, The equation of Moffat gravity with matter distribution is not yet derived.
It 's an approximation when the distribution of matter has a symmetry.
It cannot applied about a galactic collision or the structure formation of the universe etc.

○ report of progress and earlier study

about ellipse galaxy (my study)

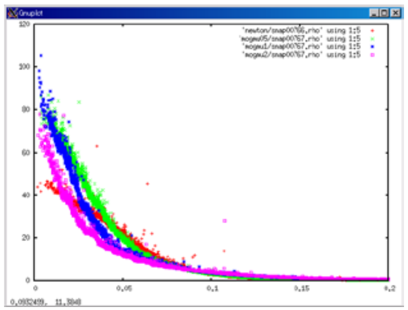

brightness distribution

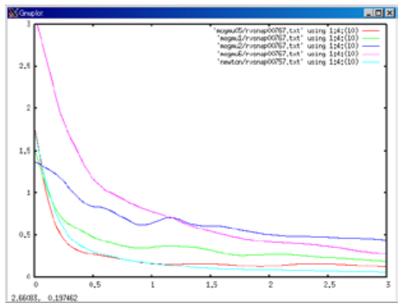

velocity distribution

red is Newtonian ,others are MOG(parameter is varied)
brightness distribution is predicted a following the Newton dynamics. *velocity* distribution is higher than Newtonian model. But the result depends on a parameter.

cf : about spiral galaxy(other earlier study)

C. S. S. Brandao and J. C. N. de Araujo, arXiv:1006.1000.

can maintain flat rotate curve

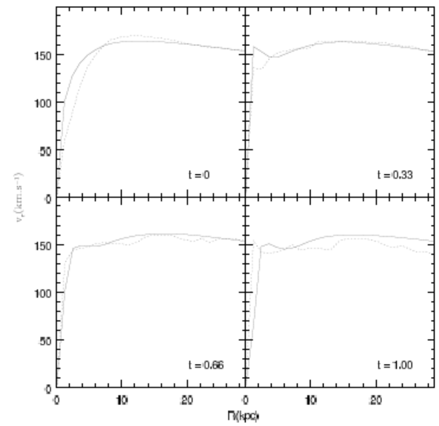

Fig. 10.— Moffatian rotation curves (model III). Solid lines stand for the rotation curve given by Equation (5) and dashed lines for the rotation curves obtained from the snapshots. Time is indicated in the respective boxes.

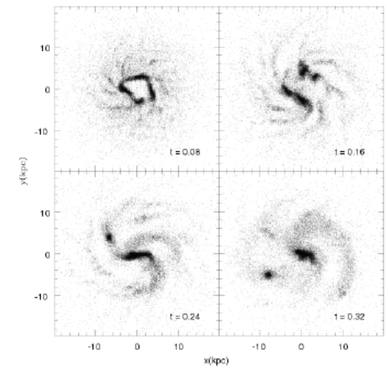

ig. 9.— First 300 Myr of simulated time to the MB disk at z-projection. Time is indicated i the respective boxes.

But, exponential disk is unstable

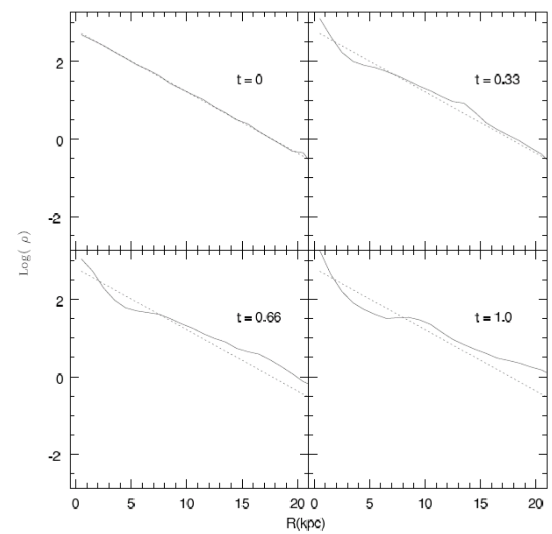

○ consideration and task for the future

- they are still toy simulation.
  - ➢ both study is few number of the particles
  - ➢ both study is not include galactic gas.

→more precisely

Constraints on the primordial non-Gaussianity from galaxy-CMB cross-correlation

Yoshitaka Takeuchi (Nagoya U.)

in collaborate with Kiyotomo Ichiki & Takahiko Matsubara

Ref : PRD 82, 023517 (2010), arXiv:[astro-ph/1005.3492]

E-mail : yositaka@a.phys.nagoya-u.ac.jp

- The primordial non-Gaussianity (NG) affects the clustering of dark matter halo through the scale-dependent bias.
- **Recent results** : ***Obs***ervations & ***For***ecasts (1-σ error)

  Obs. $f_{NL} = 53 \pm 25$ & $f_{NL} = 47 \pm 21$: from NVSS & SDSS DR6 QSOs data (Xia et al. 2010)
  For. $\Delta f_{NL} \sim 1\text{-}5$: cluster counts for DES-like survey (Cunha et al. 2010)
  For. $\Delta f_{NL} \sim$ few : CMB Bispectrum with ideal CMB experiment
- CMB lensing is a powerful tool to explore the large scale structure, which can get matter distribution without uncertainty of bias.
- Cross-correlation between galaxy & CMB lensing can be break some degeneracy of NG and bias, and will improve the constraint of NG.

Scale-dependent bias

The effect of “local” type NG,

$$\Phi = \phi + f_{\rm NL}(\phi^2 - \langle \phi^2 \rangle)$$

is seen through the scale-dependent bias.

- “local” type NG gives rise to a strong scale-dependent bias on large-scales ($\propto k^{-2}$), while the bias is roughly constant in the Gaussian case.

Gaussianity　　non-Gaussianity

$$P_g(k) = b_0^2 P(k) \longrightarrow [b_0 + \Delta b(k)]^2 P(k)$$

$$\boxed{\Delta b(k) = \frac{3(b_0 - 1) f_{\rm NL} \Omega_m H_0^2 \delta_c}{D(z) k^2 T(k)}}$$

b_0 : Linear bias
P(k) : Matter power spectrum
δ_c : Linear collapse density
D(z) : Growth factor
T(k) : Transfer function

$C_l^{\psi g}$: galaxy-CMB lensing cross-correlation

$$\boxed{C_l^{\psi g} = \frac{2}{\pi} \int k^2 dk P(k) \Delta_l^{\psi}(k) \Delta_l^{g}(k)}$$

galaxy distribution (number counts)

$$\Delta_l^g(k) = \int dz \frac{dN}{dz} b(k, z) T(k) D(z) j_l(k\chi)$$

CMB lensing potential

$$\Delta_l^{\psi}(k) = -2 \int_0^{\chi_*} d\chi T_{\Psi}(k; \eta_0 - \chi) \left(\frac{\chi_* - \chi}{\chi_* \chi} \right) j_l(k\chi)$$

$C_l^{\psi g}$ & $f_{\rm NL}$ dependence

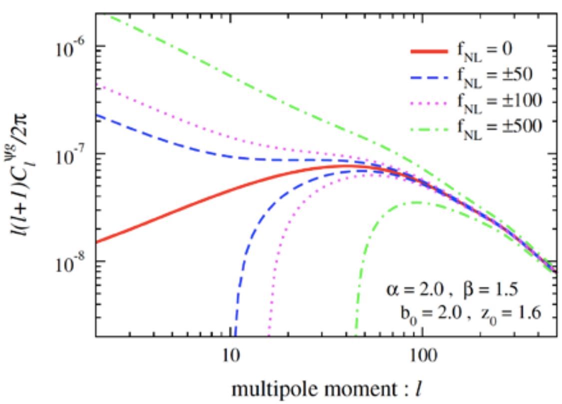

- NG raises (or lowers) the amplitude on large-scale.
- For the high-z or highly biased objects, the effect of NG appears more pronouncedly.

Signal-to-Noise

- Compare the S/N of some cross-correlations.

$$\left(\frac{S}{N}\right)^2 = f_{\rm sky}\sum_{2}^{l_{\rm max}}(2l+1)\frac{(C_l^{XY})^2}{(C_l^{XY})^2 + (C_l^{XX}+N_l^{XX})(C_l^{YY}+N_l^{YY})}$$

For high-$l_{\rm max}$, ψg get larger S/N than Tg or $T\psi$.

- ψg will be an important observation value !!

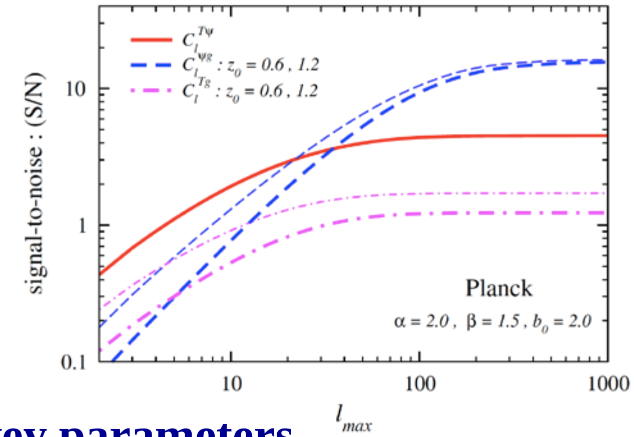

Survey parameters

- $f_{\rm sky}$: sky coverage
  for galaxy survey (C_l^{gg},C_l^{Tg},$C_l^{\psi g}$) - $f_{\rm sky}$ = 0.10
  for CMB (C_l^{TT},C_l^{EE},C_l^{TE},$C_l^{\psi\psi}$,$C_l^{T\psi}$) - $f_{\rm sky}$ = 0.65
- $N_g = 10^6$: total number of galaxies

Parameter forecast (for Plandk or CMBPol)

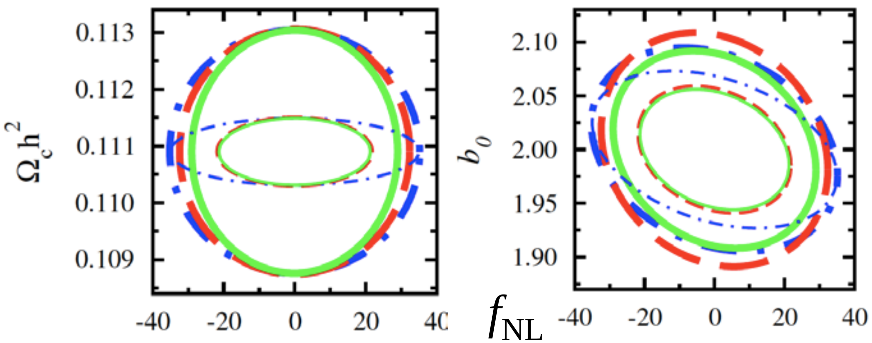

marginalized 1-σ error for **Planck (thick line)** or CMBPol (thin line)

- The error of $f_{\rm NL}$ becomes smaller by including ψg. This aspect can be seen more clearly for CMBPol.

redshift dependence of $\Delta f_{\rm NL}$

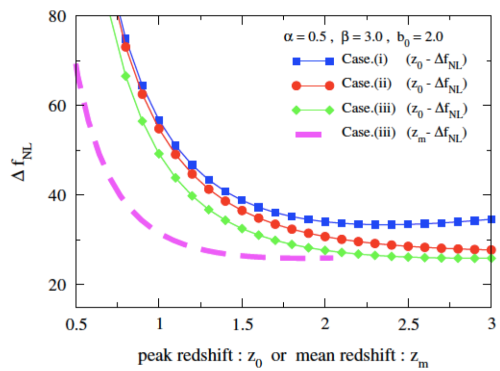

- $\Delta f_{\rm NL}$ depends extensively on the peak redshift of the galaxy distribution z_0.
- For large z_0, the change of $\Delta f_{\rm NL}$ is small.
  => the amplitude of the matter density becomes small.

- Case I : C_l^{TT}, C_l^{EE}, C_l^{TE}, $C_l^{\psi\psi}$, $C_l^{T\psi}$, C_l^{gg}, $\cancel{C_l^{Tg}}$, $\cancel{C_l^{\psi g}}$ (without C_l^{Tg}, $C_l^{\psi g}$)
- Case II : C_l^{TT}, C_l^{EE}, C_l^{TE}, $C_l^{\psi\psi}$, $\cancel{C_l^{T\psi}}$, C_l^{gg}, $\cancel{C_l^{Tg}}$, $C_l^{\psi g}$ (without C_l^{Tg}, $C_l^{T\psi}$)
- Case III: C_l^{TT}, C_l^{EE}, C_l^{TE}, $C_l^{\psi\psi}$, $C_l^{T\psi}$, C_l^{gg}, C_l^{Tg}, $C_l^{\psi g}$ (full)

Conclusion

- We estimated the error of "local" type non-Gaussianity through scale-dependent bias.
- Our analysis is based on the Fisher matrix analysis and we estimate how much the constraint of $f_{\rm NL}$ will be improved by including galaxy-CMB lensing cross-correlation.

  - Galaxy-CMB cross-correlation, ψg, improves the constraint of $f_{\rm NL}$, however, the impact is not so much for Planck.
  - Planck is not sensitive to CMB lensing so much. Therefore, the improvements by ψg can be seen more clearly for the future CMB survey which is sensitive to CMB lensing (e.g. CMBPol).

IPMU INSTITUTE FOR THE PHYSICS AND MATHEMATICS OF THE UNIVERSE

Complementarity of Future Dark Energy Probes

Jiayu Tang (IPMU)

Filipe Abdalla (UCL)

Jochen Weller (LMU, USM)

arXiv:0807.3140

Abstract: In this paper we adapt a binning approach to the equation of state factor ``w'' and discuss how future weak lensing, Sne, Cluster Counts and BAO surveys constrain the equation of state at different redshifts. We analyse a few representative future surveys, namely DES, PS1, WFMOS, PS4, EUCLID, SNAP and SKA, and perform a principal component analysis for the ``w'' bins. We study at which redshifts a particular survey constrains the equation of state best and how many principal components are significantly determined. We then point out which surveys would be sufficiently complementary. We find that weak lensing surveys, like EUCLID, would constrain the equation of state best and would be able to constrain of the order of three significant modes. Baryon acoustic oscillation surveys on the other hand provide a unique opportunity to probe the equation of state at relatively high redshifts.

w and PCA

- Model independent parameterization

$$w(z) = \begin{cases} w_{\rm i}, & z \in (z_{\rm i} - \frac{1}{2}\Delta z_{\rm i}, z_{\rm i} + \frac{1}{2}\Delta z_{\rm i}] \\ w_h, & z > z_{\rm max} \end{cases}$$

- Decorrelate *Fisher Matrix* to get the principal components, i.e., eigenmodes $e_i(z)$

To represent the redshift dependen
of the eigenmodes, we define the

$$\phi_i(z) \equiv N \left| \sqrt{\lambda_i} \mathbf{e}_i(z) \right|$$

Note that the prefactor N appears in order to make this quantity semi-independent to the number of bins.

Example: eigen modes from joint Stage III experiments (PS4 (SNe)+PS4(WL)+WFMOS(BAO))

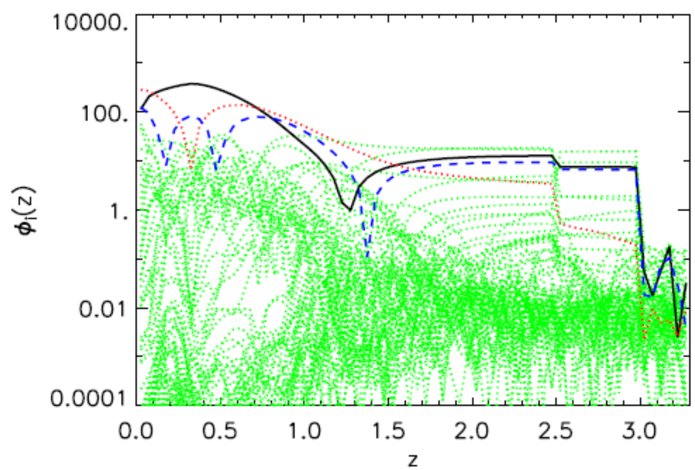

w and PCA: How many eigenmodes can be estimated by experiments

Unbiased Construction ($w=w_{fid}$)

$$B_{M+1} \approx \left| \log_{10} \left(\frac{1}{\sqrt{\lambda_{M+1}} \sqrt{N} \delta w} \right) \right| = \left| \log_{10} \left[\frac{\sigma_{M+1}}{\sqrt{N} \delta w} \right] \right|$$

By Strong evidence

$$N \lambda_M \geqslant 100 \, .$$

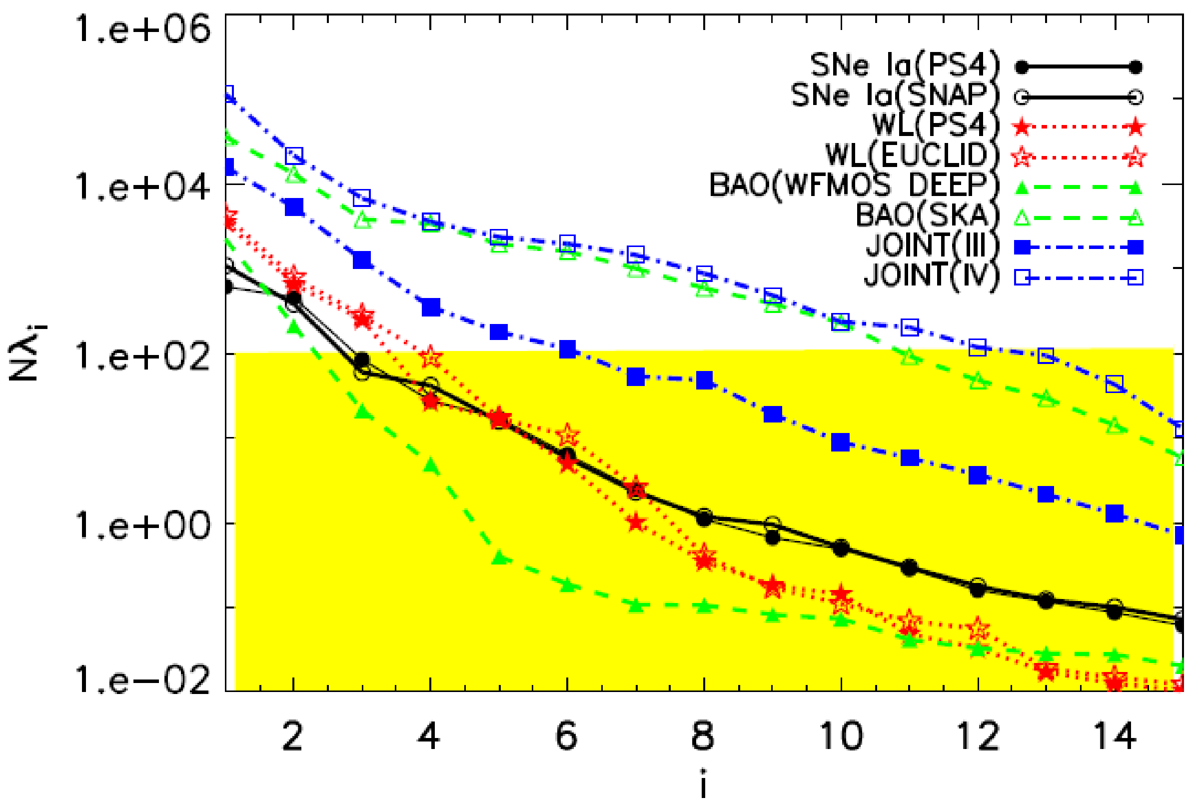

The number of w-eigenmodes with strong evidence according to Jeffrey’s scale.

Expt.	SNe Ia	WL	CC	BAO	Joint
DES	2(3)	1(3)	1(2)	1(2)	
PS1	-	2(3)	-	1(2)	
WFMOS(WIDE)	-	-	-	3(3)	
WFMOS(DEEP)	-	-	-	2(4)	
PS4	2(5)	3(3)	-	1(2)	
EUCLID	-	3(4)	-	*	
SNAP	2(5)	2(3)	-	-	
SKA	-	-	-	10(9)	
Joint III	-	-	-		6(8)
Joint IV	-	-	-		12(12)

Summary:

- Cosmological constant with large error bars is preferred by current data. We need more observation data.
- Future dark energy missions will allow us to constrain the time evolution of dark energy parameter w and hence dark energy theory.
- The statistics can be applied to distinguish dark energy, string theory and modified gravity.

The interplay between Dark Matter and the IGM during the Dark Ages

Marcos Valdés (IPMU, Tokyo)

C. Evoli, A. Ferrara, M. Mapelli, E. Ripamonti, N. Yoshida

RESCEU/DENET Summer School

Kochi, August 29th - September 1st, 2010

IPMU INSTITUTE FOR THE PHYSICS AND MATHEMATICS OF THE UNIVERSE

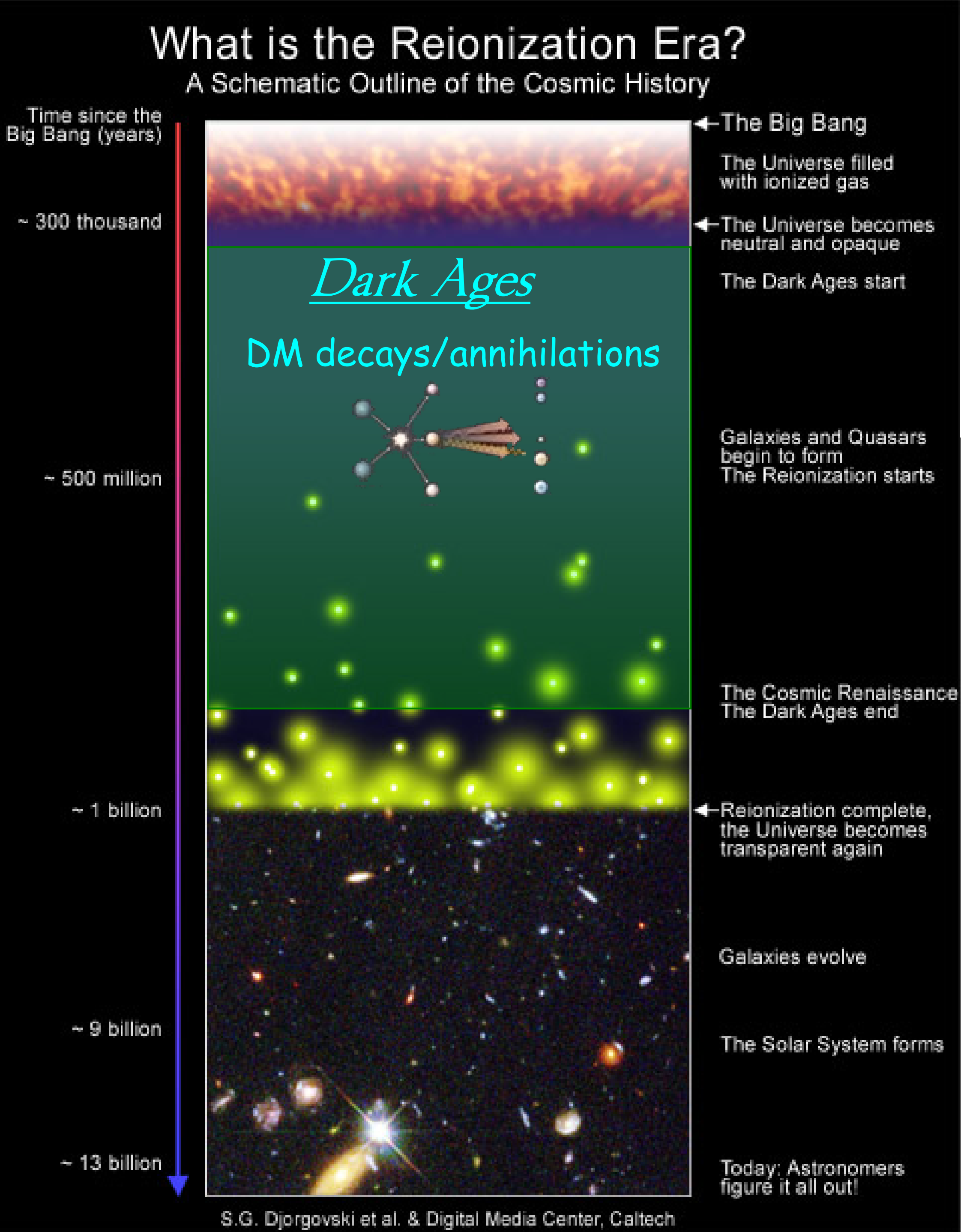

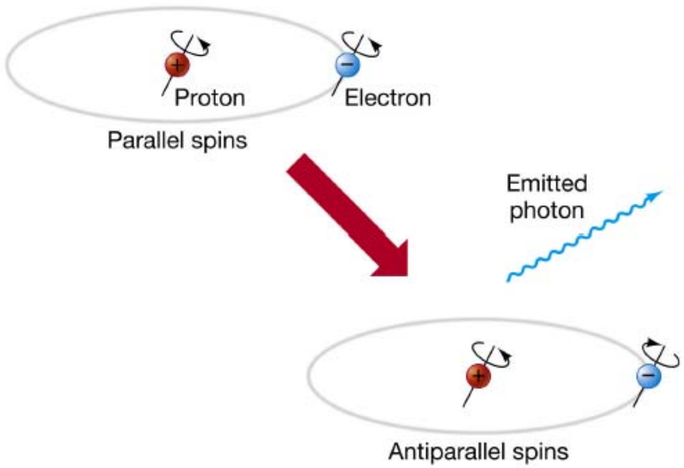

–Visualization of the two energy states of the ground level of neutral hydrogen, in which the electron has its spin either parallel or anti-parallel to that of the proton.

–The parallel state has an energy higher by ~ 5.9×10^{-6}eV, so a transition to the anti-parallel state results in the emission of a HI 21 cm photon

–Future radio interferometers such as LOFAR, MWA, SKA will probe directly the physics of the Dark Ages via HI 21 cm observations

DM decays/annihilations can leave an observable trace on the Dark Ages high-z IGM

$$T_S = \frac{T_{CMB} + y_\alpha T_k + y_c T_k}{1 + y_\alpha + y_c}$$

$$y_\alpha = \frac{P_{10} T_*}{A_{10} T_k}$$

$$y_c = \frac{C_{10} T_*}{A_{10} T_k}$$

$$\delta T_b \simeq \frac{T_S - T_{CMB}}{1+z} \tau$$

$$\tau \simeq \frac{3 c^3 h_p A_{10}}{32 \pi k_B \nu_0{}^2 T_S H(z)} \mathcal{N}_{\rm HI}$$

DM decays/annihilations can affect the thermal and ionization evolution of the IGM

→ Solve eqs. describing redshift evolution of x_e, T_k, J_α

→ Compute new values of δT_b

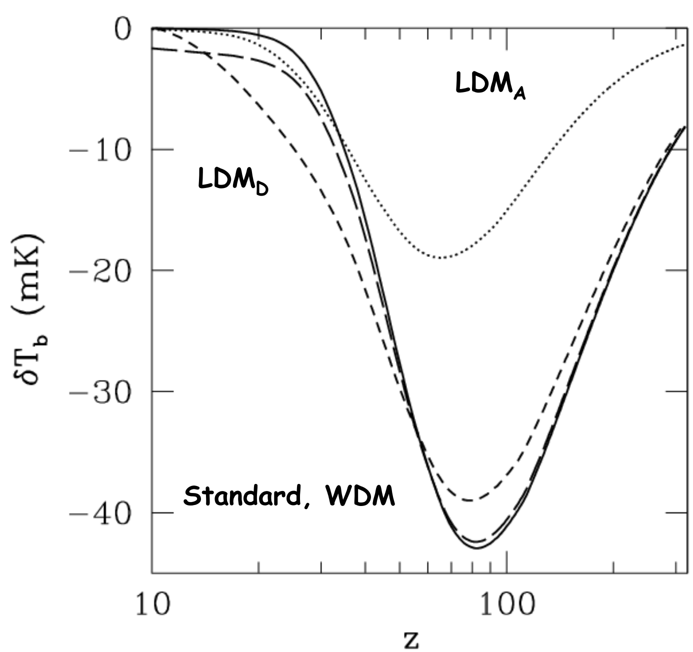

Valdés et al. 2007

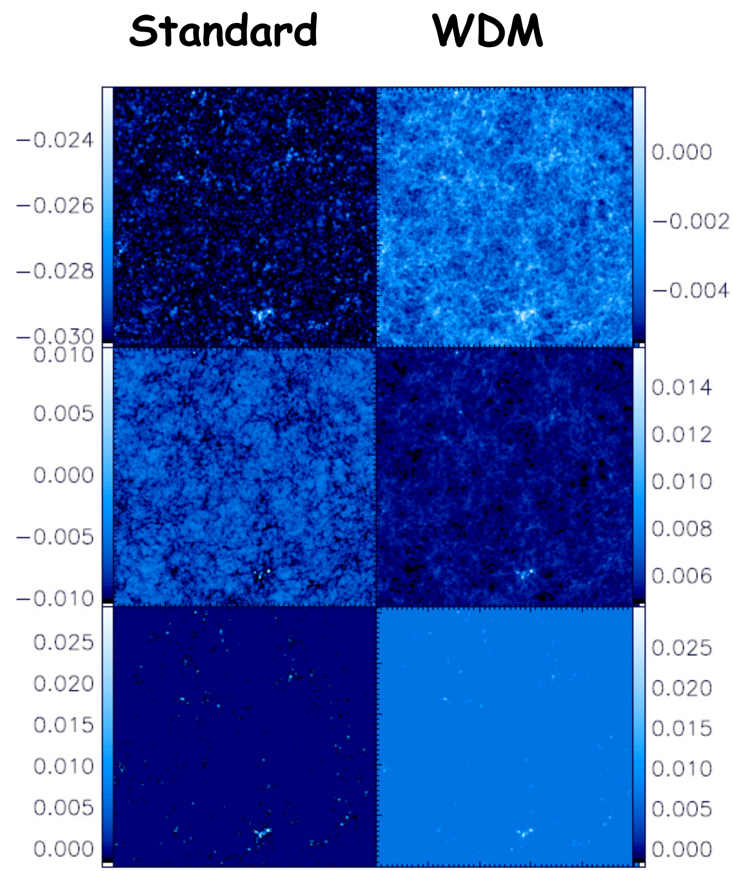

HI 21cm line differential brightness temperature, δT_b [mK]

Valdés et al. 2010 in prep

Particle energy cascade in the intergalactic medium

Valdés & Ferrara, 2008 | Valdés, Evoli & Ferrara, 2009 | Evoli, Valdés & Ferrara, 2010 in prep

<u>MEDEA - Monte Carlo Energy DEposition Analysis:</u> repeated random sampling of the relevant physical quantities and processes, i.e. *cross-sections and interaction probabilities* to follow the evolution of a relativistic electron up to 1 TeV (previous works did up to 10 keV)

LE
- (I) H, He, HeI ionization
- (II) H, He *excitation*
- (III) *Collisions with thermal electrons*
- (IV) *Recombinations*

HE
- (V) *Bremsstrahlung*
- (VI) *Inverse Compton*

→ Ensemble of secondary photons and electrons which can interact further with the gas. Start with one particle → end up with many!

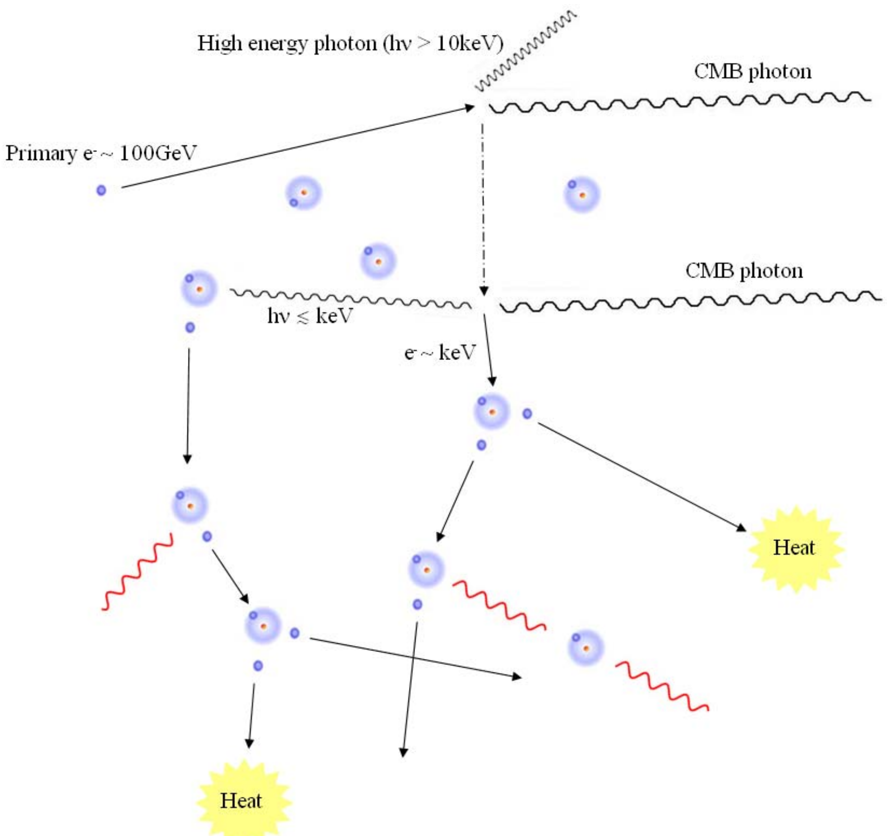

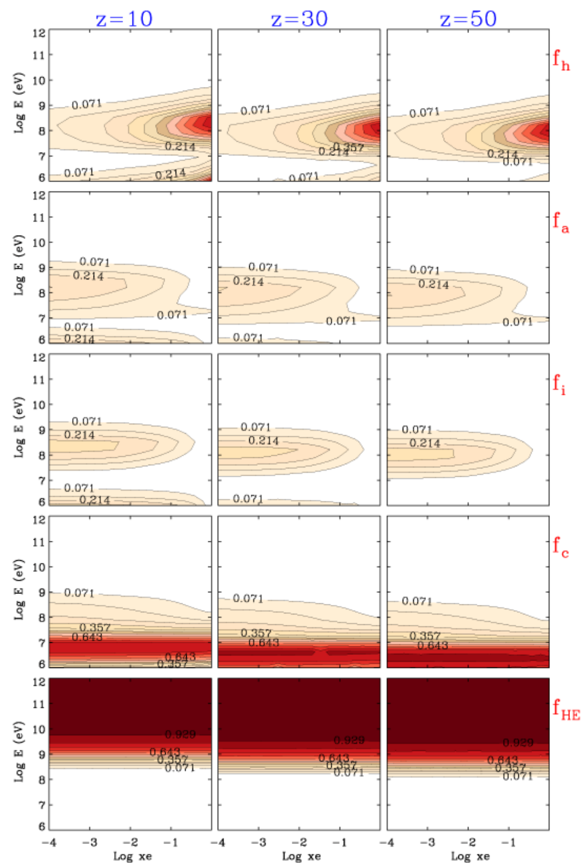

Heat

Lyα photons

Ionizations

Low energy photons $h\nu < 10.2$ eV

High energy photons $h\nu > 10$ keV

On Classification of Models of Large Non-Gaussianity

Shuichiro Yokoyama (Nagoya Univ.)

In collaboration with

T. Suyama, T. Takahashi, M. Yamaguchi

(T.Suyama, T.Takahashi, M. Yamaguchi and SY, in prep.)

◆non-Gaussian Zoo

curvaton
self-interacting curvaton
multi-brid inflation
modulated curvaton
inhomogeneous end of inflation
DBI inflation
modulated reheating
ekpyrotic scenario
ghost inflation
hilltop
multi-DBI
ungaussiton
multi-curvaton
k-inflation
modulated phase transition
preheating

....

Can we distinguish ??

How to ?

- **Shape of three point function**

  (local, equilateral, orthogonal, …)

Komatsu+(2010), Senatore+(2010)

- **fNL, tauNL, gNL**

$$\langle \zeta_{\vec{k}_1}\zeta_{\vec{k}_2}\zeta_{\vec{k}_3}\rangle = (2\pi)^3 B_\zeta(k_1,k_2,k_3)\delta(\vec{k}_1+\vec{k}_2+\vec{k}_3),$$

$$\langle \zeta_{\vec{k}_1}\zeta_{\vec{k}_2}\zeta_{\vec{k}_3}\zeta_{\vec{k}_4}\rangle = (2\pi)^3 T_\zeta(k_1,k_2,k_3,k_4)\delta(\vec{k}_1+\vec{k}_2+\vec{k}_3+\vec{k}_4),$$

$$\begin{aligned}
B_\zeta(k_1,k_2,k_3) &= \frac{6}{5} f_{\rm NL}^{\rm local}\left(P_\zeta(k_1)P_\zeta(k_2)+P_\zeta(k_2)P_\zeta(k_3)+P_\zeta(k_3)P_\zeta(k_1)\right),\\
T_\zeta(k_1,k_2,k_3,k_4) &= \tau_{\rm NL}^{\rm local}\left(P_\zeta(k_{13})P_\zeta(k_3)P_\zeta(k_4)+11\ \text{perms.}\right)\\
&\quad +\frac{54}{25} g_{\rm NL}^{\rm local}\left(P_\zeta(k_2)P_\zeta(k_3)P_\zeta(k_4)+3\ \text{perms.}\right),
\end{aligned}$$

•**current constraints**

Komatsu+(2010), Smidt+(2010), Desjacques+(2010)

$$-10 < f_{\rm NL}^{\rm local} < 74$$

$$-0.6\times10^4 < \tau_{\rm NL}^{\rm local} < 3.3\times10^4$$

$$-3.5\times10^5 < g_{\rm NL}^{\rm local} < 8.2\times10^5$$

• future experiments …

$$\Delta f_{\rm NL} \simeq 5 \qquad \Delta\tau_{\rm NL} \simeq 500 \qquad \Delta g_{\rm NL} \sim 10^4$$

fNL vs tauNL

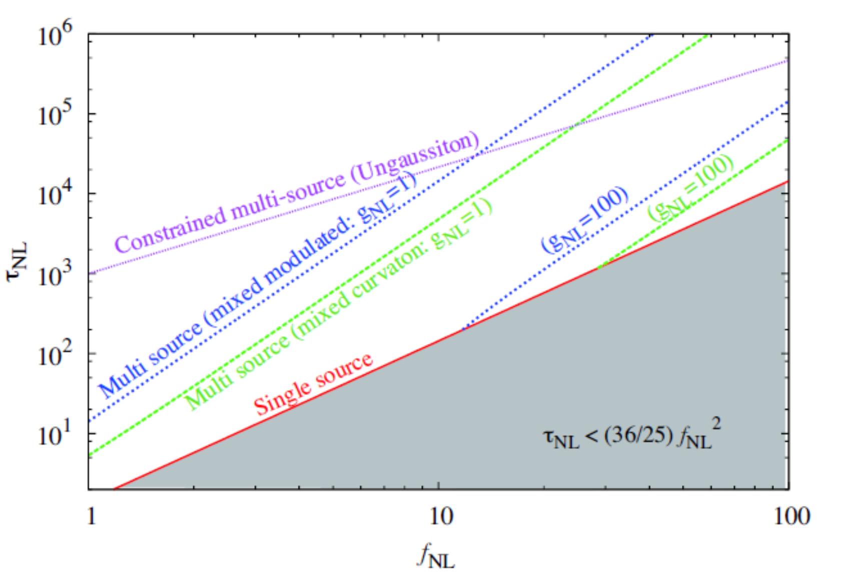

- *Local type non-Gaussianity satisfies the inequality;*

$$\tau_{\rm NL} \gtrsim \left(\frac{6}{5} f_{\rm NL}\right)^2,$$

up to the higher order corrections.

fNL vs gNL

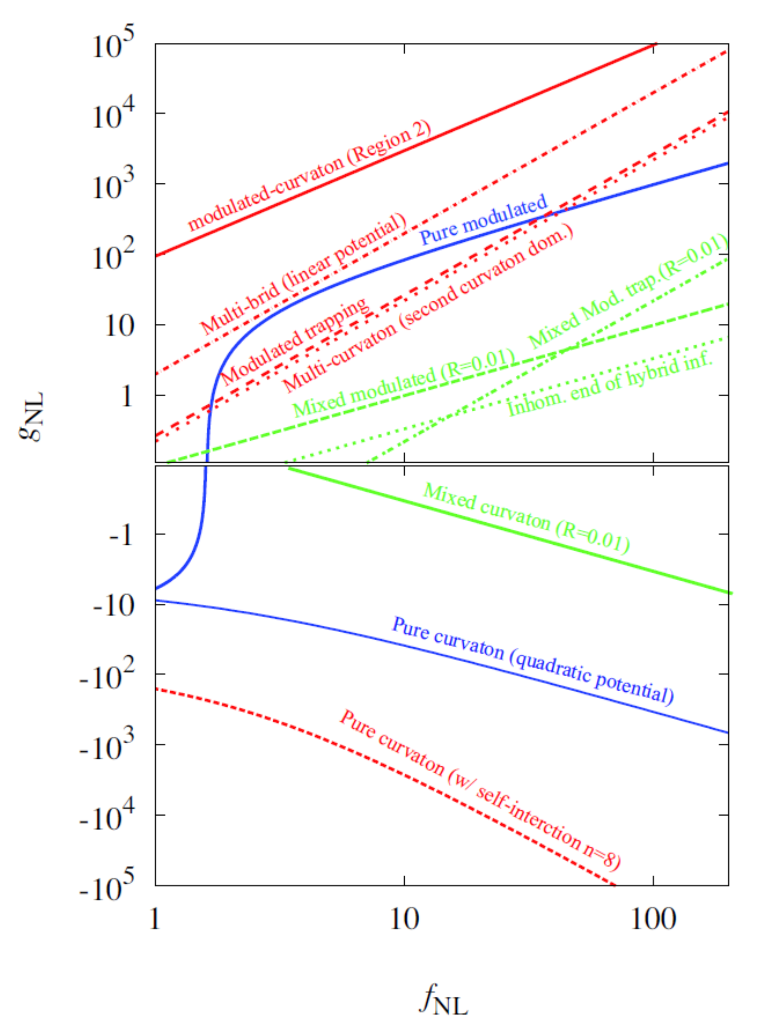

Summary of the categories

Category	$f_{\rm NL}$–$\tau_{\rm NL}$ relation	Examples and $f_{\rm NL}$–$g_{\rm NL}$ relation
Single source	$\tau_{\rm NL} = (6f_{\rm NL}/5)^2$	(pure) curvaton (w/o self-interaction) $[g_{\rm NL} = -(10/3)f_{\rm NL} - (575/108)]^{(a)}$
		(pure) curvaton (w/ self-interaction) $[g_{\rm NL} = A_{\rm NQ}f_{\rm NL}^2 + B_{\rm NQ}f_{\rm NL} + C_{\rm NQ}]^{(b)}$
		(pure) modulated reheating $[g_{\rm NL} = 10f_{\rm NL} - (50/3)]^{(c)}$
		modulated-curvaton scenario $\left[g_{\rm NL} = 3(f_{\rm NL}/r_{\rm dec})^{3/2}\right]^{(d)}$
		Inhomogeneous end of hybrid inflation $[g_{\rm NL} = (10/3)\eta_{\rm cr}f_{\rm NL}]$
		Inhomogeneous end of thermal inflation $[g_{\rm NL} = -(10/3)f_{\rm NL} - (50/27)]^{(e)}$
		Modulated trapping $[g_{\rm NL} = (2/9)f_{\rm NL}^2]^{(f)}$
Multi-source	$\tau_{\rm NL} > (6f_{\rm NL}/5)^2$	mixed curvaton and inflaton $[g_{\rm NL} = -(10/3)(R/(1+R))f_{\rm NL} - (575/108)(R/(1+R))^3]^{(g)}$
		mixed modulated and inflaton $[g_{\rm NL} = 10(R/(1+R))f_{\rm NL} - (50/3)(R/(1+R))^3]^{(h)}$
		mixed modulated trapping and inflaton $[g_{\rm NL} = (2/9)((1+R)/R)f_{\rm NL}^2 = (25/162)\tau_{\rm NL}.]^{(i)}$
		multi-curvaton $[g_{\rm NL} = C_{\rm mc}f_{\rm NL}]^{(j)}$
		Multi-brid inflation (quadratic potential) $[g_{\rm NL} = -(10/3)\eta f_{\rm NL}]^{(k)}$
		Multi-brid inflation (linear potential) $[g_{\rm NL} = 2f_{\rm NL}^2]^{(l)}$
Constrained multi-source	$\tau_{\rm NL} = Cf_{\rm NL}^n$	ungaussiton ($C \simeq 10^3,\ n = 4/3$)